Universitat Politècnica de València
Departamento de Máquinas y Motores Térmicos

Doctoral Thesis

EXPERIMENTAL STUDY OF THE UREA-WATER SOLUTION INJECTION PROCESS

Presented by:
Armando Enrique Moreno Gasparotto

Supervised by:
Dra. Gabriela Bracho León

in fulfillment of the requirements for the degree of
Doctor of Philosophy

Valencia, February 2022

Ph.D. Thesis

EXPERIMENTAL STUDY OF THE UREA-WATER SOLUTION INJECTION PROCESS

Written by:	Mr. Armando Enrique Moreno Gasparotto
Supervised by:	Dra. Gabriela Bracho León

Examination committee:

Chairman:	Dr. Jose V. Pastor Soriano
Secretary:	Dra. M. del Carmen Mata Montes
Member:	Dr. Tiemin Xuan

Reviewing board:

Dra. M. Arantzazu Gomez Esteban
Dr. Oscar Venegas Pereira
Dr. Tiemin Xuan

Valencia, February 2022

Abstract

In a global context of concern for health and the environment, the industry and research community are working hard to develop tools and technologies that contribute to the reduction of pollutant emissions. One of the sectors affected by the anti-pollution regulations is the transportation, since it is responsible for around 20% of the green house gases emissions production. New technologies are evolving, especially subsystems as fuel injection components, combustion design, after-treatment and hybridization. The selective catalytic reduction systems (SCR) have been one of the most important to reach the emission targets, specially for Nitrous Oxides (NO_x). The SCR technology is employed in the elimination of the NO_x present in the exhaust gases of a combustion engine. The injection process of the urea-water solution (UWS) determines the initial conditions for the mixing and evaporation of the fluid in the selective catalytic reduction system. For a proper operation, the UWS injector must dose an adequate amount of liquid into the exhaust pipe to avoid deposit formation and to guarantee the SCR system efficiency. This task requires the knowledge of the performance of the injector and the evolution of the spray. However, the study of the flow in this low pressure atomizers, as well as the fluid atomization and jet development, still shows significant uncertainties, constituting a major challenge for research in this field.

The goal of this thesis is the comprehension of the urea-water solution injection processes under realistic operating conditions, similar to those of an engine exhaust pipe. To this end, this work focuses on the development of new experimental facilities that enable to perform the hydraulic characterization combining momentum flux measurements and injected mass. Afterwards, the UWS jet is visualized by applying optical techniques at various levels of air temperature and mass flow, in a novel test rig designed for this purpose.

Regarding to the hydraulic performance of the UWS injector, the approach is based on measuring the spray momentum flux in order to understand the influence of different variables as injected mass, injection pressure, back pressure and cooling temperature on the flow characteristics. The measurements were carried out using an experimental facility developed at CMT-Motores Térmicos for the determination of spray momentum flux, where the configuration of the system was customized to fulfill the injector operation requirements. Also, the injected mass is obtained experimentally for the same operating conditions. The proposed methodology allowed to calculate the mass flow rate of this low pressure atomizers and the discharge coefficients, which are useful data for future computer modeling activities.

A dedicated test facility was designed to study UWS spray under conditions that resemble those of the engine exhaust pipe. The liquid spray evolution is characterized from the macroscopic point of view, developing a methodology for the determination of the spray penetration and spreading angle. The method is based on the optical setup known as back-light in a far-field configuration. The spray penetration was divided in two zones, the spray burst and the body, where it was observed that the initial part of the injected spray is not particularly affected by the injection pressure but was rather influenced by the cooling temperature of the injector.

Besides, the liquid atomization process of the UWS dosing system is investigated using optical diagnosis through back-light imaging coupled with a special lens. The droplet diameter distribution and the droplet velocity (in the injector axial and tangential components) of the liquid spray are quantified under different air flow and injection pressure levels. A high-speed camera was used for capturing the liquid phase images, comparing the atomized liquid drops in three different regions of the plume: the first one near the nozzle exit, and the other two in the developed region of the spray, one aligned with the injector axis and the other at the spray periphery. The results of this study demonstrated that injection pressure produces more droplets with smaller diameters favoring the atomization process.

Resumen

En un contexto mundial de preocupación por la salud y el medio ambiente, la industria y la comunidad investigadora están trabajando arduamente para desarrollar herramientas y tecnologías que contribuyan a la reducción de emisiones contaminantes. Uno de los sectores afectados por la normativa anticontaminación es el transporte, ya que es responsable de alrededor del 20 % de la producción de emisiones de gases de efecto invernadero. Nuevas tecnologías están evolucionando, especialmente componentes de los sistemas de inyección, diseño de cámaras de combustión, elementos de postratamiento, la hibridación, entre otros. Los sistemas de reducción catalítica selectiva (SCR) han sido una de las claves para alcanzar los objetivos de las normativas de emisiones, especialmente de Óxidos Nitrosos (NO_x). La tecnología SCR se emplea para eliminar los NO_x presentes en los gases de escape de un motor. El proceso de inyección de la solución de urea-agua (UWS) determina las condiciones iniciales para la mezcla y evaporación del fluido en el sistema de reducción catalítica selectiva. Para un correcto funcionamiento, el inyector UWS debe dosificar una cantidad adecuada de líquido en el tubo de escape para evitar la formación de depósitos y garantizar la eficiencia del post-tratamiento. Esta tarea requiere la caracterización hidráulica del inyector y de la evolución del spray. Sin embargo, el estudio del flujo en estos atomizadores de baja presión, tanto de la atomización del fluido como el desarrollo del chorro, aún presenta importantes incertidumbres, lo que constituye un gran desafío para la investigación en este campo.

El objetivo de esta tesis es la comprensión de los procesos de inyección de solución urea-agua en condiciones de funcionamiento realistas, similares a las que se encuentran en un tubo de escape de motor. Para ello, este trabajo se centra en el desarrollo de nuevas instalaciones experimentales que permitan realizar la caracterización hidráulica combinando medidas de flujo de cantidad de movimiento y masa inyectada. Posteriormente, el chorro de UWS se visualiza aplicando técnicas ópticas a varios niveles de temperatura y flujo másico de aire, en un banco de pruebas diseñado para este propósito.

En cuanto a la caracterización hidráulica del inyector de UWS, el método se basa en medir el flujo de cantidad de movimiento para comprender la influencia de diferentes variables como el fluido inyectado, la presión de inyección, la contrapresión y la temperatura del sistema sobre las características del flujo. Las medidas se realizaron utilizando una instalación experimental desarrollada en CMT-Motores Térmicos para la determinación del flujo de cantidad de movimiento, la cual fue modificada para cumplir con los requisitos de operación de estos inyectores. Además, la masa inyectada se obtiene experi-

mentalmente para las mismas condiciones de funcionamiento. La metodología propuesta permitió calcular el flujo másico de estos atomizadores de baja presión, así como el coeficiente de descarga, que son datos útiles para futuras actividades de modelado.

Se diseñó una instalación experimental para estudiar la atomización del fluido UWS en condiciones similares a las del tubo de escape del motor. La evolución del spray se caracterizó desde el punto de vista macroscópico, desarrollando una metodología para la determinación de la penetración y del ángulo del chorro. El método se basa en la configuración óptica conocida como diffused-back-light en una configuración de campo lejano. La penetración del spray se dividió en dos zonas: el inicio del chorro y el cuerpo principal. Se observó que la parte inicial del spray inyectado no se ve particularmente afectada por la presión de inyección sino más bien por la temperatura de la camisa de enfriamiento del inyector.

El proceso de atomización se investigó mediante la misma técnica de diagnóstico óptico, diffused-back-lighting, acoplado a una lente microscópica especial. Se cuantificó la distribución del diámetro de las gotas y la velocidad de las gotas (en los componentes axial y tangencial) del chorro, en diferentes niveles de presión de inyección y flujo de aire. Se empleó una cámara de alta velocidad para capturar las imágenes de la fase líquida, comparando las gotas de líquido atomizado en tres regiones diferentes del chorro: la primera cerca de la salida de la tobera y las otras dos en la región desarrollada del spray, una alineado con el eje del inyector y el otro en la periferia del mismo. Como resultado de este estudio, se puede observar que una mayor presión de inyección produce más gotas con diámetros menores favoreciendo el proceso de atomización.

Resum

En un context mundial de preocupació per la salut i el medi ambient, la indústria i la comunitat investigadora estan treballant àrduament per a desenvolupar eines i tecnologies que contribuïsquen a la reducció d'emissions contaminants. Un dels sectors afectats per la normativa anticontaminació és el transport, ja que és responsable d'al voltant del 20 % de la producció d'emissions de gasos d'efecte d'hivernacle. Noves tecnologies estan evolucionant, especialment components dels sistemes d'injecció, disseny de cambres de combustió, elements de posttractament, la hibridació, entre altres. Els sistemes de reducció catalítica selectiva (SCR) han sigut una de les claus per a aconseguir els objectius de les normatives d'emissions, especialment d'Òxids Nitrosos (NO_x). La tecnologia SCR s'empra per a eliminar els NO_x presents en els gasos de fuita d'un motor. El procés d'injecció de la solució d'urea-aigua (UWS) determina les condicions inicials per a la mescla i evaporació del fluid en el sistema de reducció catalítica selectiva. Per a un correcte funcionament, l'injector UWS ha de dosar una quantitat adequada de líquid en el tub d'escapament per a evitar la formació de depòsits i garantir l'eficiència del post-tractament. Aquesta tasca requereix la caracterització hidràulica de l'injector i de l'evolució de l'esprai. No obstant això, l'estudi del flux en aquests atomitzadors de baixa pressió, tant de l'atomització del fluid com el desenvolupament del doll, encara presenta importants incerteses, la qual cosa constitueix un gran repte per a la investigació en aquest camp.

L'objectiu d'aquesta tesi és la comprensió dels processos d'injecció de solució urea-aigua en condicions de funcionament realistes, similars a les que es troben en un tub d'escapament de motor. Per a això, aquest treball se centra en el desenvolupament de noves instal · lacions experimentals que permeten realitzar la caracterització hidràulica combinant mesures de flux de quantitat de moviment i massa injectada. Posteriorment, el doll de UWS es visualitza aplicant tècniques òptiques a diversos nivells de temperatura i flux màssic d'aire, en un banc de proves dissenyat per a aquest propòsit.

Quant a la caracterització hidràulica de l'injector de UWS, el mètode es basa a mesurar el flux de quantitat de moviment per a comprendre la influència de diferents variables com el fluid injectat, la pressió d'injecció, la contrapressió i la temperatura del sistema sobre les característiques del flux. Les mesures es van realitzar utilitzant una instal · lació experimental desenvolupada en CMT-Motores Térmicos per a la determinació del flux de quantitat de moviment, la qual va ser modificada per a complir amb els requisits d'operació d'aquests injectors. A més, la massa injectada s'obté experimentalment per a les mateixes condicions de funcionament. La metodologia proposada va permetre calcular

el flux màssic d'aquests atomitzadors de baixa pressió, així com el coeficient de descàrrega, que són dades útils per a futures activitats de modelatge.

Es va dissenyar una instal · lació experimental per a estudiar l'atomització del fluid UWS en condicions similars a les del tub d'escapament del motor. L'evolució de l'esprai es va caracteritzar des del punt de vista macroscòpic, desenvolupant una metodologia per a la determinació de la penetració i de l'angle del doll. El mètode es basa en la configuració òptica coneguda com diffused-back-light en una configuració de camp llunyà. La penetració de l'esprai es va dividir en dues zones: l'inici del doll i el cos principal. Es va observar que la part inicial de l'esprai injectat no es veu particularment afectada per la pressió d'injecció sinó més aviat per la temperatura de la camisa de refredament de l'injector.

El procés d'atomització es va investigar mitjançant la mateixa tècnica de diagnòstic òptic, diffused-back-lighting, acoblat a una lent microscòpica especial. Es va quantificar la distribució del diàmetre de les gotes i la velocitat de les gotes (en els components axial i tangencial) del doll, en diferents nivells de pressió d'injecció i flux d'aire. Es va emprar una càmera d'alta velocitat per a capturar les imatges de la fase líquida, comparant les gotes de líquid atomitzat en tres regions diferents del doll: la primera prop de l'eixida de la tovera i les altres dues a la regió desenvolupada de l'esprai, una alineada amb l'eix de l'injector i l'altra en la perifèria del mateix. Com a resultat d'aquest estudi, es pot observar que una major pressió d'injecció produeix més gotes amb diàmetres menors afavorint el procés d'atomització.

"There is a driving force more powerful than steam, electricity and atomic energy: the will."
Albert Einstein

Contents

List of Figures

List of Tables

Nomenclature

Latin

A	Area
C_a	Area Coefficient
C_d	Discharge Coefficient
Cp	Back pressure or Counter pressure
C_v	Velocity Coefficient
d	Diameter
D_{eq}	Equivalent Diameter
F	Force
K	Calibration Constant
L	Length
$\dot{m}$	Mass flow rate
$\dot{M}$	Momentum Flux
m	Mass
P	Pressure
$P1$, $P2$, $P3$,	Position 1, Position 2, Position 3
P_{inj}	Injection Pressure
S	Spray penetration
T	Temperature
t	Time
T_{amb}	Ambient Temperature
T_{ref}	Coolant Temperature
u	Flow Velocity
u_b	Bernoulli Velocity
V_x	Droplet Velocity in horizontal direction
V_y	Droplet Velocity in vertical direction

Greeks

λ	Wave length
μ	Viscosity
ρ	Density
σ	Surface tension
τ	Optical depth

Subscripts

air	Referred to air conditions
eff	Effective
exp	Experimental
f	Referred to the fluid
L	Referred to liquid
max	Maximum
opt	Optimal

Initials and acronyms

ASOE	After Start of Energizing
CFD	Computational Fluid Dynamics
DBI	Diffused Back Illumination
ECU	Engine Control Unit
EGR	Exhaust Gas Recirculation
ET	Energizing Time
fps	frames per second
HSMI	High-Speed Microscopic Imaging
ICE	Internal Combustion Engine
LED	Light Emitting Diode
LIF	Laser Induced Fluorescence
LNC	Lean NO_x Catalyst
NSC	NO_x Storage Catalyst
PDA	Phase Doppler Anemometry
PIV	Particle Image Velocimetry
PM	Particle Matter
ROI	Rate of Injection
SCR	Selective Catalytic Reduction
SMD	Sauter Mean Diameter
TDC	Top Dead Center
UWS	Urea-Water Solution

Chapter 1

Introduction

This chapter introduces the motivations for analysing the urea-water solution injection process, and the reasons for understanding the hydraulic behaviour of the flow as well as the spray atomization characteristics. The first section explains the context of this work in the research community. The second section presents the objectives and the methodology employed to fulfil the goals. The last section details the structure of the subsequent chapters of this thesis.

1.1 General context

The reciprocating Internal Combustion Engines (ICE) is one of the most used powertrain in transportation [1] for marine and land propulsion systems. Beyond transportation, this technology is also used in other fields like agriculture, industry, and power generation. The interest in these machines is the reasonable durability and the high thermal efficiency [2–4]. However, it is estimated that the mobility sector is responsible for approximately 20% of the total production of the green-house-gases emissions [3]. In order to accomplish the emission regulations, several efforts have been made in the engine industry, especially to improve combustion systems and to develop auxiliary devices. The reduction of pollutant emissions is a challenge because it should consider the fuel consumption quantity without deteriorating the engine efficiency, which have an opposite behavior [5]. Thanks to the efforts of the scientific community and the industry, the technologies are rapidly evolving, improving several

subsystems, such as fuel injection components, combustion system design and after-treatment. The development of the latter has been one of the key factors for reaching the emission targets, specifically for Nitrous Oxides (NO_x).

Recent studies [6] showed that for the enhancement of de-NO_x technologies, the preferential solution is the implementation of Selective Catalytic Reduction (SCR), which reduced the real drive emissions. At the beginning, in the 1970s, SCR technology was used in stationary engines of thermal power plants in Japan. A little later, it was used in plants in Europe and in the United States. As regulations have evolved (becoming more restrictive), the use of ammonia had to be implemented in land transport vehicles. First, in 2008 with the introduction of Euro V [1], it was installed on heavy duty systems, such as trucks or buses. Later on, since 2014, SCR has been incorporated into light duty vehicles with diesel engines in order to fulfill the Euro VI normative. Unlike heavy duty vehicles, passenger cars hardly have room to connect the SCR system, for this reason incomplete mixing of urea with the exhaust flow might occur. As a consequence, important solid deposits are formed that would damage the exhaust system of the vehicle, as well as improper SCR de-NO_x efficiencies.

As explained by Payri et al in [7], the SCR works as a chemical reactor in conjunction with the injection of a Urea-Water Solution (UWS) upstreams in the exhaust pipe [8]. The UWS mixes with the combustion gases, passing through a catalyst where the NO_x byproducts of combustion are reduced with ammonia into water and nitrogen [9]. To ensure an effective reduction of NO_x (also known as de-NO_x process), the UWS should decompose into ammonia before the flow reaches the inlet section of the SCR with an adequate distribution and correct quantity [8–10]. For that reason, a good design must include uniform injection and fast urea decomposition. The UWS injector unit is responsible for the accurate dosing and homogeneous droplet distribution. Considerable efforts are being done in the improvement and understanding of these systems, as can be seen in the literature [11–13]. The reason is that injecting incorrect quantity of UWS into the exhaust pipe could cause ammonia slip into the atmosphere or incomplete NO_x transformation [13, 14]. This scenario obliges to determine experimentally the UWS injected mass per shot and the mass flow rate. Currently, most estimations of the mass flow rate are calculated by CFD models of inlet and/or outlet flow [15, 16], or by collecting the injected quantity in a vessel and assuming uniform injection events [12]. However, more accurate techniques are still required.

[1] Regulation that governs emissions in the European Union.

Moreover, the interest in the determination of the macroscopic and microscopic spray parameters at various exhaust flow conditions has increased recently, especially for a deeper comprehension of the UWS jet, from the global point of view (for example, spreading angle and spray penetration) and from local perspective (for example, droplet shape, diameter and velocity distribution) [7]. Improper quantities of UWS may generate deposits that could block the exhaust pipes of the engine and reduce the system efficiency. Several researchers have investigated the spray behaviour of the UWS using both experimental and numerical methods.

Regarding experimental approaches, different studies have applied visualization techniques in simplified test rigs that allow to analyse the liquid phase of the jet in cross-flows of air. Some of the works have been performed injecting water instead of the UWS solution because the physical properties are analogous [12]. Nevertheless, other authors preferred the use of urea, in particular when deposits are the subject of interest. Previous studies [10, 14] showed the effect of spray pattern, wall impingement and droplet diameter on the NO_x conversion efficiency and the formation of deposits. From a global perspective, other works [13, 17] carried out visualization measurements using an aqueous-urea solution in a test bench with hot air, reaching air and fluid temperatures of 490 °C and 130 °C respectively. Based on their results, they concluded that the fluid temperature had a strong influence on the macroscopic spray parameters, due to the boiling point of the fluid. They also found that gas temperature slightly affects the spray development. Besides, the impact of exhaust pipe geometry was evaluated by LeCompte et al. [18]. They also considered the effect of the gas temperature and mixer location on the homogenization and vaporization of the mixture using optical methods [7].

Similarly, droplet and velocity distributions have been investigated in previous researches. Concerning the velocity field, some studies [19] are reported using experimental facilities to characterize the spray flow field using particle image velocimetry apparatus and Phase Doppler Anemometry (PDA) for droplet determination [20]. Even though this optical approach based on lasers is widely used, the hypothesis of completely spherical droplets might limit its implementation for some boundary conditions, such as low injection pressures and in regions of the spray near the nozzle exit, where ligaments and blobs can be seen.

Based on the necessity of quantifying the injected mass flow and the spray structure of UWS dosing units, the purpose of this thesis is to contribute in the understanding of the injection event of this low-pressure atomizer. To

this end, new experimental facilities were developed for the hydraulic characterization, as well as for the study of the spray morphology and atomization analysis, with the construction of a test rig with optical accesses and dedicated post-processing tools. The design of the experimental equipment was done to reproduce realistic operating conditions, in terms of exhaust gas flow, temperature and pressure.

This thesis has been carried out at the research institute CMT-Motores Térmicos at the Universitat Politècnica de València. This institute is a research and educational center dedicated to the development of new technologies related to transportation and combustion engines. It was founded more than four decades ago, and is devoted to the understanding of processes within propulsion systems, combining high quality experimental capabilities with theoretical and computational tools. The research activities carried out in this institute are the outcome of the collaboration between academia and industry, both from national and international companies. During the first decades, it was committed to the study of diesel engines, but in the last 10 years they have extended the investigation field to gasoline engines and electrified powertrains as well. The main research lines are the injection-combustion, air management, after-treatment systems, noise, 1D and 3D simulations, among others. The center has human resources with a long history and extensive experience, producing more than 500 research articles in international journals, more than 180 books published and about 160 doctoral thesis. Specifically, the injection research line is one of the few places in Spain dedicated to the study of injection systems. The available facilities make it possible to measure the different parameters that characterize a dosing unit, such as the injection flow rate, the dispersion of the jet or the size of the drops, under different operating conditions. Regarding the injection of urea in particular, this work represents one of the first studies under realistic conditions carried out in CMT. In recent years, due to the necessity of a deeper understanding of the urea-water-solution injection process in the SCR system, the institute decided to invest and extend the knowledge in this technology. The current thesis is the first one in the department focused on this topic.

1.2 Objectives and methodology

The main objective of this work is to contribute to the understanding of the urea-water solution injection process under realistic operating conditions, analogous to the exhaust pipe of a combustion engine. In this context, this thesis focuses on the development of new experimental facilities that enable

the characterization of the UWS spray performance, both in terms of flow characteristics at the nozzle exit, and in terms of the spray development. In order to achieve the main goal of the work, specific objectives were defined:

- To develop an experimental methodology for determining the rate of injection based on the spray momentum measurement. After the configuration and validation of the system, the test rig is used for understanding the effect of different parameters on the evolution of the mass flow rate and UWS injected mass.
- To design and build an experimental facility that resembles the flow conditions at the exhaust manifold of a combustion engine, in terms of gas mass-flow and temperature. This is coupled to a rig with optical accesses that permits the visualization of the UWS spray for different boundary conditions.
- To perform a comprehensive analysis of the spray through two aspects: quantification of the global characteristics of the jet (spray penetration and spreading angle), and calculation of the microscopic structure of the spray in terms of droplet size distribution and velocity. Both approaches are determined by means of dedicated optical techniques. The obtained results will provide a robust database for model validation.

As was mentioned in previous section, the research group dedicated to injection systems has wide expertise in experiments for hydraulic flow characterization and spray analysis. Most of the studies performed so far were focused on diesel and gasoline technologies. Few investigation are available on USW dosing systems, being this thesis the first formal study performed at the Department. However, the significant know-how available in the research team for characterizing other dosing systems was transferred to this work. Especially, precedent works are the baseline and the reference texts for the different topics considered: the hydraulic behavior of injector units [21–23], the theoretical-experimental study of the jet development [24–26] and the droplet characterization [27, 28].

Since the current thesis is the first one in the department focused on UWS injection process, new experimental facilities were designed and calibrated. The proposed methodology can be summarized as:

1. Hydraulic characterization

- Spray momentum flux
- Rate of injection

2. Determination of global spray parameters
   - Optical technique: Diffused Back-Illumination
   - Development of the post-processing tools for the calculation of spray penetration and spreading angle
3. Droplet Characterization
   - Optical technique: Diffused Back-Illumination with microscopic lens.
   - Development of the post-processing tools for tracking and quantification of droplet size and velocity.

The first stage of the methodology is focused on the implementation of the approach for determining the rate of injection based on the measurements of the momentum flux in a UWS dosing unit. After the configuration and validation of the measuring system, the test rig is used for understanding the effect of several boundary conditions on the evolution of the injected mass and rate of injection. The system is tested using water and UWS. The reason for injecting water in experimental settings is because it has similar properties than the urea and it avoids the deposit formation in the laboratory equipment. The state-of-the art UWS dosing system tested in this work has a cooling system that avoids overheating of the nozzle tip and the fluid.

The second part of the methodology is dedicated to the UWS spray characterization by means of optical analysis, obtaining global parameters of the spray. The methodology is based on the optical setup known as back-light in a far-field configuration. The spray penetration and spreading angle are calculated from a proposed methodology that takes into account the particularities of this low pressure atomizer.

The third phase is related to the determination of the UWS spray structure in terms of particle size distribution and droplet velocity in various conditions that resemble the exhaust pipe flow of an engine. The estimations of the droplet size distribution are made using the back-light technique coupled with a microscope at three different regions of the spray jet: one near the exit of the nozzle, and two others in the developed zone of the spray. Additionally, a novel post-processing script is programmed for the calculation of the velocity, which is based on a particle tracking algorithm. This is possible thanks to

the back-light imaging and the high-speed camera that delivers high frame rates. This is an alternative method to the Particle Image Velocimetry (PIV) that only provides averaged velocities of the flow, or to PDA that is based on particles with spherical shape. The quantification of the velocity and the distribution of the droplet size is essential to provide robust experimental data for the configuration and validation of computational fluid dynamic models.

1.3 Thesis outline

The document is organized in seven chapters. The current Chapter (**chapter 1**) that presents an introduction, the general motivation and main objectives of the work carried out.

The second chapter (**Chapter 2**) is focused on the description of the NO_x formation and the main techniques available for the reduction of these pollutant emissions. The SCR system is detailed in order to understand the requirements and necessities for an efficient aftertreatment. Then, the UWS dosing system is described, as well as the fundamental concepts of the injection process. Afterwards, a literature review on the hydraulic characterization and spray measurements is done and serves as a reference for explaining the procedures used in this work.

Chapter 3 is centered on the facilities, equipment and experimental methodologies designed and calibrated in this thesis. Each test rig is described with the respective measurement procedure. Moreover, it explains the optical techniques employed and the details of the algorithms used for the processing of the images.

The results of the hydraulic characterization of the UWS injector are presented in **Chapter 4**. Momentum flux measurements and injected mass results are reported, paying special attention on the influence of the boundary conditions on the rate of injection (ROI) behaviour. The discharge coefficient of the nozzle is analyzed for the low pressure atomizer. Hence, this chapter proposes a novel approach for the ROI determination based on the momentum flux signal.

Chapter 5 outlines the results of the liquid spray development. The chapter includes the spray penetration and spreading angle analysis for different boundary conditions. The novel image processing tool implemented allows to divide the spray penetration of this low pressure atomizer in two regions: the spray burst and the body.

The analysis related with the droplet characterization are detailed in **chapter 6**. Results are given in terms of droplet size distribution and droplet ve-

locity evolution. The data is acquired at three different zones of the plume. The new image processing algorithm allowed the evaluation and quantification of the droplet diameter for various operating conditions.

The last chapter (**chapter 7**) presents a summary and review of the main results of the thesis, as well as the main conclusions. Finally, some future works are proposed to continue this research line, based on the knowledge gained during the development of this work.

References

[1] Kalghatgi, Gautam. "Is it really the end of internal combustion engines and petroleum in transport?" In: *Applied Energy* 225 (2018), pp. 965–974. DOI: https://doi.org/10.1016/j.apenergy.2018.05.076.

[2] Johnson, Timothy and Joshi, Ameya. "Review of Vehicle Engine Efficiency and Emissions". In: *SAE Technical Paper Series* 1 (2018), pp. 1–23. DOI: 10.4271/2018-01-0329.

[3] Yang, Liuhanzi et al. "Experimental Assessment of NOx Emissions from 73 Euro 6 Diesel Passenger Cars". In: *Environmental Science and Technology* 49.24 (2015), pp. 14409–14415. DOI: 10.1021/acs.est.5b04242.

[4] Degraeuwe, Bart and Weiss, Martin. "Does the New European Driving Cycle (NEDC) really fail to capture the NOX emissions of diesel cars in Europe?" In: *Environmental Pollution* 222.X (2017), pp. 234–241. DOI: 10.1016/j.envpol.2016.12.050.

[5] Payri, Francisco and Desantes, Jose Maria. *Motores de combustion interna alternativos*. Editorial Universitat Politecnica de Valencia, 2011.

[6] Triantafyllopoulos, Georgios, Katsaounis, Dimitrios, Karamitros, Dimitrios, Ntziachristos, Leonidas, and Samaras, Zissis. "Experimental assessment of the potential to decrease diesel NOxemissions beyond minimum requirements for Euro 6 Real Drive Emissions (RDE) compliance". In: *Science of the Total Environment* 618.x (2018), pp. 1400–1407. DOI: 10.1016/j.scitotenv.2017.09.274.

[7] Payri, Raul, Bracho, Gabriela, Gimeno, Jaime, and Moreno, Armando. "Investigation of the urea-water solution atomization process in engine exhaust-like conditions". In: *Experimental Thermal and Fluid Science* 108.June (2019), pp. 75–84. DOI: 10.1016/j.expthermflusci.2019.05.019.

[8] Zheng, Guanyu. "Development of Air-Assisted Urea Injection Systems for Medium Duty Trucks". In: *SAE Technical Papers* 2017-Septe.September (2017). DOI: 10.4271/2017-24-0112.

[9] Koebel, M., Elsener, M., and Kleemann, M. "Urea-SCR: a promising technique to reduce NOx emissions from automotive diesel engines". In: *Catalysis Today* 59.3 (2000), pp. 335–345. DOI: 10.1016/S0920-5861(00)00299-6.

[10] Oh, Jungmo and Lee, Kihyung. "Spray characteristics of a urea solution injector and optimal mixer location to improve droplet uniformity and NOx conversion efficiency for selective catalytic reduction". In: *Fuel* 119 (2014), pp. 90–97. DOI: 10.1016/j.fuel.2013.11.032.

[11] Payri, Raúl, Bracho, Gabriela, Martí-Aldaraví, Pedro, and Moreno, Armando. "Using momentum flux measurements to determine the injection rate of a commercial Urea Water Solution injector". In: *Flow Measurement and Instrumentation* 80 (2021), p. 101999. DOI: https://doi.org/10.1016/j.flowmeasinst.2021.101999.

[12] Kapusta, Łukasz Jan, Sutkowski, Marek, Rogóż, Rafał, Zommara, Mohamed, and Teodorczyk, Andrzej. "Characteristics of Water and Urea–Water Solution Sprays". In: *Catalysts* 9.9 (2019), p. 750. DOI: 10.3390/catal9090750.

[13] Vuuren, Nic van, Ungaro, Carmine, Brizi, Gabriele, Buitoni, Giacomo, and Postrioti, Lucio. "AUS-32 Injector Spray Imaging on Hot Air Flow Bench". In: *SAE 2015 World Congress and Exhibition*. SAE International, 2015. DOI: https://doi.org/10.4271/2015-01-1031.

[14] Varna, Achinta, Spiteri, Alexander C., Wright, Yuri M., Dimopoulos Eggenschwiler, Panayotis, and Boulouchos, Konstantinos. "Experimental and numerical assessment of impingement and mixing of urea-water sprays for nitric oxide reduction in diesel exhaust". In: *Applied Energy* 157 (2015), pp. 824–837. DOI: 10.1016/j.apenergy.2015.03.015.

[15] Kim, Chang Su and Park, Sung Young. "A design-variable-based computational study on the unsteady internal-flow characteristics of the urea-SCR injector for commercial vehicles". In: *Defect and Diffusion Forum* 379 (2017), pp. 64–72. DOI: 10.4028/www.scientific.net/DDF.379.64.

[16] Lee, Sang In and Park, Sung Young. "Numerical analysis of internal flow characteristics of urea injectors for SCR dosing system". In: *Fuel* 129 (2014), pp. 54–60. DOI: 10.1016/j.fuel.2014.03.031.

[17] Vuuren, Nic van, Postrioti, Lucio, Brizi, Gabriele, Ungaro, Carmine, and Buitoni, Giacomo. "Experimental Analysis of the Urea-Water Solution Temperature Effect on the Spray Characteristics in SCR Systems". In: *SAE Technical Paper Series* 1 (2015). DOI: 10.4271/2015-24-2500.

[18] Lecompte, Matthieu, Raux, Stephane, and Frobert, Arnaud. "Experimental Characterization of SCR DeNOx-Systems: Visualization of Urea-Water-Solution and Exhaust Gas Mixture". In: *SAE Technical Paper Series* 1 (2014). DOI: 10.4271/2014-01-1524.

[19] Spiteri, Alexander and Dimopoulos Eggenschwiler, Panayotis. "Experimental fluid dynamic investigation of urea-water sprays for diesel selective catalytic reduction-denox applications". In: *Industrial and Engineering Chemistry Research* 53.8 (2014), pp. 3047–3055. DOI: 10.1021/ie404037h.

[20] Liao, Yujun, Furrer, Roman, Dimopoulos Eggenschwiler, Panayotis, and Boulouchos, Konstantinos. "Experimental investigation of the heat transfer characteristics of spray/wall interaction in diesel selective catalytic reduction systems". In: *Fuel* 190 (2017), pp. 163–173. DOI: 10.1016/j.fuel.2016.11.035.

[21] Salvador, Francisco Javier. "Estudio teórico experimental de la influencia de la geometría de toberas de inyección Diésel sobre las características del flujo interno y del chorro". PhD thesis. Valencia: E.T.S. Ingenieros Industriales. Universidad Politécnica de Valencia, 2003.

[22] Gimeno, Jaime. "Desarrollo y aplicación de la medida de flujo de cantidad de movimiento de un chorro Diesel". PhD thesis. E.T.S. Ingenieros Industriales, Universidad Politécnica de Valencia, 2008. DOI: 10.4995/Thesis/10251/8306.

[23] Venegas, Oscar. "Estudio del fenómeno de la cavitación en la inyección Diesel mediante la visualización del flujo interno en orificios transparentes." PhD thesis. Universitat Politècnica de València, 2014. DOI: 10.4995/Thesis/10251/37375.

[24] Bardi, Michele. "Partial Needle Lift and Injection Rate Shape Effect on the Formation and Combustion of the Diesel Spray". PhD thesis. Universitat Politècnica de València, 2014. DOI: 10.4995/Thesis/10251/37374.

[25] Viera, Juan Pablo. "Experimental study of the effect of nozzle geometry on the performance of direct-injection diesel sprays for three different fuels". PhD thesis. Universitat Politècnica de València, 2017. DOI: 10.4995/Thesis/10251/81857.

[26] Bracho, Gabriela. "Experimental and theoretical study of the direct diesel injection process at low temperatures". PhD thesis. E.T.S. Ingenieros Industriales, Universidad Politécnica de Valencia, 2011.

[27] Soare, Vlad. "Phase Doppler Measurements in Diesel Dense Sprays: Optimisation of Measurements and Study of the Orifice Geometry Influence over the Spray at Microscopic Level". PhD thesis. E.T.S. Ingenieros Industriales, Universidad Politécnica de Valencia, 2007.

[28] Giraldo Valderrama, Jhoan Sebastián. "Macroscopic and microscopic characterization of non-reacting diesel sprays at low and very high injection pressures". In: November (2018).

Chapter 2

Urea water injection process

2.1 Introduction

The use of ammonia as a reducing agent within an SCR system began in the 1980s in stationary and marine engines. With the consecutive emission regulations for vehicles, both by the European Union (Euro standards) and in other countries such as the United States (Tier Bin), it has been necessary to implement these SCR systems in vehicles, starting with heavy duty vehicles in 2008 with the Euro V standard [3], as well as for light vehicles , with the Euro 6 standard. The efficiency improvement of SCR systems in light vehicles is more difficult due to the limited space available for the aftertreatment system and the dimensions of the exhaust pipe, therefore the jet of urea water solution impinges the walls due to the small volume available [4], interfering with the evaporation and proper homogenization of the urea-exhaust gas mixture. The development of the injection system is a promising way to improve the efficiency of the SCR system. Therefore, this chapter presents the fundamental definitions and technologies implemented for NO_x reduction and a summary of the urea water solution injection process.

2.2 Emissions and pollutants from internal combustion engines

The Internal Combustion Engines (ICEs) are currently the most important technology in transportation systems, from light to heavy duty vehicles. Since

its invention in the XIX century, massive efforts have been dedicated to the improvement of its technology in order to improve the performance of the engine without compromising the efficiency and maintaining the pollutants as low as possible. Over the past few decades, the demand for cleaner vehicles alongside the need to diminish the use of fossil fuels as an energy source, have driven carmakers to the introduction of new technologies to replace the ICEs, such as electric vehicles, hydrogen engines or fuel cells. Nonetheless, these alternatives still have to develop enough to reach the efficiency and reliability that the ICEs offer. These technologies are still in research and it is likely that in the coming future they will represent the alternative to the traditional ICE. However, for the time being the transportation systems will be ICE based with increasing levels of hybridization and electrification [1]. Therefore, the transportation industry still should develop the technologies for internal combustion engines, in order to improve the performance of the system, while reaching zero emission levels.

The main issues coming from the ICEs are related to the processes in which the power is generated. The use of fossil fuels as a primary energy source is convenient due to the huge amount of energy that can be stored, leading to high driving ranges. Nevertheless, there are important drawbacks related to the fossil fuels which are the low energy efficiency and the high emission levels.

The thermal processes that occur inside the engine are characterized by the low energy conversion efficiency, and together with the heat losses in the powertrain of the vehicle, the overall efficiency can be reduced significantly. The high levels of emissions present in the exhaust gases are the by-products of the combustion process inside the engine. This process takes place in a very short period of time, making it difficult to reach the steady state of the flame and therefore creating the conditions to form a significant amount of pollutants.

Given these conditions, the development of advanced after-treatment systems for the exhaust gases has been important in the past years and many efforts have been directed into researching and developing new technologies. One of the most promising technologies is the SCR system which is an effective technology for the reduction of Nitrogen Oxide (NO_x) emissions.

2.2.1 European regulations on automotive internal combustion engines pollutant emissions

Reciprocating internal combustion engines, specially diesel engines, are subject to public scrutiny and legislation such as the EURO standards, which have set

strict limitations for the pollutant matter emissions since 1990. The decline of air quality and the ambient pollution in urban areas is mostly attributed to vehicles.

Europe regulation is represented by the EURO standard and its application is set to be applied in different steps. This segmentation allows the car manufacturers to properly develop the technologies that are required to comply with the emission limits.

The emission limits are defined taking into account the mass of the vehicle, where three classes can be distinguished:

- **CL1**: vehicles with mass below 1305 kg.
- **CL2**: vehicles with mass between 1305-1760 kg.
- **CL3**: vehicles with mass above 1760 kg.

Limits are higher as the mass increases due to the greater fuel consumption and emissions expected for such vehicles. The limited species are nitrogen oxides (NO_x), carbon monoxide (CO) hydrocarbons and particulate matter (PM). Currently, the regulation in force for heavy-duty applications is the EURO VI. Particularly, in this latest standard, a particulate number has been introduced, which coupled with the PM total mass defines a limitation on particle size distribution. Specially for diesel engines a significant reduction has taken place for its pollutant emissions as is shown in Figure 2.1.

In Figure 2.1, the maximum allowed limits for NO_x and PM in diesel engines from the EURO I standard from 1993 to the EURO VI in 2014 are plotted. It is known nowadays that the NO_x and PM emissions are of utmost importance for diesel engines. These pollutants are one of their major disadvantages compared to other types of propellers. From EURO I to EURO VI there was a 95% reduction in the NO_x limits. Since the implementation of the first EURO standard, the overall reduction for the PM is about 97%, with an additional reduction of 10% in the last five years. The actual challenge for the survival of the diesel engines relies on the capacity to comply with these limits, without affecting the engine performance and efficiency.

2.2.2 The homologation cycles

Until the final quarter of 2017 the homologation procedure used the driving cycle known as the New European Driving Cycle (NEDC). This test was the result of joining together two elementary driving cycles:

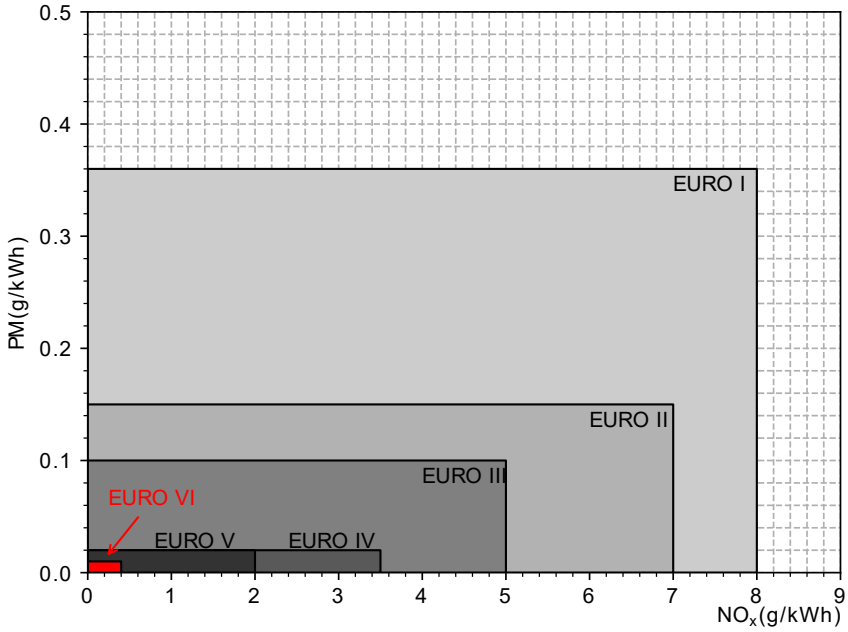

Figure 2.1: EURO Standards maximum limits for PM and NO_x in light duty diesel engines [2].

- **The Urban Driving Cycle (UDC, ECE-15)**: top speed 50 km/h, conformed by the elementary urban cycle repeated four times.
- **The Extra Urban Driving Cycle (EUDC)**: top speed 120 km/h.

The NEDC test started with the UDC phase followed by the EUDC, with a total duration of 1180 s and a theoretical travel distance of 11 km with an average speed of 33.6 km/h. Figure 2.2 illustrates a common NEDC test velocity profile.

Although the NEDC was globally accepted, it was not fully reliably due to the few acceleration phases present, thus not representing real stressing conditions of an engine. Taking these considerations into account, the introduction of the new Worldwide harmonized Light duty vehicles Test Cycle (WLTC) replaced the NEDC. Figure 2.3 shows the vehicle velocity over time in a standard WLTC.

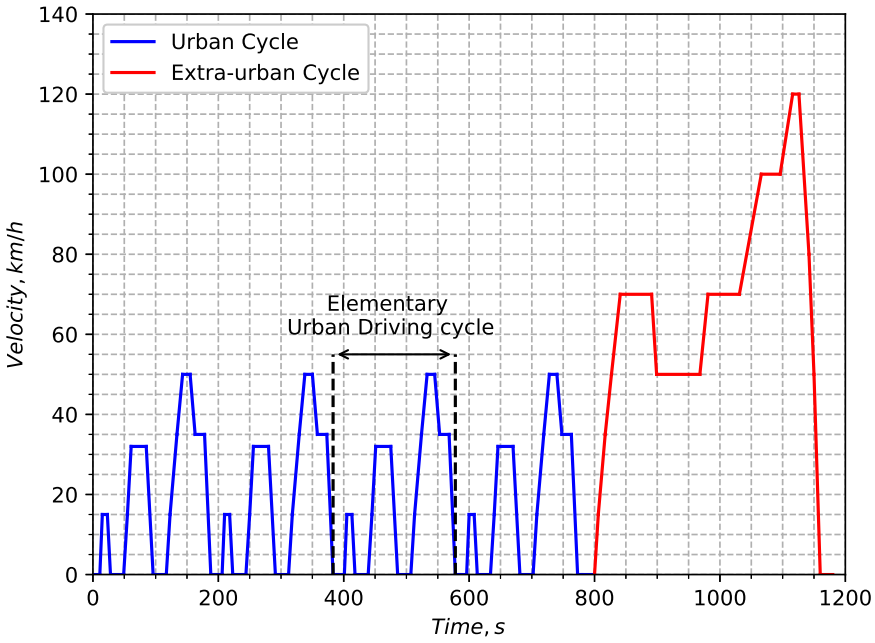

Figure 2.2: New European Driving Cycle (NEDC) velocity profile over time (Adapted from [3]).

The WLTC has four phases, including velocities from low to extra-high and greater accelerations than the previous test cycle. Furthermore, the travel distance in the WLTC is increased to 23.25 km with an average and top velocity of 46.5 km/h and 131 km/h. An increase of 37% and 9% respect with the NEDC and the operating range of the engine is largely investigated, regarding load and speed.

The aforementioned tests are performed using a chassis dynamometer, keeping all the ambient conditions carefully monitored, including the exhaust gases which are studied using gas analysers. Nevertheless, since 2014, the behaviour of the vehicle has to be tested in conditions that resemble the real driving. With that purpose in mind, the Real Driving Emission (RDE) test was introduced in the beginning of 2014.

Thus, for light-duty vehicles, the current regulations (EURO 6d-Temp) establish that the vehicle must be tested both in a test bench (according to the WLTC cycle) and in the road in real driving conditions (RDE) according to

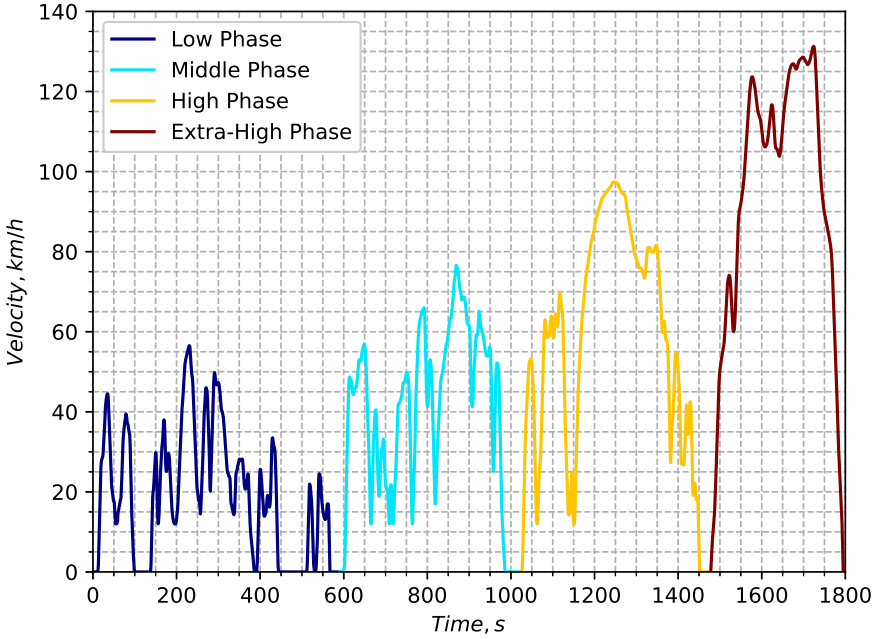

Figure 2.3: Worldwide harmonized Light duty vehicles Test Cycle (WLTC) velocity profile curve over time(Adapted from [3]).

certain specifications. The RDE test is performed by installing in the subject vehicle a Portable Emission Measuring System (PEMS). It is equipped with a gas sampling probe that is introduced inside of the exhaust line and measures the vehicle emissions while it is being driven on open road. The test has to reproduce specific driving conditions, based on the speed and routes that resemble those typical of Europe:

- **Urban route**: Velocity of up to 60 km/h.
- **Rural route**: Velocity between 60 and 90 km/h.
- **Highway route**: Velocity above 90 km/h.

These routes have to be evenly combined with a tolerance up to 10%. Conditions of altitude, temperature, stop times and maximum vehicle speed have to be taken into account. Furthermore, the cumulative elevation cannot

exceed the 1200 m per 100 km in order to prevent the drivers to drive in an aggressive or smooth tendency, taking into account the acceleration patterns [4]. In Table 2.1 some of the boundary conditions for the RDE test cycle are presented (extracted from [5]).

Table 2.1: Real Driving Emission test trip speed and distance characteristics.

RDE Trip specifications		Provision set in the normative
Total trip duration		Between 90 and 120 min
Distance	Urban	Greater than 16 km
	Rural	Greater than 16 km
	Motorway	Greater than 16 km
Trip Composition	Urban	28% to 43% of total distance
	Rural	23% to 43% of total distance
	Motorway	23% to 43% of total distance
Average Speeds	Urban	15 to 30 km/h
	Rural	60 to 90 km/h
	Motorway	>90 km/h

2.2.3 NO_x formation process in Internal Combustion Engines

Nitrogen oxides are a class of chemical species composed of nitrogen and oxygen that have differing atom-to-atom relationships. In ICEs, NO_x forms during the combustion phase and three different NO_x formation mechanisms can be distinguished:

- **Thermal NO_x**: since extremely high temperatures are achieved in the volume accompanying the combustion area, the nitrogen (N_2) and oxygen (O_2) molecules found in the oxidizing air undergo a dissociation process, resulting in the formation of atomic nitrogen and oxygen. The reaction between them, aided by the high temperatures, results in the production of NO_x.
- **Prompt NO_x**: they are produced in the area where combustion is developing by the reaction of oxygen, nitrogen, and other chemical species, constituting intermediate products of hydrocarbon molecule oxidation.
- **Fuel NO_x**: in the past two cases, the nitrogen used in the chemical reactions was that which was present in the air. In this case, however, a significant amount of nitrogen is found in the fuel itself, and its oxidation results in the generation of additional NO_x.

Figure 2.4 shows the contribution of each NO_x category to the overall amount of nitrogen oxides emitted during the combustion process.

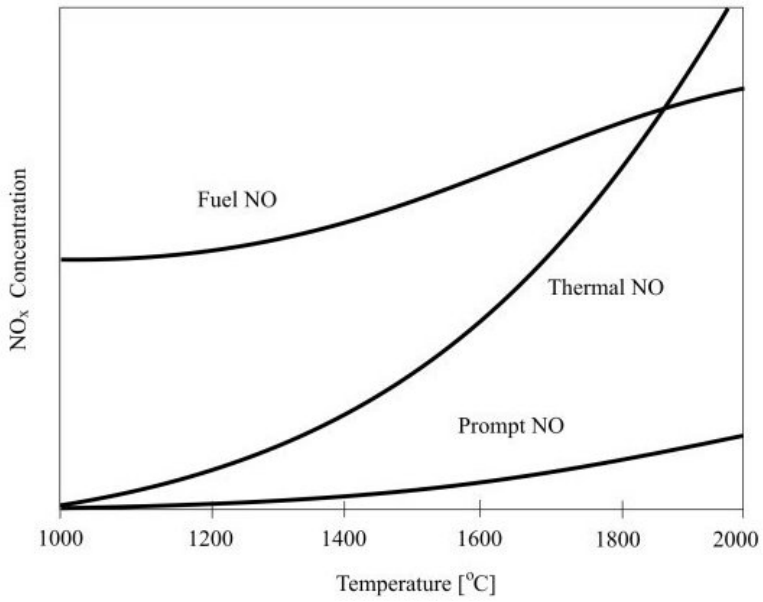

Figure 2.4: Relative concentrations for the three different formation of nitrogen oxides (thermal, prompt, fuel), with the increase of flame temperature [6].

It should be acknowledged that when the combustion temperature increases, the bulk of the overall NO_x quantity is defined by thermal NO_x, while fuel and prompt NO_x percentages become marginal. Local temperatures in an ICE will typically reach 2200-2500 °C during the combustion process. As a result, the total volume of NO_x found in the combustion products can be considered to belong to the thermal NO_x class.

The amount of nitrogen oxides produced during the combustion process in ICEs is influenced by two major parameters: local temperature and the availability of oxygen to facilitate nitrogen oxidation. The fuel/air equivalence ratio determines both of these two quantities. Numerous experiments have shown that using a slightly rich fuel mixture results in the highest combustion temperatures, with a fuel/air equivalence ratio of about 1.05-1.1 kg_{fuel}/kg_{air}. However, under these conditions, the overall amount of oxygen available in the combustion chamber is insufficient to enable full fuel oxidation and consumption, and some hydrocarbons will be emitted. Therefore, NO_x formation

is prevented. Lower fuel/air ratios induce a drop in flame temperature, as well as a rise in excess oxygen. The maximum volume of NO_x is generated when a slightly lean fuel mixture is present, as a result of the combination of these two phenomena, when the fuel/air equivalence ratio is about 0.9. At larger amounts of oxygen excess, the fuel/air ratio is reduced, but combustion temperatures are too low to allow molecular nitrogen dissociation, and NO_x formation is clearly avoided.

As previously mentioned, pollutant concentrations in ICEs are substantially higher than those in the equilibrium state at a given temperature. This effect is directly attributable to the limited period of time available for the combustion phase to be completed (typically of few milliseconds). Consequently, kinetics must be addressed in a systematic analysis of pollutant formation processes, both for species that are specifically created during the combustion phase (such as CO, HC and PM) and for those on which combustion can have a major effect (such as NO_x).

The bulk of NO_x in ICEs is in the form of nitrogen monoxide (NO). According to Zeldovich's [7] condensed kinetic model, NO production is primarily caused by the following three chemical reactions:

$$O + N_2 \rightarrow NO + N \tag{2.1}$$

$$N + O_2 \rightarrow NO + O \tag{2.2}$$

$$N + OH \rightarrow NO + H \tag{2.3}$$

According to the preceding equations, molecular nitrogen reacts with atomic oxygen to form nitrogen monoxide and pure atomic nitrogen. (Equation 2.1), that then combines with molecular oxygen (Equation 2.2) and hydroxyl (Equation 2.3), resulting in an additional NO volume formation. The following theory is proposed in order to examine the kinetics of the three preceding reactions:

- As soon as the first reaction is done, the remaining two follow suit. This suggests that these two reactions are much quicker than the first, and hence the atomic nitrogen concentration can be assumed constant over time (as soon as atomic nitrogen is produced according to the first chemical equation, it is immediately consumed according to the second and third reactions).

- All chemical species concentrations involved are much higher than those of NO and N. Therefore, their concentrations can be considered as those in equilibrium conditions.

With these two assumptions, the following equation can be used to determine the rate of nitrogen monoxide production/destruction:

$$\frac{d[NO]}{dt} = \frac{6{\cdot}10^6}{T^{0.5}} e^{-\frac{69000}{T}} [O_2]^{0.5} [N_2] \tag{2.4}$$

Where T is the absolute temperature, $[O_2]$ and $[N_2]$ are the concentration of molecular oxygen and nitrogen, in equilibrium state, at a given temperature, and d[NO]/dt is the production/destruction rate for nitrogen monoxide.

$$\tau_{NO}^{-1} = \frac{d[NO]}{dt} \frac{1}{[NO]} \tag{2.5}$$

The preceding parameter must be contrasted with the temporal gradient of inner cylinder temperature for a complete explanation of the nitrogen monoxide production mechanism. Temperatures usually increase very rapidly during the combustion process, and the high values of it guarantee high NO output rates. As a result, temperature and NO concentration gradients are comparable during this first step, and equilibrium conditions can almost be reached. However, once the combustion process is complete and during the expansion stage, the temperature decreases significantly and rapidly. As a consequence, the rate of NO destruction is greatly reduced, and the drop of its concentration is considerably delayed. When the exhaust valve opens, the resulting NO concentrations are unquestionably greater than those of the equilibrium state.

The Zeldovich model is useful for understanding the physical processes that occur during NO_x formation/consumption during combustion. These phenomena are much more complex in a real ICE, especially one with compression ignition, since they are controlled by many operational parameters and can be regulated using appropriate control strategies.

2.2.4 NO_x formation process in Compression Ignition Engines

The NO_x development method in compression ignition ICEs can still be represented using the Zeldovich model. However, the phenomena involved with a true Diesel engine are unquestionably more complicated. Within the cylinder, a highly heterogeneous fuel/air mixture occurs during the ignition and

combustion phases. This is largely due to the peculiar fuel injection technique used by these ICEs, in which fuel injection is conducted directly into the combustion chamber as the piston reaches Top Dead Center (TDC). Upon auto-ignition, there is no time for the injected fuel to fully combine with the oxidizing air. In consequence, temperature levels and the fuel/air local equivalence ratios can differ widely and are subject to significant changes as the combustion progresses. The aforementioned conditions promote the NO_x formation.

NO_x production is particularly significant in the first regions where auto-ignition occurs, leading to the development of the premixed combustion phase. Once the combustion has completed, the gases present in this region are further compressed and heated by the combustion of the surrounding fuel/air mixture. As a result, their temperature is likely to remain very high for an extended period of time. However, a very rapid temperature drop happens during the expansion stroke. Furthermore, the additional NO_x formation, as well as the consumption of those that have already been created, is effectively stopped. Therefore, when exhaust valve opens, nitrogen oxides concentration is still significant and definitely higher than equilibrium concentration.

Another significant distinction between Zeldovich's theoretical model and NO_x output in a real Diesel engine is the presence of a significant amount of nitrogen dioxide (NO_2). During the combustion process, an overall lean mixture is found in the cylinder under normal compression ignition engine operating conditions. Then, a massive amount of extra oxygen is accessible for the completion of oxidation processes, resulting in NO oxidation to NO_2. The NO_2/NO_x ratio is affected by engine operating conditions, especially engine speed and load. Normally, the concentration of NO_2 increases as engine load decreases. This phenomenon can be explained by considering the two major reactions that occur during NO_2 formation/destruction (Equation 2.6, 2.7).

$$NO + HO_2 \rightarrow NO_2 + OH \tag{2.6}$$

$$NO_2 + O \rightarrow NO + O_2 \tag{2.7}$$

The first reaction is exothermic and its completion is favoured by the high temperature present during the combustion process. On the contrary, the second reaction is endothermic and requires a certain amount of heat coming from the external environment to develop. However, during the expansion stroke, burned gases mix with the excess air and cool down, so that the second chemical reaction comes to be prevented. The cooling of exhausts and unreacted

fresh air is particularly strong at low loads, since a greater amount of mixture does not take part in the combustion process in these conditions. Indeed, a smaller amount of fuel increases the portion of oxidizing air that does not contribute to the combustion completion; therefore, a higher dilution between burned gases and fresh air takes place, with a quite more remarkable charge cooling effect.

2.2.5 NO_x Reduction strategies for diesel engines

As mentioned previously, critical Diesel engine pollutants are nitrogen oxides and particulate matter. Since combustion conditions and control methods that favor NO_x reduction often cause a rise in soot emissions and fuel usage, some important considerations regarding the trade-off between behaviors of these contaminants may be taken into account [8]. This is referred to as the well-known NO_x-soot trade-off, as depicted in Figure 2.5.

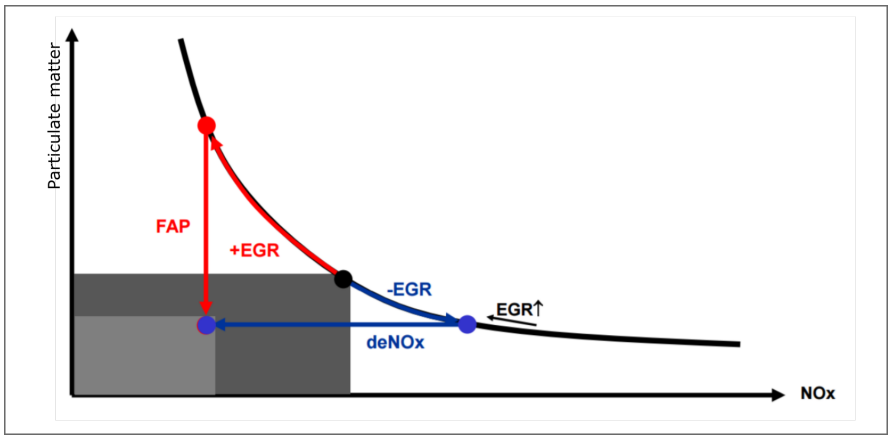

Figure 2.5: Particulate matter vs NO_x trade-off [9].

The standard output of a Diesel engine, as seen in Figure 2.5, allows the working points to travel along the black curve (for example, shifting from the blue point towards points black or red). Besides, that plot shows two strategies to reduce these contaminants and to achieve compliance with the new emissions (light gray area). On the one hand, the red trajectory, starting from the black point, increases the EGR rate in order to reduce the production of nitrogen oxides. This means an increase in the production of particles, so a particle filter must be installed to eliminate them. On the other hand, the blue line shows an opposite strategy, where the EGR rate is decreased, thus

reducing the production of particles to comply with the new limits, at the cost of increasing the nitrogen oxides generation. This path should be combined with de-NO_x technology to eliminate them, either by means of a NO_x trap or with an SCR system. To control emissions levels in diesel engines, a variety of strategies are available, as depicted in Figure 2.6.

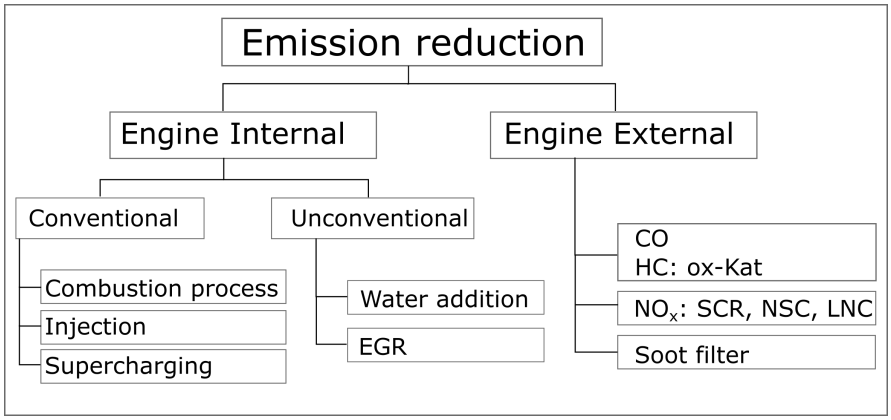

Figure 2.6: Methods to reduce pollutant emissions for Diesel engines [8].

The main approaches used to minimize emission levels can be categorized as traditional or unconventional. Conventional methods attempt to change the combustion mechanism through adjusting the geometry of the combustion chamber, air movement inside the engine (also by supercharging), and the fuel injection method. The aim is to reduce or eliminate the generation of contaminants. The fuel/air mixture's composition remains unchanged in this situation. The primary purpose of conventional measures is to control the combustion process so that peak temperatures within the cylinder are minimized (a reduction in peak temperature prevents NO_x formation). Simultaneously, there could be a rise in PM emissions, requiring the use of appropriate particle-reduction techniques. The following are some of the key parameters that have a significant impact on the combustion process:

- **Combustion chamber design:** number of inlet and exhaust valves, shape, compression ratio.
- **Air feeding:** compression ratio, turbulence, air motion inside the cylinder.

- **Fuel injection:** injection pressure, injection start and duration, injection rate, localization of injector nozzle and number of orifices, size and geometry of the nozzle.

The target of these measures is to manage the combustion process by controlling the following variables:

- The proportion of premixed combustion.
- Fuel/air mixture uniformity and local fuel/air ratios.
- Mixture ignition and combustion duration.

These parameters have an effect one on another and could have opposite effects on pollutant levels. As a result, to predict the effect of particular parameters is difficult.

Unconventional approaches, on the other hand, are taken on purpose to influence the composition of the fuel/air mixture. Unconventional steps, such as a heavy alteration of the combustion mechanism, are to partially or fully eradicate pollutant emissions. Water injection and Exhaust Gas Recirculation (EGR) are the most powerful methods.

The measures described so far were intended to intervene, more or less directly, in the combustion process, in order to prevent NO_x formation to the greatest extent possible. However, the latest emissions legislation has become more and more severe in terms of pollutants and carbon dioxide emissions. The previous technologies revealed to be effective in pollutants abatement, but their adoption is restricted to a reduced number of engine operating conditions; otherwise, a strong penalization in engine performances is unavoidable unless higher fuel consumption is accepted. Consequently, the stand-alone application of these measures is not enough anymore and, in the recent future, strong efforts will be required to develop advanced pollutants after-treatment systems to be properly coupled with engine internal technologies. In terms of NO_x emissions reduction, one of the most promising technology is the Selective Catalytic Reduction (SCR), which will be fully outlined in the next chapter. Beside SCR systems, other possibilities are currently being investigated, which will be briefly described in the following.

Lean NO_x Catalyst (LNC)

In these systems, the abatement of nitrogen oxides is achieved by means of the unburned hydrocarbons present in the exhausts [10]. In order to make the reduction process more effective, a proper catalyst is used, on which noble metals are laid. Two different main LNC technologies can be distinguished:

- Passive LNC: the unburned hydrocarbons present in the exhausts serve as the reductant agent. Conversion efficiency is quite low (about 20%) and the HC/NO_x ratio must be in the range 5-10, which is possible only when engine is running in low load conditions (when NO_x are low).
- Active LNC: an additional amount of fuel is injected in the cylinder or directly in the exhaust pipe in order to artificially increase HC concentration. The conversion efficiency raises to about 60-70%, but an increase in fuel consumption is unavoidable, along with higher unburned hydrocarbons emission levels.

Moreover, a significant conversion efficiency can be achieved only within a restricted temperature range; too high temperatures can easily damage the catalyst.

NO_x Storage Catalysts (NSC)

These systems are also referred as NO_x adsorbers. Their operation is divided into two main phases [11]:

- O_x storage: the engine is operated with a lean fuel mixture (as the typical Diesel engine operation requires). Nitrogen oxide (NO) is firstly converted to nitrogen dioxide (NO_2) thanks to the presence of a proper catalyst (often Platinum) and then stored in a carbonate-based matrix substrate. The duration of this first phase is typically around 60 s.
- O_x reduction: for few seconds, the engine is fed with a fuel rich mixture, in order to produce H_2, CO and HC, which further favor stored NO_x release. After that, rhodium acts as a catalyst for the reaction between NO_x and CO, with the production of N_2 and CO_2.

The second phase leads to a 2% increase in fuel consumption. Operating temperatures should not exceed 750 °C, because the carbonate substrate could be damaged, with a consequent worsening of its adsorption capabilities.

2.3 Selective catalytic reduction systems

The Selective Catalytic Reduction (SCR) systems are a passive solution with the objective of reducing the NOx emissions from the internal combustion engines exhaust gases. Therefore, it is an after treatment system that works as a chemical reactor.

This technology was first implemented in stationary engines used for energy production in the 1970s, mostly in Japan. Later on, this technology began its use in Europe and North America. As the emissions regulations evolved and became more stringent, the use of ammonia in the exhaust gases of vehicles was also implemented [12]. Since directly using this gas can be dangerous, in the heavy and light duty vehicles an urea water solution (UWS) diluted at 32.5%, commercially known as AdBlue, is used to obtain the gas through the hydrolysis and thermolysis of the fluid. It is a non toxic, biodegradable and low cost but very corrosive fluid. In Figure 2.7 an example of the system for commercial vehicles is shown.

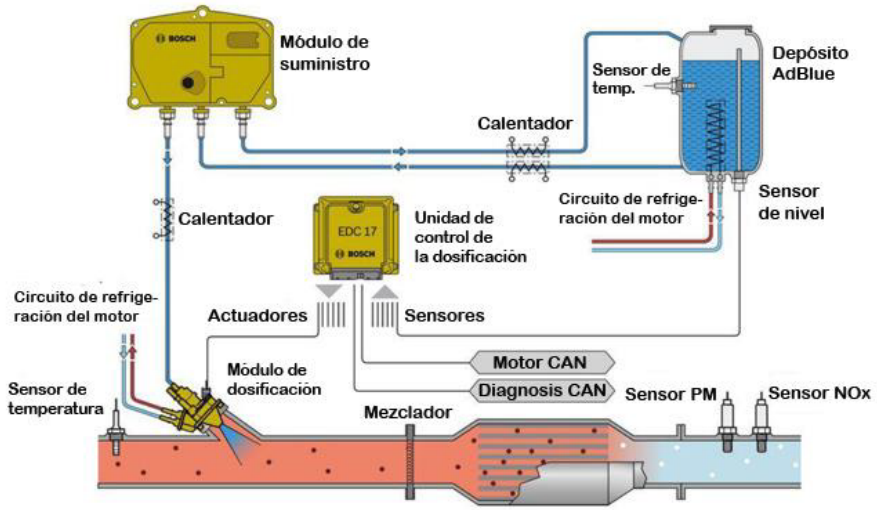

Figure 2.7: Example of an SCR system.

The selected concentration of 32.5% is used due to the low freezing point of the solution that under this condition is -11°C, as can be appreciated in Figure 2.8.

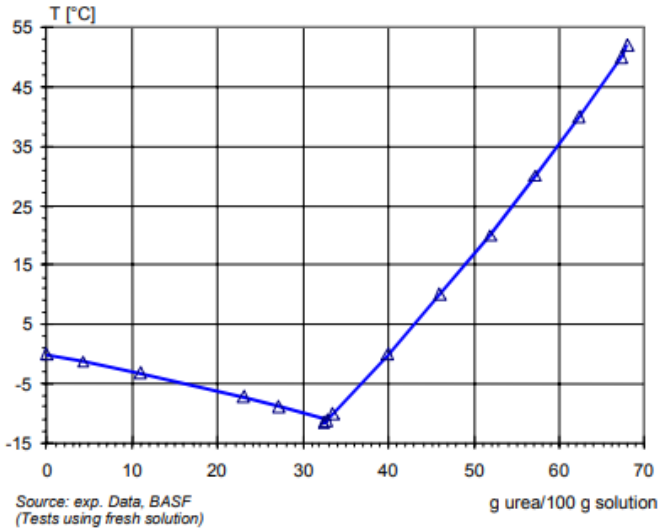

Figure 2.8: Freezing point of the solution versus concentration of urea. [13]

Normally, during the aftertreatment procedure the exhaust gases pass through an oxidation catalyst to reduce the CO concentration and unburned hydrocarbons, but more importantly, the NO gases are transformed into NO_2.

After this process is completed, the UWS is injected and mixed with the gases, which then go into the SCR catalyst. Inside of it, a reaction occurs where the extracted NH_3 from the UWS reacts with the titanium and vanadium oxides present in the catalyst and the NO_x reduction takes place. Finally, the gases pass through an oxidation catalyst where the excess NH_3 is eliminated and not ejected to the atmosphere.

The main advantages of the SCR catalyst are:

- The SCR is one of the most efficient aftertreatment systems with a conversion rate of over 80%.
- The system can work in almost any regime of the engine thanks to its great thermal stability.
- Compared to other NO_x reduction systems, the SCR is relatively cheaper.
- The SCR complements the EGR system, which helps to diminish the amount of recirculated gases, and then enhancing the combustion process efficiency.

On the other hand, the main disadvantages of this system are:

- The need of an additive that is not necessary for other systems (the UWS consumption is nearly 2-4% of the fuel consumption).
- The cost of introducing the system into the vehicle since several parts are needed, and fueling stations are also necessary.
- These new parts occupy the limited space of a light duty vehicle.
- The chemical reactions during the UWS decomposition produce additional CO_2.

Current vehicles with the SCR system installed consume around 1.5l per 1.000 km, with an autonomy of 20.000 km to match the vehicle service.

The space reduction is a critical issue since all the elements of the system have to be compact. This directly translates into a reduced space for the mixture of gases. Therefore, the optimization of all dosing parameters and exhaust conditions is important to achieve a proper mixture of the fluids.

The optimization of the dosing of UWS can result in removing the mixer put before the injection section or the last oxidation catalyst that reduces the excess NH_3, which could make the whole system occupy less space and cheaper.

2.3.1 SCR operating principle

It is well known that three way catalysts represent the most effective NO_x reduction system on vehicles, but require the absence of oxygen. Indeed, in these systems, unburned CO and HC serve as reductant agents for NO_x on a Rhodium catalyst. It is of paramount importance to have a near-stoichiometric mixture, otherwise, if excess oxygen is present in the exhausts, CO and HC will react with it, rather than with the NO_x. Some technologies are being developed to successfully employ CO and HC for NO_x abatement in a lean environment, but their industrial application is still unavailable. On the other hand, SCR systems have been developed to perform a selective catalysis of nitrogen oxides by means of an "external" reductant agent, which is ammonia. As mentioned before, ammonia is a toxic compound, then the aqueous solution of urea is preferred. The UWS is injected into the exhaust system, where ammonia is produced thanks to the high temperatures. The main reactions through which ammonia is produced are reported below:

$$(NH_2)_2CO \cdot 7H_2O \rightarrow (NH_2)_2CO + 7H_2O \tag{2.8}$$

$$(NH_2)_2CO \rightarrow NH_3 + HNCO \tag{2.9}$$

$$HNCO + H_2O \rightarrow NH_3 + CO_2 \tag{2.10}$$

According to the first reaction (Equation 2.8) a preliminary process of water evaporation takes place, leading to the formation of pure urea and water vapor. The presence of a hot environment further favors urea decomposition through a thermolysis reaction, whose products are ammonia and isocyanic acid (Equation 2.9). At last, the third chemical reaction (Equation 2.10 corresponding to hydrolysis process) converts the isocyanic acid into ammonia and carbon dioxide.

Ammonia is then dragged by the exhausts into a proper catalyst, characterized by a wide active surface where NO_x abatement reactions can take place. The combination between ammonia and nitrogen oxides is explained by the following equations:

$$4NO + 4NH_3 + O_2 \rightarrow 4N_2 + 6H_2O \tag{2.11}$$

$$2NO_2 + 2NO + 4NH_3 \rightarrow 4N_2 + 6H_2O \tag{2.12}$$

$$6NO_2 + 8NH_3 \rightarrow 7N_2 + 12H_2O \tag{2.13}$$

The first reaction (Equation 2.11) is typically considered the standard one. However, since NO_2 is always present in Diesel exhausts to some extent ($NO_2/NO_x \approx 10\%$), also the second reaction (2.12) becomes possible. This is actually the fastest NO_x reduction reaction and is therefore promoted by the presence of a proper Diesel Oxidation Catalyst (DOC), placed upstream the SCR one. If too much NO_2 is produced ($NO_2/NO > 1$), the third reaction (Equation 2.13) occurs. However, this reaction is undesirable because the excess NO_2 can lead to the formation of N_2O, which is a pollutant and a strong greenhouse gas (see Equation 2.14):

$$6NO_2 + 6NH_3 \rightarrow 3N_2 + 3N_2O + 9H_2O \tag{2.14}$$

The reduction process is referred to as selective because of the particular chemical property of ammonia to have a high affinity for NO_x. Therefore, the reaction between ammonia and NO_x is definitely favored against the reaction

with excess oxygen. However, when exhaust gases temperature is higher than 450 ºC, ammonia chemical affinity for NO_x strongly decreases and the reaction between ammonia and oxygen comes to be predominant, thus leading to a possible worsening of catalyst performances (i.e. lower NO_x conversion efficiencies). At the same time, reaching good low temperature (below 200 ºC) performances is limited by urea injection related issues (evaporation and hydrolysis processes). In these conditions, the obtainable NO_x reduction rate is mainly dependent on exhaust/urea mixing capabilities. Therefore, improved mixing devices are being developed [14] in order to achieve a faster mixing, enabling the SCR catalyst to be placed closer to the engine for a faster heat-up, thus shortening the cold start phase, during which conversion efficiency is not adequately high. In the same frame, a different solution is represented by the adoption of urea hydrolysis catalysts, which were found to be effective in ammonia production even at very low temperatures (150-160 ºC), while preventing the formation of other unexpected decomposition products [15].

The real efficiency of the whole SCR system is surely dependent upon the performances of its single elements. However, it is also strongly influenced by several other factors, most of them related to the architecture of the exhaust line itself and the control strategies applied to the various components. In particular, the kinetics of urea decomposition and NO_x abatement processes are first influenced by exhausts mass flow rate and temperature. Therefore, a sophisticated control system has to be implemented in the Electronic Control Unit (ECU) and several sensors have to be installed on the vehicle exhaust line, in order to record the thermal conditions present. This data can be extremely useful to apply the most suitable urea dosing strategy, so that the maximum possible NO_x conversion efficiency can actually be achieved.

In an effort to improve SCR system performances, some other mandatory goals have to be met:

- A uniform distribution of the UWS solution should be present upstream the SCR catalyst. This way, it is likely that the largest portion of the active surface of the catalyst will take part in the reduction process. On the other hand, regions where ammonia concentration is low or where ammonia is not present at all will likely determine a poor concentration of the reductant in the corresponding regions of the catalyst.

- A proper mixing between UWS and the exhaust gases should be established before the beginning of chemical processes. The largest part of available ammonia will take part in the conversion reactions, while

preventing ammonia slip phenomena downstream the catalyst. Moreover, if a suitable stoichiometric amount of ammonia is introduced in the exhaust line, all the NO_x present should be properly converted.

- The UWS spray characteristics, both in terms of targeting and drops sizing, should correctly match with the geometry of the exhaust line where the injector has to be installed. An incorrect targeting, indeed, may result in spray/wall impingement phenomena and, in a long-term period, in the formation of undesired deposits inside the pipe. On the other hand, a proper spray atomization can accelerate urea decomposition processes and, therefore, NO_x abatement reactions.

2.3.2 Components of a SCR system

The SCR systems begun their automotive application in heavy duty vehicles, and for this reason the initial configurations used compressed air (already present in this type of vehicles) to assist the atomization of the spray. This kind of system is depicted in Figure 2.9.

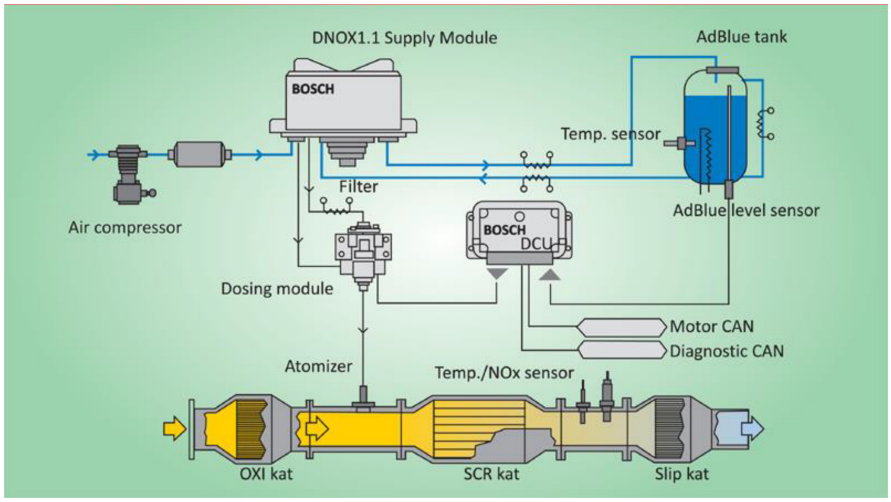

Figure 2.9: Bosch Denoxtronic 1.1 system components for heavy duty vehicles (Adapted from [16]).

The system is usually composed of the following components:

- **Deposit**: it is a storage unit destined to contain the liquid. This item has level and temperature sensors to control the system.

- **Supply module**: this part is responsible of pumping the fluid from the deposit to the dosing unit at a set pressure.
- **Dosing module**: this element is the injector. It receives the signals from the control unit to dose the proper fluid quantity. Here is where the mixture of UWS and compressed air occurs. The injector nozzle is inside the exhaust line.
- **Control sensors**: In addition to the sensors present in the deposit, there are sensors to quantify the characteristics of the exhaust gases and NO_x levels, which, once the signals are processed, will control the characteristics of the injection event.

When the SCR systems were implemented in the light duty vehicles, the compressed air system was no longer available, therefore their name of "non-air assisted". Figure 2.10 depicts a light duty vehicle SCR system scheme.

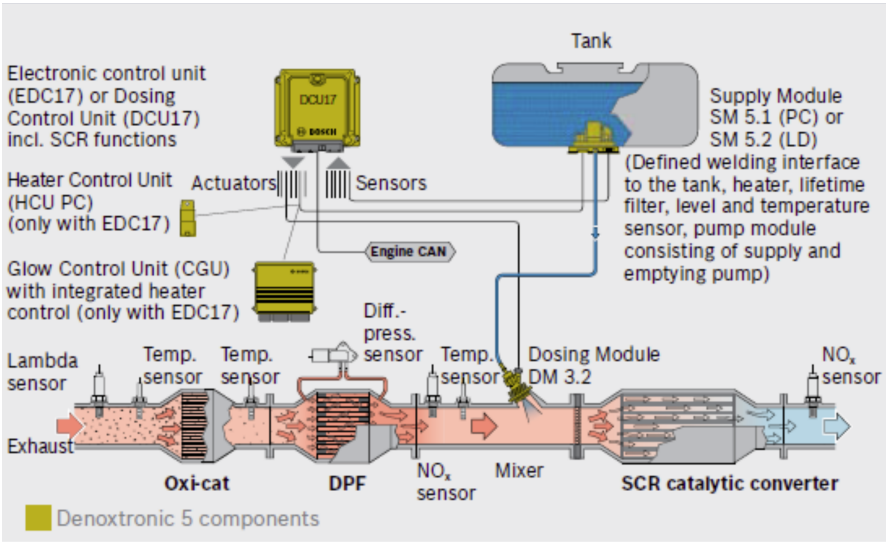

Figure 2.10: Bosch Denoxtronic 5.0 system components (Adapted from [16]).

In both setups (light and heavy duty) injectors need cooling, may it be either by air or a coolant fluid coming from the engine cooling system.

The injector position is often selected to favour the mixing of the gases with the injected fluid and depending on the layout of the exhaust line, even allowing setups where the injector axis is parallel to the gas flow (Figure 2.11).

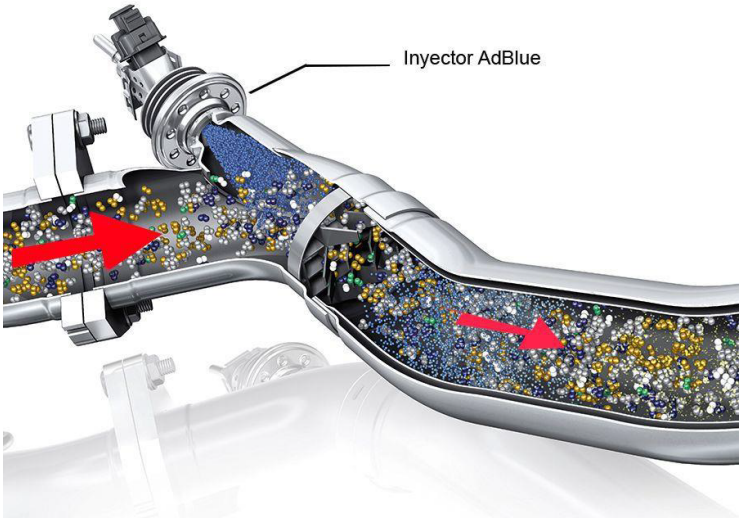

Figure 2.11: Exhaust line "Y" layout.

2.3.3 UWS dosing unit

As it was mentioned in previous sections, the dosing element plays an important role in the delivery of the UWS. These injection systems usually operate between 3.5 and 8.5 bar and the injected quantity is calculated by the control unit depending on the working conditions and the information obtained from the sensors. Different injector types are available nowadays in the market, which are classified depending on their characteristics:

Air-cooled injectors:

These are the first type of injectors developed and installed in vehicles. They are mounted distant from the exhaust manifold, then the temperature level is not very high. The maximum tip fluid temperature can be 120 ºC. They can provide Sauter Mean Diameters of 70 μm up to 155 μm. An example of this injector type can be seen in Figure 2.12.

Figure 2.12: Air-cooled UWS injector.

Liquid-cooled injectors:

These dosing systems have a cooling jacket that prevents overheating of the nozzle tip due to the high exhaust gas temperatures. The cooling temperature range is 80-90 ºC. This temperature can affect the properties of the injected fluid. This injector type is the one used in this Thesis and is depicted in Figure 2.13.

There is another classification that depends on the pressure supply:

- Low pressure units: use the same technology than gasoline dosing systems employed for port fuel injection. The operating pressure is around 5-6 bar. It is employed in SCR systems for light-duty engines.
- Injector with integrated high pressure pump: The injector is coupled with a small reciprocating pump in the same unit. It can operate with higher pressure levels up to 70 bar, producing droplets with smaller diameters around 50 μm. Since this system is more complex, it is also more expensive.
- Air-assisted injector: This type of unit has two nozzles, the first one delivers the UWS, and the second one is used for injecting pressurized air. This technology is more complex, but it enhances the atomization

Figure 2.13: Liquid-cooled UWS injector.

process since the liquid UWS mixes with the pressurized air downstream the nozzle producing smaller droplets. These are used in heavy-duty engines where the air supply is available.

Independently of the injector type, the correct operation of the dosing unit faces challenges that require a deep understanding. Some issues that may compromise an appropriate injection process are the formation of huge droplets that are difficult to evaporate or that require a long time for decomposition. When this happens, the ammonia production is not fast enough, and the mixture preparation with the exhaust gases is inefficient, producing wall impingement and ammonia slip. Additionally, the spray/wall impingement phenomena combined with low temperatures (in the range of 220-250 ^{o}C) lead to the formation of deposits in the internal wall of the exhaust line, mixer elements and in the injector nozzle itself, as depicted in Figure 2.14.

Figure 2.14: Example of deposit formation in a commercial nozzle.

To overcome these problems previous works have been dedicated to the understanding of this specific component, using computational and experimental tools. In the following sections, a literature review of techniques that are used for the characterization of UWS injector units is presented.

2.3.4 Hydraulic characterization of UWS injector

During the design of the SCR system and in the calibration of the engine the UWS injection process plays a key role. For that reason, it should be understood and characterized for a suitable selection of the injector [17]. Until few years ago, the information regarding to UWS injection systems for light duty applicatios was very limited. Recently, some researchers have devoted their investigations to the characterization of this system. They have realized that the determination of the injected mass is necessary [18], since it is an essential parameter for correct initialization and validation of Computational Fluid Dynamics (CFD) models [19, 20].

In the paper [21] written by the author, it is indicated that the most used methods for the determination of the mass flow are the Zeuch and the Bosch methodologies [18, 22]. In the Bosch instrument, the measuring principle is based on injecting the liquid into a closed volume and registering the pressure wave using a piezoelectric pressure sensor. Then, the rate of injection is proportional to the pressure wave. In the Zeuch-type device, it is possible

to perform measurements of absolute pressure level along with the pressure wave intensity, thanks to a piezoresistive pressure transducer that is used to avoid derive effects. In this device, the rate of injection is proportional to the pressure derivative. In the last decade, both systems have been widely used for gasoline and diesel dosing applications, where injection pressures are very high (in particular in diesel it can reach values up to 250 MPa). One of the main characteristics of those instruments is that the injection is performed into a chamber filled with liquid where the signal is registered downstream of the injector.

Besides, another methodology have been implemented by Ferrari et al. [23]. They measure the instantaneous flow rate based on the pressure time variation in the line that connects the injector with the rail. The pressure is registered in the connection line, and then the curve is converted into mass flow rate. The procedure has been validated for pilot injections, tipically with small pulses. Another technique based on fast Coriolis flow meters has been employed by Leach et al. [24]. They showed promising results, but reported some challenges such as the calibration of the device for very small pulses [18].

To implement those methodologies directly in UWS injectors could have some issues. The injection pressure levels in UWS units are low in comparison with gasoline or diesel direct injection systems. Besides, real UWS injection process is in exhaust gas conditions are considerably different to injecting into liquid. Additionally, the discharge ambient pressure is relatively low compared to those of diesel and gasoline, surrounding the atmospheric pressure.

To address those issues, other authors have implemented a different method based on the measurement of the momentum flux [25–28], injecting into gas and obtaining good results. This has been used in the past for gasoline and diesel sprays. The fact that this procedure is capable of measuring the injection event evolution in a gaseous medium makes it attractive for the application that concerns UWS dosing systems. The measurement of momentum flux allows injecting into air, and also enables to do an analysis of the shot-to-shot dispersion, usually impossible with a weight. This is the approach chosen for this thesis and will be described in detail in the following chapter (Section 3.3).

2.3.5 Spray development characterization of UWS injectors

The literature evidences that efforts are dedicated to the understanding of the UWS jet characteristics, from the global spray (liquid penetration, spreading angle and vapor penetration) to the microscopic perspective (droplet shape,

diameter distribution and velocity). The determination of these properties has become of great importance due to the consequences of inadequate dosing and mixing on the formation of deposits, which can block the injector and the exhaust components affecting the efficiency of the engine. This section presents a summary of previous works, exposing the most recent technologies used for the characterization of the urea spray development.

Lecompte et al. [29] developed a test bench for the visualization of UWS sprays. The gas flow in the test rig is supplied by a supercharged 4-stroke Diesel engine. They used two rig configurations depicted in Figure 2.15.

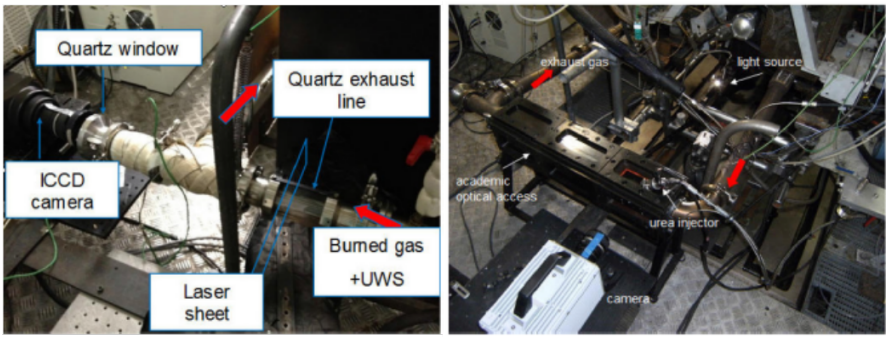

Figure 2.15: Visualization test rig and optical setup used in [29].

They applied two optical diagnoses, shadowgraphy and laser induced fluorescence (LIF), for measuring the spray evolution and the mixture, respectively. The visualization setup was composed by three consecutive modules, with rectangular cross-section, designed to hold quartz windows. In this way, they could see the flow in three different areas along the exhaust pipe, including the first millimeters of the jet. They also designed several pieces to insert the injector in one side of the chamber at different angles relative to the direction of flow. Additionally, the test rig had a tubular optical access with a quartz cylinder to maintain the geometry and avoid disturbances. The purpose of this window is to have access to apply a laser beam for studying the vaporization and homogeneity of urea through LIF. From the measurements, they obtained an improvement in the homogeneity of the urea-gas mixture in the exhaust line at higher temperature. This homogeneity is hardly affected by the mass flows studied.

Spiteri and Eggenschwiler [30], unlike the previous study, developed a specific test bench for urea studies where the air flow is not coming from the engine exhaust gas. The air flow was generated by a blower or a compressor.

The visualization test rig had a square section of 80 *mm* on each side with optical accesses. The injector was located at the top of the chamber, as shown in Figure 2.16 with an inclination angle of 50 degrees to the flow direction. It was used a commercial injector designed for SCR system applications. The injected fluid was water instead of urea, as it has a similar behavior according to [31]. They used three different optical imaging techniques, such as Mie scattering, shadowgraphy and particle image velocimetry (PIV).

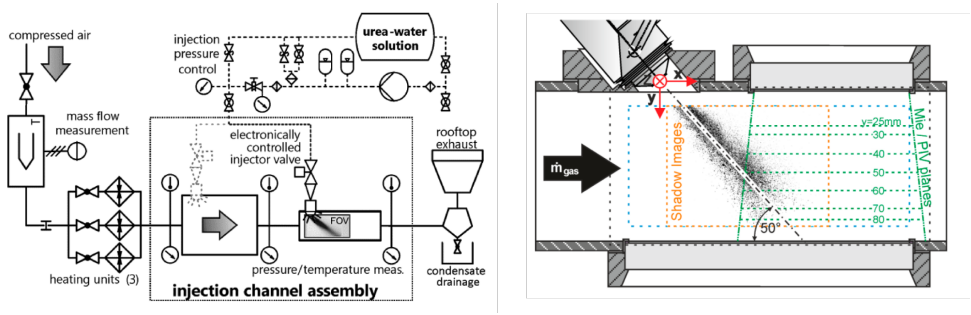

Figure 2.16: Scheme of the flow rig and visualization chamber used in [30].

In this test bench, 12 points were studied varying the gas flow rate and the temperature. They simulated different loads and regimes of the engine. The jet penetration was studied based on the progress of the jet tip. They determined that there is no appreciable variation in penetration due to the effect of the gas flow. The iso-contours of the jet were also studied, and they concluded that the spray penetration and cone angle were independent of gas flow conditions. On the other hand, they carried out a study of the droplet axial velocity. They suggested that the flow conditions are insufficient to induce secondary breakup, in the tested range.

Like the previous study, Shi et al. [32] simulated the exhaust gas using a blowing fan and a heater. The injected fluid used was urea. The windows of the visualization test rig were made of a quartz tube that imitates the exhaust pipe with a diameter of 127 *mm*. The urea injector was single-hole non-air-assisted, and was located at the upper side of the test rig. Figure 2.17 shows the diagram of the test bench. Regarding the test conditions, those were selected to simulate one engine operating point, with constant flow and temperature. They varied the injection pressure and the injector angle position. The droplet distribution and wall impingement were characterized. Results showed that when the injection pressure increased, the mixing distance was larger due to the increment in the axial and perpendicular velocity of the

droplets, causing a higher spray penetration and more possibilities of wall impingement.

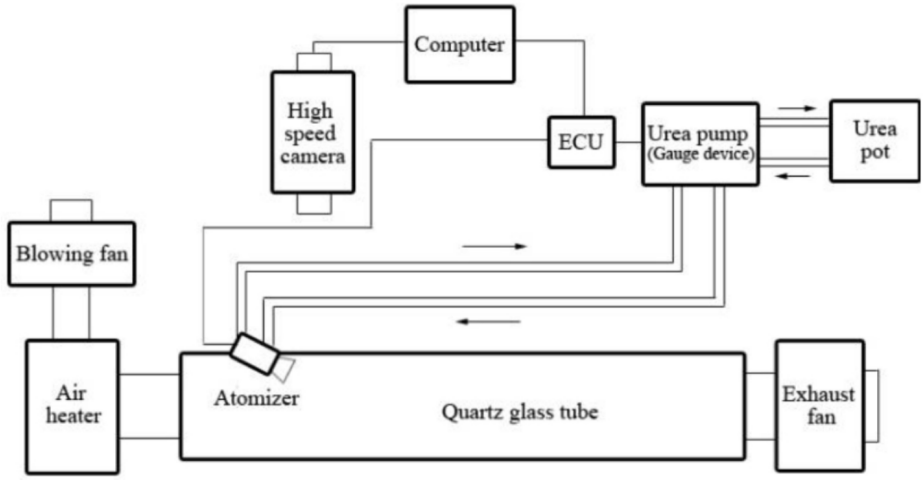

Figure 2.17: Diagram of the visualization system used in [32].

Regarding the microscopic characterization, several studies have been done for determining the droplet size distribution and velocity.

Postrioti et al. [33] proposed a methodology based on back-light imaging for diameter determination and validated the results against PDA. They used a hot-air flow test rig, with four optical accesses, where the injector is placed axially to the gas flow. The backlight imaging set-up is depicted in the left side of Figure 2.18 and the PDA arrangement is depicted in the right side of the same figure. They obtained a good agreement between both measurement methods for the droplet diameter determination. They also concluded that the backlight imaging procedure is a reasonable alternative that can be applied when the complexity of the geometry avoids the use of the PDA technique.

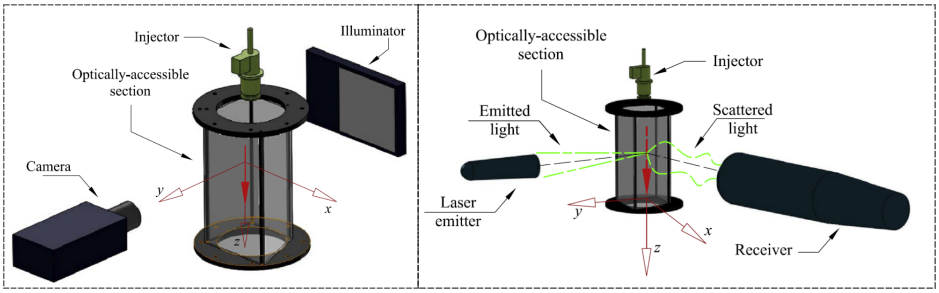

Figure 2.18: Test rig used in [33]. Left side: Laser backlight imaging setup. Right side: PDA arrangement.

Later, in the work of Brizi et al [34], the UWS spray was studied under different chamber and fluid temperatures, founding that fluid temperature has big influence over the spray and droplet formation. Brizi in [2] used the technique based on laser backlight optical setup. The configuration of the optical layout is depicted in Figure 2.19, where the spray is located between the CCD camera and the backlight source. He used a field of view of 15x15 mm with a pixel resolution of about 7.3 $\mu m/pixel$. The spray was injected in a quiescent environment. He confirmed that the air temperature has little influence on the spray droplet diameter evolution.

Lieber, Koch and Bauser [35] studied an air assisted UWS injector with high-temperature coaxial flow, determining the velocity of the gas by approximating it to the velocity of the smallest droplets and predicting the turbulent dispersion of the droplets. They remarked the difficulties of the droplet detection for these types of atomizers where the images might have a degradation due to density gradients in the measurement volume. They implemented a cooling system in the test rig windows to minimize these issues. Also, they described the post-processing, which was based on the application of a threshold for separating the droplets from the background. The threshold used was chosen arbitrarily as an empirical value that provided a good compromise between enough assignment of droplets and background noise elimination. They quantified the droplet size distribution in the radial direction of the spray and noticed that the spray was not symmetric. In the second part of their work, they determined the droplet velocity in a radial direction.

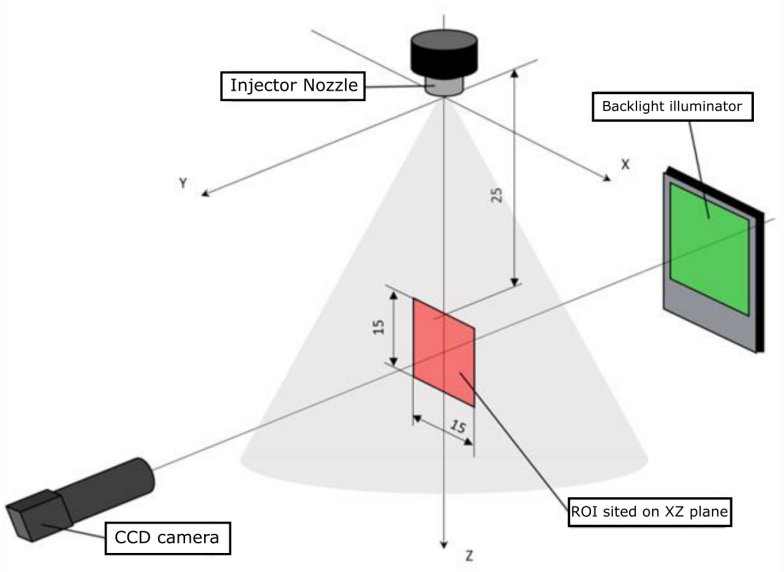

Figure 2.19: Laser backlight imaging setup used in [2].

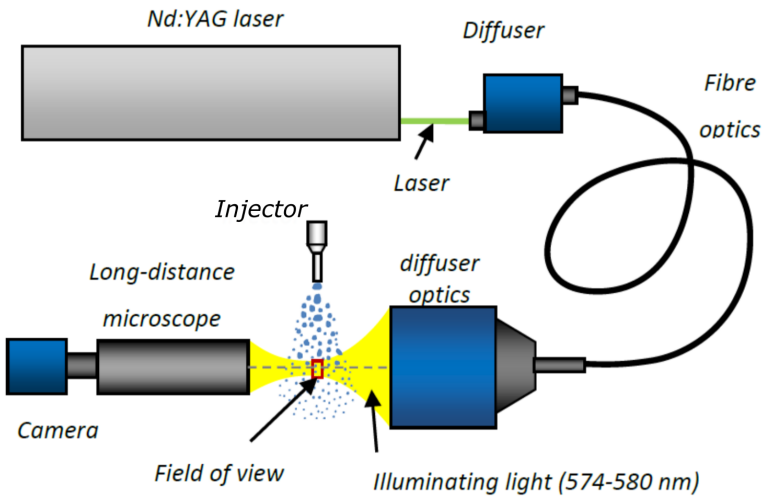

Figure 2.20: Experimental setup with shadowgraphy and microscope used in [36].

Kapusta et al. in [36] compared the behaviour of a commercial UWS injector using UWS and water, analysing various spray characteristics and droplet

distribution. The set-up was based on the shadowgraphy optical method with a long-distance microscope (depicted in Figure 2.20), where the area of interest was located 20 mm below the nozzle exit, in the plume axis. They were able to measure diameter values in the range between 20 μm and 300 μm for different injection pressures. They reported that there are some differences in the droplet size distribution when water is used as a substitute fluid. The main differences appear at smaller droplet size (25-65 μm), obtaining larger droplets when water is the injected fluid, whereas this difference is negligible at big sizes.

Moreover, Kapusta characterized the break-up regimes of the UWS jet, and represented the tested conditions considering the criterion of the Ohnesorge number and the Reynolds number, as depicted in Figure 2.21. They found that when UWS is injected, the jet break-up regime is placed in the first wind-induced regime. When water is used as injecting fluid, the jet droplet breakup process moves towards the right side of the chart, and could be in a different break-up regime than the one observed for UWS. From the reports available in the literature, the parameters that affect the atomization process are related to the liquid properties (fluid density, fluid viscosity, surface tension), to the ambient properties (gas density), relative velocity between the gas and the liquid, and the effective nozzle diameter of the nozzle [37]. Therefore, the atomization regimes presented in the chart might be different if one of those parameters changes.

For a deeper understanding of the spray atomization process theory, the next section describes the fundamentals of the jet breakup process.

2.4 Spray atomization process

One of the first theoretical studies on jet breakup was carried out by Rayleigh [40], who considered a laminar jet with a diameter equal to d_j in its initial stages and coming from a circular orifice, which led to surface disturbances. He concluded that symmetric disturbances characterized by an optimal wavelength $\lambda_{opt} = 4.15 d_j$ will increase over time, leading to the breakup of the jet into smaller structures like ligaments that will become spherical droplets. The diameter, d, could be calculated from:

$$\lambda_{opt} \frac{\pi}{4} d_j^2 = \frac{\pi}{6} d^3 \rightarrow d = 1.89 d_j \tag{2.15}$$

Later Weber extended Rayleigh's theory, adding the effect of the fluid viscosity by means of the Ohnesorge number [41]. Weber's theory express the

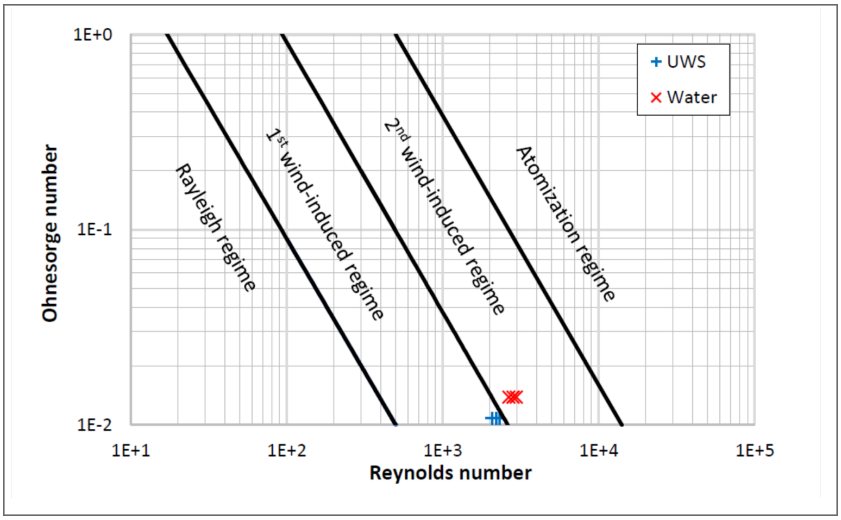

Figure 2.21: Break-up regimes at the tested conditions of [36], based on [38, 39].

optimal unstable wavelength as:

$$\lambda_{opt} = \sqrt{2}\pi d_j (1 + 3Oh)^{0.5} \tag{2.16}$$

The characteristic length scale in the Ohnersorge number is the diameter of the cylindrical jet and the Oh number is defined as:

$$Oh = \frac{\mu_L}{\sqrt{\rho_L \sigma d_j}} \tag{2.17}$$

where μ_L is defined as:

$$\lambda_{opt} \frac{\pi}{4} d_j^2 = \frac{\pi}{6} d^3 \rightarrow d = \left(\frac{3\pi}{\sqrt{2}}\right)^{\frac{1}{3}} d_j (1 + 3Oh)^{\frac{1}{6}} \tag{2.18}$$

In addition to the viscosity of the liquid, other significant quantity that strongly influences the atomization process is the initial velocity of the jet released from the orifice [42]. The phenomena described by the theories of Weber and Rayleigh are representative for the breakup of the jet only at low liquid velocities. As the relative velocity between the air and the liquid increases, aerodynamic interactions between the two fluids become stronger, usually leading to smaller droplets. According to recent experiments, the

classification of breakup regimes was proposed by Reitz [40] and can be divided in four regimes as a function of the liquid Ohnesorge and Reynolds number, as shown in Figure 2.22, and are also described as follow:

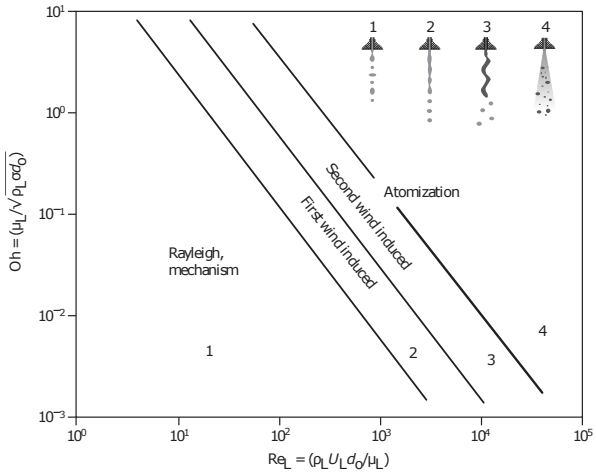

Figure 2.22: Diagram of the jet breakup regimes classification (extracted from [41]).

- *Rayleigh mechanism*: if the flow remains in low velocities, the breakup mechanism that governs is the one studied by Rayleigh. The rupture of the liquid vein is due to the increase of symmetric oscillations under the action of surface tension, which is able to enlarge their amplitude for disturbance wavelengths greater than a minimum value. The drops originated from this breakup mechanism have quite a uniform diameter, which is approximately two times the initial jet diameter.

- *First wind-induced breakup*: the relative velocity between the gas phase and the spray increases the surface tension effect, reducing the optimal wavelength for the breakup of the liquid vein and therefore forming smaller droplets upon rupture.

- *Second wind-induced breakup*: as the velocity of the spray increases, droplets begin to form due to the unstable growth of small waves in the liquid vein surface, which are generated by interaction of the gas and the spray. The waves become unstable and separate from the spray surface as ligaments that will break up into droplets of much smaller diameter than the initial orifice. This process occurs at several orifice diameters below the nozzle exit.

- *Prompt atomization*: the spray disintegrates as soon as it exits the nozzle and the droplet diameters are considerably smaller than the orifice diameter.

2.4.1 Secondary atomization

Droplets travelling in a gaseous medium are governed by aerodynamic forces and this could lead to the deformation and fragmentation of the droplet. The breakup of droplets into smaller particles is referred to as secondary atomization.

Critical Weber number

Simple study about droplet stability can be described by considering a particular droplet subjected to a moving airflow. When the aerodynamic force, in this case the drag force, is equivalent to those of the surface tension, the critical condition for droplet breakup is obtained [41]:

$$C_D \frac{\pi}{8} d^2 \rho_g U_g^2 = \pi d \sigma \tag{2.19}$$

A critical Weber number can be calculated by arranging this equation, allowing a measure of the maximum diameter of stable droplet that can be found in the spray:

$$\left(\frac{\rho_g U_R^2 d}{\sigma} \right)_c = We_c = \frac{8}{C_D} \rightarrow d_{max} = \frac{We_c \sigma}{\rho_g U_R^2} \tag{2.20}$$

For low viscosity fluids, experimental data on several C_D points towards a value of critical Weber number We_c of approximately 12. Equation 2.20 can be modified by introducing the Ohnesorge number and by doing so the influence of the liquid viscosity is taken into account. The following expression is proposed:

$$We_{c,lv} = We_c + 14 \left(\frac{\mu_L}{\sqrt{\rho_L \sigma d}} \right)^{1.6} = We_c + 14 Oh^{1.6} \tag{2.21}$$

It can be observed in Equation 2.21 that an increase in the viscosity of the liquid usually leads to a greater Weber number. Nevertheless, the effect of this property over the critical Weber number is only relevant at high fluid viscosities.

Secondary breakup regimes

Experimental results indicate that various breakup regimes can be identified, as can be observed in Figure 2.23. Droplet Weber number is defined as Equation 2.22:

$$(We = \rho_g U_R^2 d/\sigma) \tag{2.22}$$

Weber and Ohnesorge number define the transition between the different breakup regimes, with the later taking into account the effects of the fluid viscosity. When the Ohnesorge number is low enough, the effects of the fluid viscosity are negligible and the aforementioned transition is governed only by the Weber number. Some values for different breakup regimes are also shown in Figure 2.23 for Ohnesorge numbers below 0.1.

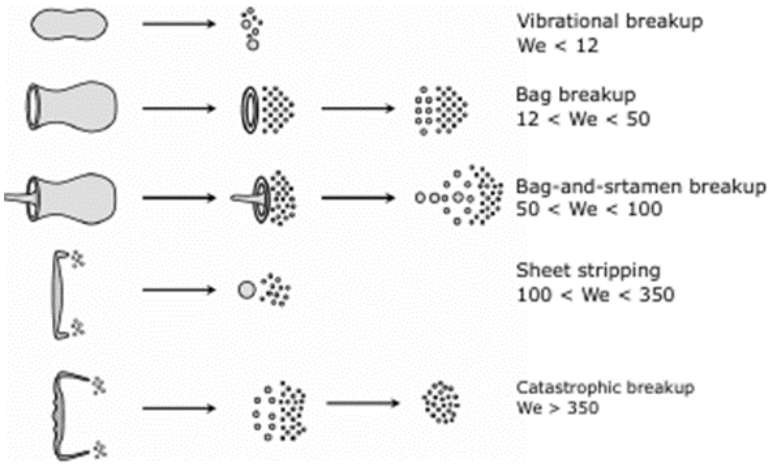

Figure 2.23: Breakup regimes for a low viscosity Newtonian droplet in a horizontal air stream (adapted from [43]).

An important deformation of the droplet occurs when the Weber number is equal to one. The deformation due to the interaction of the gas flow and the droplet is countered by the surface tension and viscous forces. The droplet deformation will lead to a breakup if the aerodynamic forces are large enough. The vibrational droplet breakup is rarely observed and consists of oscillations at the natural frequency of the droplet. The droplets generated after breakup have diameters comparable to those of the parent drop. In the "bag breakup regime", the deformation of the droplet triggers the formation of

a thin hollow bag that is attached to a wider rim with toroidal shape. The bag disintegrates first, and generates several small drops, followed by the toroidal rim that results in a smaller number of big fragments. The "bag-and-stamen breakup" is analogous to the bag breakup, but with the addition of a stamen oriented anti-parallel to the motion of the drop. Like the bag breakup, the first to disintegrate is the bag, and subsequently the rim and the stamen. In "sheet stripping", on the surface of the droplet a film is generated, and from there small droplets are continuously torn off. This produces a cloud of small droplets and, in some cases, a core whose size is comparable to that of the parent droplet. Lastly, the "catastrophic regime" appears for Weber numbers > 350. The surface of the droplet is corrugated by waves of large amplitude and long wavelengths. This produces very small droplets.

For Oh numbers greater than 0.1, due to the effect of liquid viscosity, the critical Weber numbers that distinguish the different regimes may change. Typical expressions for the critical Weber number as a function of the Ohnesorge number have the same form of Equation 2.21. Some indications about the transition between the different regimes as a function of both We and Oh numbers can be found in reference [44].

2.5 Summary

This chapter presented the complex technological challenges that the internal combustion engine industry faces, which has been evolving continuously in the past twenty years to overcome the emissions standards and legislations. From the literature review performed, it is possible to identify that the development of effective aftertreatment system has been a key in the reduction of pollutant emissions. In particular, the SCR has been developed to abate the NO_x in the exhaust gases. Several efforts have been made in the comprehension of the processes that occur inside that system, paying special attention to the UWS injection performance.

This review has shown that previous studies have been dedicated to study the UWS injection in modified engines, that have been adapted to visualize the spray in the most realistic environment. Due to the complexity of the infrastructure and the geometry of the ICE system, the optical techniques implemented are complex, also, they have to deal with particles and contaminants present in the exhaust gas that can distort the analysis of the spray evolution. Some other works have been done in dedicated facilities, that simulate the flow conditions artificially with a gas generation system. The limitation of previous studies is that some of them have been performed for old generations

of injection systems (that used to work at lower injection pressures, or without any integrated cooling), and at a narrower range of operation in terms of gas mass flow and temperature. Additionally, the main technique used for droplet characterization has been the PDA which is expensive. Finally, most of the experiments available in the literature have been performed with water as a substitute of the UWS. Hence, this work pretends to answer some aspects that are still not clear:

- Shed some light in the hydraulic performance of the UWS injectors. To quantify the differences of its operation when UWS is replaced by water as testing fluid. For this study, it is necessary to develop a methodology that allows measuring the rate of injection of this low-pressure atomizer. So far, very little studies have been reported in this subject.
- To characterize the global spray development, in conditions that resemble the engine exhaust pipe flow and to quantify the effect of important parameters as injection pressure and flow temperature on the spray penetration.
- The droplet diameter distribution has been obtained mainly using the PDA technique. This work aims to find an alternative optical method to quantify the diameter, and at the same time to determine the velocity of the particles in two components. The experimental determination of these parameters would be useful to initialize and validate CFD simulations that are being done in other studies of the research institute.

References

[1] Reitz, R D et al. “IJER editorial: The future of the internal combustion engine”. In: *International Journal of Engine Research* (2019), p. 146808741987799. DOI: 10.1177/1468087419877990.

[2] Brizi, Gabriele. “Experimental analysis of Urea-Water Solution injectors for automotive Selective Catalytic Reduction systems”. PhD thesis. Universita degli Studi di Perugia, 2018.

[3] Giechaskiel, Barouch et al. “Evaluation of NOx emissions of a retrofitted Euro 5 passenger car for the Horizon prize “Engine retrofit””. In: *Environmental Research* 166 (2018), pp. 298–309. DOI: https://doi.org/10.1016/j.envres.2018.06.006.

[4] Yang, Zhiwen et al. "Real-world gaseous emission characteristics of Euro 6b light-duty gasoline- and diesel-fueled vehicles". In: *Transportation Research Part D: Transport and Environment* 78 (2020), p. 102215. DOI: https://doi.org/10.1016/j.trd.2019.102215.

[5] García-Contreras, Reyes et al. "Impact of regulated pollutant emissions of Euro 6d-Temp light-duty diesel vehicles under real driving conditions". In: *Journal of Cleaner Production* 286 (2021), p. 124927. DOI: https://doi.org/10.1016/j.jclepro.2020.124927.

[6] Kohl, Arthur L. and Nielsen, Richard B. "Control of Nitrogen Oxides". In: *Gas Purification* II (1997), pp. 866–945. DOI: 10.1016/b978-088415220-0/50010-0.

[7] Zeldovich, Yakov Borisovich. "Oxidation of nitrogen in combustion and explosions". In: *Selected Works of Yakov Borisovich Zeldovich, Volume I*. Princeton University Press, 2014, pp. 404–410.

[8] Zhao, Hua. *Advanced direct injection combustion engine technologies and development: diesel engines*. Vol. 2. Elsevier, 2009.

[9] Payri, Francisco and Desantes, Jose Maria. *Motores de combustion interna alternativos*. Editorial Universitat Politecnica de Valencia, 2011.

[10] Iwamoto, Masakazu et al. "Removal of nitrogen monoxide through a novel catalytic process. 2. Infrared study on surface reaction of nitrogen monoxide adsorbed on copper ion-exchanged ZSM-5 zeolites". In: *The Journal of Physical Chemistry* 96.23 (1992), pp. 9360–9366. DOI: 10.1021/j100202a055.

[11] Liu, Gang and Gao, Pu-Xian. "A review of NOx storage/reduction catalysts: mechanism, materials and degradation studies". In: *Catal. Sci. Technol.* 1 (4 2011), pp. 552–568. DOI: 10.1039/C1CY00007A.

[12] Blakeman, Phil, Arnby, Karl, Marsh, Per, Newman, Colin, and Smedler, Gudmund. "Optimization of an SCR Catalyst System to Meet EUIV Heavy Duty Diesel Legislation". In: *2008 SAE International Powertrains, Fuels and Lubricants Congress*. SAE International, 2008. DOI: https://doi.org/10.4271/2008-01-1542.

[13] BASF. "AdBlue® Technical Leaflet". In: November (2006), pp. 1–6.

[14] Zhan, Reggie, Li, Wei, Eakle, Scott, and Weber, Phillip. "Development of a Novel Device to Improve Urea Evaporation, Mixing and Distribution to Enhance SCR Performance". In: 2010. DOI: 10.4271/2010-01-1185.

[15] Alano, Eduardo et al. "Compact SCR for Passenger Cars". In: *SAE Technical Paper*. SAE International, 2011. DOI: 10.4271/2011-01-1318.

[16] Raff, Michael, Weingarten, Erik, and Muslija, Manuel. "Denoxtronic 5.3 – A modular system for applications worldwide". In: *19. Internationales Stuttgarter Symposium*. Ed. by Michael Bargende, Hans-Christian Reuss, Andreas Wagner, and Jochen Wiedemann. Wiesbaden: Springer Fachmedien Wiesbaden, 2019, pp. 113–127.

[17] Payri, Raul, Bracho, Gabriela, Gimeno, Jaime, and Moreno, Armando. "A Methodology for the hydraulic characterization of a Urea-Water Solution injector by means of Spray Momentum Measurement". In: *ILASS - Europe 2019, 29th Conference on Liquid Atomization and Spray Systems* September (2019), pp. 2–4.

[18] Postrioti, Lucio, Caponeri, Giulio, Buitoni, Giacomo, and Van Vuuren, Nic. "Experimental Assessment of a Novel Instrument for the Injection Rate Measurement of Port Fuel Injectors in Realistic Operating Conditions". In: *SAE International Journal of Fuels and Lubricants* 10.2 (2017), pp. 1–8. DOI: 10.4271/2017-01-0830.

[19] De Rudder, Korneel and Chauvin, Corine. "Close coupled DOC - mixer - SCR for Tier 4 final". In: *7th AVL International Commercial Powertrain Conference* (2013), pp. 1–10.

[20] Montenegro, G. et al. "CFD analysis applied to the design of aqueous urea SCR dosing system with reduced risk of solid deposit formation". In: *THIESEL 2018 Conference on Thermo- and Fluid Dynamic Processes in Direct Injection Engines High-pressure*. 2018.

[21] Payri, Raúl, Bracho, Gabriela, Martí-Aldaraví, Pedro, and Moreno, Armando. "Using momentum flux measurements to determine the injection rate of a commercial Urea Water Solution injector". In: *Flow Measurement and Instrumentation* 80 (2021), p. 101999. DOI: https://doi.org/10.1016/j.flowmeasinst.2021.101999.

[22] Payri, R., Salvador, F. J., Gimeno, J., and Bracho, G. "A new methodology for correcting the signal cumulative phenomenon on injection rate measurements". In: *Experimental Techniques* 32.1 (2008), pp. 46–49. DOI: 10.1111/j.1747-1567.2007.00188.x.

[23] Ferrari, A. and Paolicelli, F. "An indirect method for the real-time evaluation of the fuel mass injected in small injections in Common Rail diesel engines". In: *Fuel* 191 (2017), pp. 322–329. DOI: https://doi.org/10.1016/j.fuel.2016.11.053.

[24] Leach, Felix et al. "Fast Coriolis mass flow metering for monitoring diesel fuel injection". In: *Flow Measurement and Instrumentation* 58 (2017), pp. 1–5. DOI: https://doi.org/10.1016/j.flowmeasinst.2017.09.009.

[25] Pickett, Lyle M, Manin, Julien, Payri, Raul, Bardi, Michele, and Gimeno, Jaime. "Transient Rate of Injection Effects on Spray Development". In: *SAE Technical Paper 2013-24-0001* (2013). DOI: 10.4271/2013-24-0001.

[26] Mariani, Alessandro, Cavicchi, Andrea, Postrioti, Lucio, and Ungaro, Carmine. "A Methodology for the Estimation of Hole-to-Hole Injected Mass Based on Spray Momentum Flux Measurement". In: *SAE Technical Paper Series* 1 (2017). DOI: 10.4271/2017-01-0823.

[27] Payri, Raul et al. "Momentum Flux Measurements on an ECN GDi Injector". In: *SAE Technical Paper 2015-01-1893*. Vol. 1. 2015. DOI: 10.4271/2015-01-1893.

[28] Payri, R., Bracho, G., Soriano, J. A., Fernández-Yáñez, P., and Armas, O. "Nozzle rate of injection estimation from hole to hole momentum flux data with different fossil and renewable fuels". In: *Fuel* 279.March (2020), p. 118404. DOI: 10.1016/j.fuel.2020.118404.

[29] Lecompte, Matthieu, Raux, Stephane, and Frobert, Arnaud. "Experimental Characterization of SCR DeNOx-Systems: Visualization of Urea-Water-Solution and Exhaust Gas Mixture". In: *SAE Technical Paper Series* 1 (2014). DOI: 10.4271/2014-01-1524.

[30] Spiteri, Alexander and Dimopoulos Eggenschwiler, Panayotis. "Experimental fluid dynamic investigation of urea-water sprays for diesel selective catalytic reduction-denox applications". In: *Industrial and Engineering Chemistry Research* 53.8 (2014), pp. 3047–3055. DOI: 10.1021/ie404037h.

[31] Spiteri, A., Srna, A., and Dimopoulos Eggenschwiler, P. "Characterization of sprays of water and urea-water solution from a commercial injector for SCR DeNOx applications". In: *The Proceedings of the 13th Stuttgart International Symposium "Automotive and Engine Technology"*. 2013.

[32] Shi, Xian, Deng, Jun, Wu, Zhijun, and Li, Liguang. "Effect of Injection Parameters on Spray Characteristics of Urea-SCR System". In: *SAE International Journal of Engines* 6.2 (2013), pp. 873–881. DOI: https://doi.org/10.4271/2013-01-1067.

[33] Postrioti, Lucio, Brizi, Gabriele, Ungaro, Carmine, Mosser, Mark, and Bianconi, Francesco. "A methodology to investigate the behaviour of urea-water sprays in high temperature air flow for SCR de-NOx applications". In: *Fuel* 150.x (2015), pp. 548–557. DOI: 10.1016/j.fuel.2015.02.067.

[34] Brizi, Gabriele, Postrioti, Lucio, and Vuuren, Nic van. "Experimental analysis of SCR spray evolution and sizing in high-temperature and flash boiling conditions". In: *SAE International Journal of Fuels and Lubricants* 12.2 (2019), pp. 87–107. DOI: 10.4271/04-12-02-0006.

[35] Lieber, Christian, Koch, Rainer, and Bauer, Hans-jörg. "Microscopic Imaging Spray Diagnostics under High Temperature Conditions : Application to Urea – Water Sprays". In: *Applied sciences* (2019). DOI: 10.3390/app9204403.

[36] Kapusta, Łukasz Jan, Sutkowski, Marek, Rogóż, Rafał, Zommara, Mohamed, and Teodorczyk, Andrzej. "Characteristics of Water and Urea–Water Solution Sprays". In: *Catalysts* 9.9 (2019), p. 750. DOI: 10.3390/catal9090750.

[37] Giraldo Valderrama, Jhoan Sebastián. "Macroscopic and microscopic characterization of non-reacting diesel sprays at low and very high injection pressures". In: November (2018).

[38] Reitz, Rolf Deneys and Bracco, Frediano V. "Mechanism of breakup of round liquid jets". In: *Encyclopedia of Fluids Mechanics* 3 (1984). Ed. by N Cheremisnoff, pp. 233–249.

[39] Baumgarten, C. *Mixture Formation in Internal Combustion Engines.* Springer: Berlin/Heidelberg, Germany, 2006.

[40] Reitz, Rolf D. "Atomisation and other breakup regimes of a liquid jet". PhD thesis. Ph.D. Thesis, Princeton University, 1978.

[41] Lefebvre, Arthur H. and McDonell, Vincent G. *Atomization and Sprays.* Vol. 45. 5. CRC Press, 1990, p. 1435. DOI: 10.1016/0009-2509(90)87140-N.

[42] Venegas, Oscar. "Estudio del fenómeno de la cavitación en la inyección Diesel mediante la visualización del flujo interno en orificios transparentes." PhD thesis. Universitat Politècnica de València, 2014. DOI: 10.4995/Thesis/10251/37375.

[43] Pilch, M. and Erdman, C. A. "Use of breakup time data and velocity history data to predict the maximum size of stable fragments for acceleration-induced breakup of a liquid drop". In: *International Journal of Multiphase Flow* 13.6 (1987), pp. 741–757. DOI: 10.1016/0301-9322(87)90063-2.

[44] Guildenbecher, D. R., López-Rivera, C., and Sojka, P. E. "Secondary atomization". In: *Experiments in Fluids* 46.3 (2009), pp. 371–402. DOI: 10.1007/s00348-008-0593-2.

Chapter 3

Materials and Methods

3.1 Introduction

The experimental tools and data-processing methodologies are listed in this chapter. First, the fluid delivery system and the dosing unit are defined. The next two parts present the experimental instruments where the tests were carried out: the momentum flux test rig, and the high-flow high-temperature test vessel for the visualization. Finally, the optical set-up and techniques for image processing are explained. All the experiments were carried out in the CMT-Motores Térmicos laboratories.

3.2 Injection system

In this thesis, a commercial injection system is employed for the UWS characterization, specifically the Denoxtronic 5 from Bosch, which is used for passenger cars (SUV type) and was depicted in Figure 2.10 in previous chapter. This system should deliver the urea water solution into the exhaust flow with precision. It is composed by the adblue tank, the control unit, the supply module and the dosing unit. The tank contains a heating kit that is used for warming up the UWS when it is at negative temperatures. It is also equipped with a level sensor and a filter to collect any dust or impurity. The control unit calculates the required amount, the supply module brings the fluid to the required pressure and feeds it to the dosing module. The dosing module ensures that precise quantity of UWS is injected and atomized into the

exhaust stream. In order to facilitate the control and the installation of the UWS circuit, the system was adapted for the research and laboratory use.

3.2.1 Dosing system in the laboratory

Figure 3.1 illustrates a diagram of the injection system adapted to laboratory requirements. The basic components of the system are the injector, the pressure unit, and the pulse controllers (frequency controller and injector pulse generator). Since the dosing unit used in this work was a liquid-cooled injector, the temperature of the cooling fluid was controlled using a dedicated heat exchanger. This generic configuration was the one employed in all the experiment campaigns, and the test rig was modified according to the characterization. Each of these components are explained below.

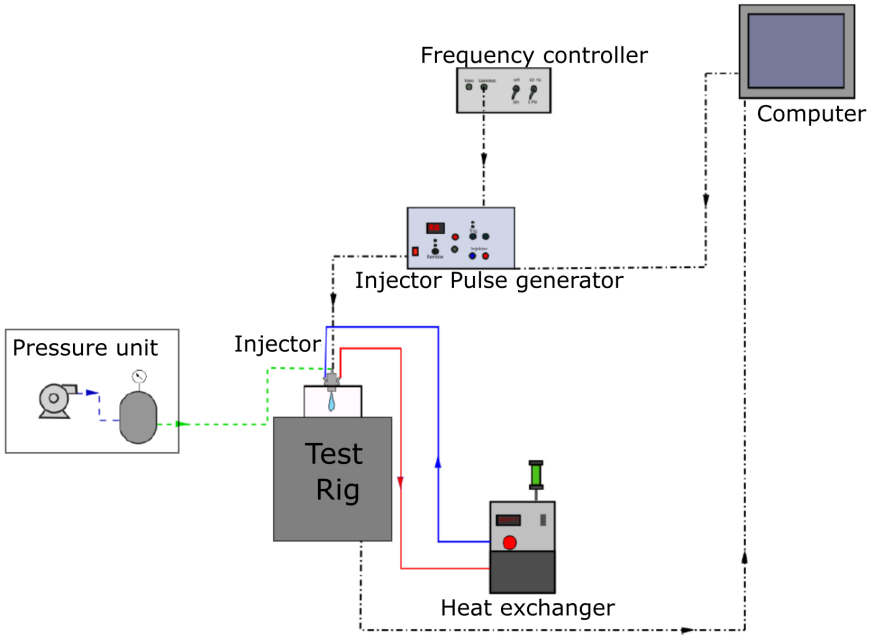

Figure 3.1: Schematic diagram of the dosing system adapted to laboratory requirements.

Pressure unit

A pneumatic system is used to pressurize the injection circuit. The pressure levels for these type of injectors are relatively low (between 3 and 9 bar)

and could be supplied by the compressed air installation available at CMT laboratories. A set of valves and manometers were used to regulate the air delivered by the main compressor of the building that reaches up to 10 bar. Figure 3.2 presents a schematic diagram of the UWS pressure system used in the experiments. The compressed air entered the deposit from the upper part, pressurizing the UWS inside of it. The deposit was connected to a pressure relief valve to avoid over-pressure of the system. Another control valve was used to adjust the injection pressure that goes to the injector. Flexible lines transported the UWS from the deposit to the injector unit. A purger was used to prevent that any air or solid particles reached the dosing unit.

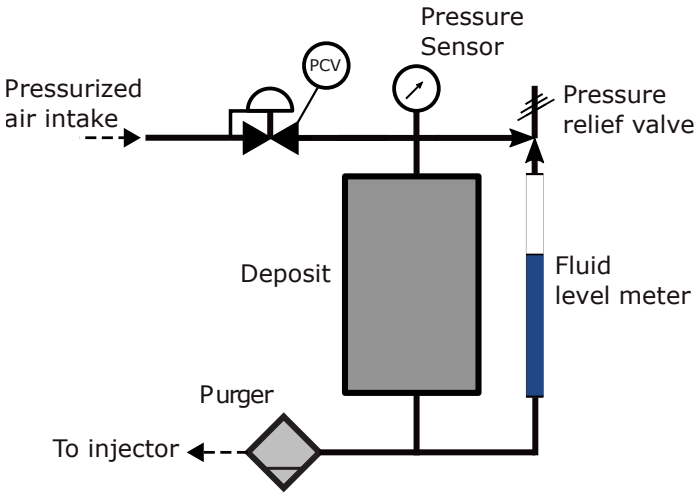

Figure 3.2: Pressure unit schematic diagram.

Urea water solution dosing Unit

As mentioned before, the injector used is a commercially available Denoxtronic 5 dosing unit, with 3 holes from Bosch. The device has a solenoid actuator and operates with injection pressures that are in the range from 3 to 9 bar, to dose quantities from 200 g to 2000 g per hour. The injector is cooled by liquid to preserve the mechanical integrity of the unit. The main characteristics of the injector are summarized in Table 3.1 and pictures of the dosing unit are presented in Figure 3.3. The images at the left side show the external region of the nozzle where the three orifices are visible. The top-left image is a picture of the new injector before the measurements. The bottom-left image depicts the same injector after the operation of the system in the experimental facilities,

showing the formation of urea deposits, which is one of the main issues of this technology. Usually, these deposits are a consequence of improper evaporation of the fluid that are undesired because they block and damage the nozzle. At the end of each test campaign, the dosing unit was unmounted and cleaned for removing the deposits to avoid that those solid particles could affect the functionality of the injector and reliability of the measurements.

Figure 3.3: Dosing unit.

Table 3.1: Injector technical features.

Parameter	**Value**	**Units**
Number of holes	3	-
Avg. outlet diameter ($\overline{D}_o$)	135	µm
Operating pressure	3-9	bar
Operating voltage	12	V
Max. Fluid Temperature	120	°C
Dosing quantity min./max.	200/2000	g/h
Emission target	Euro 6	-

The determination of the real inner geometry of the injector was a difficult task, due to the complexity of the nozzle and because the covering material used as cooling jacket restricted to perform direct measurements of the interior of the holes. Therefore, for the geometrical characterization of the orifices, it was possible to measure only the outer diameter of the three holes, using the optical microscope available at Universitat Politècnica de València. An

example of the images obtained from the microscope is depicted in Figure 3.4. Each frame had its own scale, then the outlet diameter of the nozzle was calculated using a homemade script in Matlab. After 3 repetitions per hole, the average outlet diameter obtained was 135 μm.

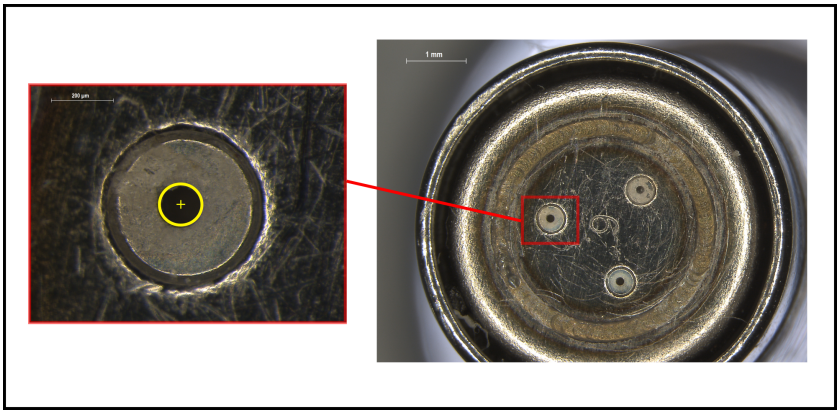

Figure 3.4: Geometrical characterization of the hole outlet with the optical microscope.

Later, for a deeper understanding of the system, the injector nozzle was scanned using X-rays tomography at the "Museo Nacional de Ciencias Naturales" (MNCN - CSIC). One of the main advantages of the tomography scan is that the waves can penetrate through the metal, which permits to visualize the geometry inside the nozzle without disassembling it. The image reconstruction was done using the software "Volumegraphics" provided by the MNCN-CSIC. the Figure 3.5 illustrates an example of the 2D slice images acquired with this technique. The internal inspection reveals that this is a complex element with different layers for temperature isolation. Also, it can be seen that the sac and the orifice configuration is very different from other injection systems used for vehicle applications. The data obtained was rendered and then represented in SolidWorks, specifically in the region near the orifice. This facilitates the analysis of the flow evolution, and will be presented in the next chapter dedicated to the internal flow characterization.

Injector controller

The injector unit has a solenoid valve that controls the opening and closing of the nozzle very precisely. The electrical signal for the solenoid is commanded by the Engine Control Unit (ECU), which in this case was manufactured by

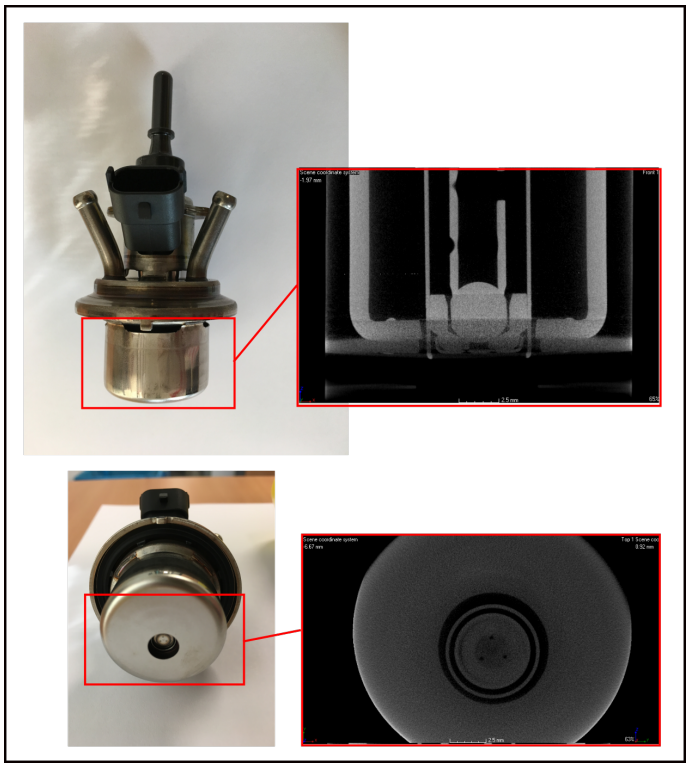

Figure 3.5: Internal inspection of the nozzle using X-rays tomography.

Bosch (depicted in the left side of Figure 3.6). To facilitate the operation of the system in the laboratory, a commercial injector driver was used instead of the ECU. This driver permits to configure the electrical signal required by the injector, reproducing the original signal generated by the ECU. A picture of the driver can be seen in the right side of Figure 3.6. It is controlled with a computer software that defines the parameters of the electrical signal.

There are two main parameters that define the current signal. The first one is the peak current, which is the intensity level needed to break the forces to lift the needle. The second parameter is the current level required to maintain the injector open. The first one indicates the beginning of the injection, and the second one determines the duration of the injection event, also known as energizing time (ET), and the injection quantity is proportional to this variable. Figure 3.7 shows an example of the electrical signal employed.

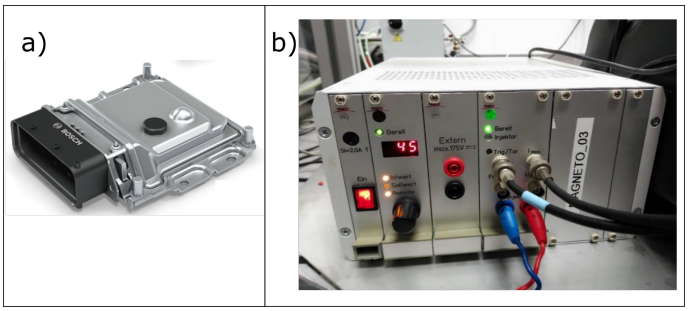

Figure 3.6: Injector signal controller. a) Engine Control Unit from Bosch. b) Commercial injector driver.

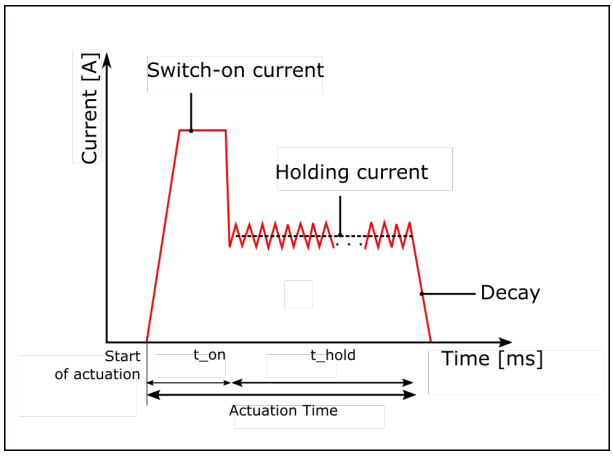

Figure 3.7: Electrical signal definition.

Temperature controller

The temperature of the cooling fluid in the injector was also controlled. This prevents any overheating in the injector tip during operation, and permits to inject the fluid at a constant temperature value during each test condition. The cooling fluid was ethylene glycol ($C_2H_6O_2$), and was regulated using the heat exchanger and a PID shown in Figure 3.8.

3.3 Momentum flux

Momentum flux measurements of the UWS spray were performed in a modified version of the facility built at CMT-Motores Térmicos and developed by

Figure 3.8: Temperature controller.

Gimeno in [1]. Figure 3.9 shows the measurement principle, which consists of a piezoelectric sensor that registers the impact force induced by the spray over it. The sensor should be aligned with the spray plume and placed at a certain distance from the nozzle exit, so all the jets collide with the surface of the target.

If a cylindrical control volume that contains the region comprehended between the nozzle and the piezoelectric transducer is considered, the assumptions listed below can be made [1, 2]:

- The forces related to gravity can be neglected.
- Inside the test vessel the pressure is uniform.
- The flow direction of the gas entering the control volume are perpendicular to the spray axis. Moreover, the direction of the UWS going out after hitting the target of the sensor is perpendicular to the spray axis.

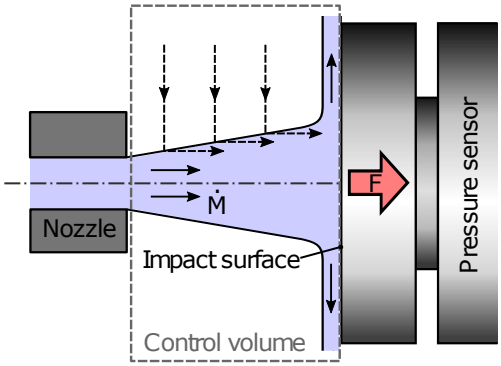

Figure 3.9: Measurement principle of the Spray momentum flux [2].

Thus, the axial component of momentum flux of both fluids through the external surface of the cylindrical control volume, as well as the viscous stress, can be neglected.

Hence, considering the momentum conservation law, and taking into account the simplifications cited, the force F produced by the spray over the surface of the sensor can be expressed as:

$$F = \frac{\partial}{\partial t} \int_{CV} \rho \, u \, d\varpi + \dot{M} \tag{3.1}$$

Where ρ is the density and u is the velocity of the fluid mixture that passes through the control volume. The surface of the control volume is denoted by ϖ is and $\dot{M}$ is the momentum flux at the nozzle exit, which is considered parallel to the axis of the nozzle. For the steady state conditions, the first term which represents the momentum flux variations can be neglected, simplifying Equation 3.1 as:

$$F = \dot{M} \tag{3.2}$$

Therefore, the momentum flux measurement is registered directly from the the signal provided by the sensor. This statement is only true if the spray and the sensor are properly aligned, the target surface is larger than the impact area and the deflected fluid is perpendicular.

3.3.1 Measurement setup

The momentum flux was measured using the setup presented in Figure 3.10 and its main characteristics are shown in Table 3.2. The injector was mounted in the top of the test rig using a customized lid to align the injector axis with the centre of the vessel. The cooling circuit was connected to the heat exchanger to keep a constant dosing unit temperature throughout the experiments. The pressure sensor was placed into a holder that aligns the transducer with the injector axis. Spacers of different sizes were used to set the distance from the sensor to the outlet of the nozzle. The pressure in the chamber was controlled by a set of valves connected to a compressed air line with a pressure regulator or to a vacuum pump, depending on the operating conditions [3]. The gas temperature range in Table 3.2 refers to the limits for which the test rig was designed in [1]. At CMT laboratories there are different ways to achieve those temperatures (in the climatic chamber for low temperatures, and with gas heaters for high temperatures). However, in this part of the work, the gas temperature was kept at standard conditions near $T_{amb} = 298K$.

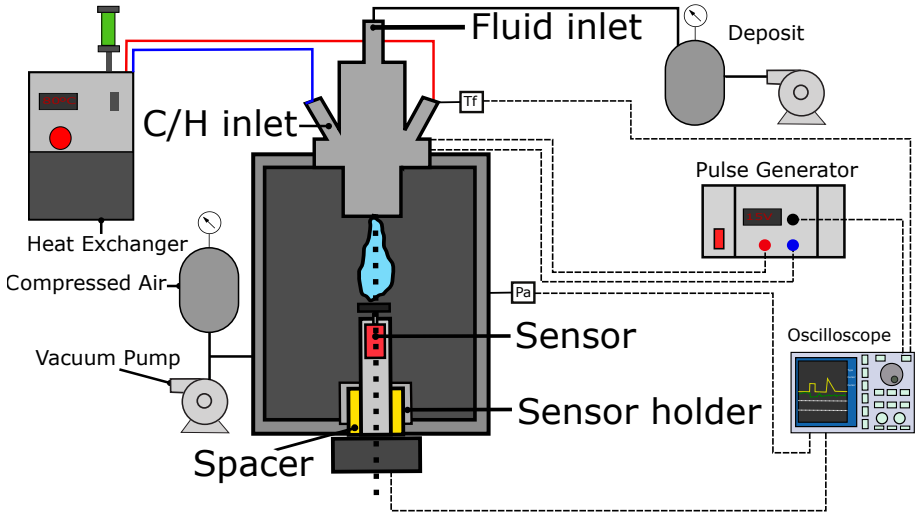

Figure 3.10: Diagram momentum flux test rig.

3.3.2 Measurement procedure

The voltage signals, chamber pressure and momentum flux were recorded using a digital oscilloscope. A total of 50 repetitions per test point were registered with a 1 Hz of frequency (a rate of 1 injection per second). The obtained

Table 3.2: Momentum Flux test rig properties.

Parameter	Range	Units
Facility pressure	0 - 100	bar
Gas Temperature	0 - 300	°C
Cooling system Temperature	5 - 120	°C
Ambient gas	N_2	-

signals have considerable noise. Regarding this aspect, Gimeno [1] made some considerations to explain the possible source of this noise:

- Pressure waves that appear in the feeding lines during the injection event. These waves produce fluctuations in the signal. This effect on the signal is often minimal.
- Dispersion between repetitions due to turbulence inside the injector nozzle that affects internal flow behaviour, as well as in the mixing process of the ambient gas with the injected fluid, which disturbs spray development. The influence of this effect is decreased by measuring several injection events and averaging the momentum flux signal, since turbulence is a random phenomenon.
- Fluctuations in the measured signal due to background noises, mechanical vibrations and acoustic waves that appear in the interaction between the ambient gas and the spray. These three effects are relatively small compared with the momentum flux signal.

The average signal is then calculated using the 50 measurements and the accumulation phenomenon is then corrected [4].

3.4 Injected mass

Injected mass measurements were carried out using the same vessel used for momentum flux measurements but with some modifications to collect the injected mass under different ambient pressures.

3.4.1 Measurement setup

The setup used for the injected mass measurements is displayed in Figure 3.11. It is the same chamber that was employed for measuring the momentum flux,

but the piezoelectric transducer was removed and replaced by a lid. The injected mass was collected using a flask that was attached to the injector holder. The flask had four small orifices at the top that allowed to have the same pressure inside than in the vessel. The chamber volume is big enough to maintain constant the pressure level after all the injection events are done.

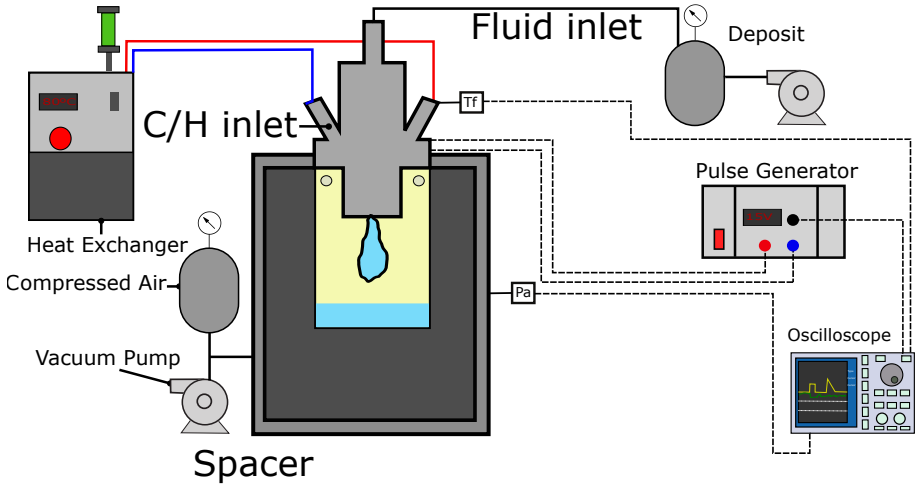

Figure 3.11: Injection Measurement setup schematic diagram.

3.4.2 Measurement procedure

The injected mass was measured using a scale, after 500 injections were collected in the flask. The test conditions for these experiments were the same used for the momentum flux measurements. The injected mass corresponds to the integral of the mass flow rate curve, between the begining and the end of the injection, then it was used to adjust the mass calculated from the momentum flux signals.

3.5 Rate of injection

The rate of injection (ROI) curves can be determined combining the measurements of momentum flux and injected mass. The mathematical definition of mass flow rate and momentum flux is given by Equations 3.3 and 3.4:

$$\dot{m} = A \cdot \rho \cdot u \tag{3.3}$$

$$\dot{M} = A{\cdot}\rho{\cdot}u^2 \tag{3.4}$$

Where $\dot{m}$ is the rate of injection, A is the area of the nozzle exit, ρ is the fluid density, u is the flow velocity at the nozzle exit and $\dot{M}$ is the momentum flux.

Combining both equations 3.3 and 3.4, rate of injection and the momentum flux can be related as:

$$\dot{m} = \sqrt{A.\rho{\cdot}\dot{M}} \tag{3.5}$$

The actual mass flow rate at the hole exit is determined by the fluid density and the velocity profile [2, 5]. The real shape of the velocity profile is difficult to be determined experimentally, but it is possible to define an effective area and an effective velocity that are representative of the flow, as shown in figure 3.12.

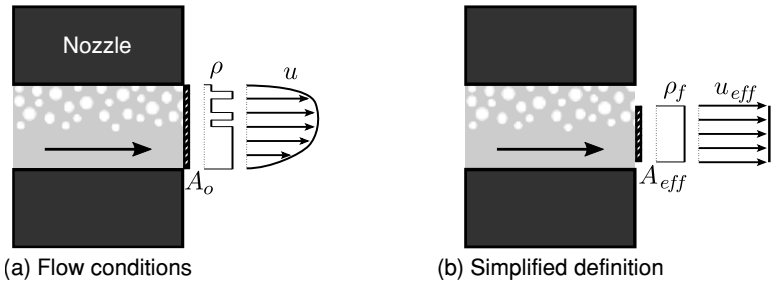

Figure 3.12: (a) Representation of the real flow behaviour: area, density and velocity profile. (b) Representation of the effective area, density, and effective velocity in a nozzle. Adapted from [1].

The definition of those parameters is based on the consideration of a simplified flow that is characterized by an effective area, which is smaller than the geometrical area, and with an effective velocity and density (equal to the density of the fluid) uniform in the entire section. From this assumption, equations 3.3 and 3.4 can be expressed as:

$$\dot{m} = A_{eff}{\cdot}\rho{\cdot}u_{eff} \tag{3.6}$$

$$\dot{M} = A_{eff}{\cdot}\rho{\cdot}u_{eff}^2 \tag{3.7}$$

Equations 3.6 and 3.7 can be written as a function of the velocity u and the area A by means of the discharge coefficient C_d:

$$C_d = \frac{\dot{m}}{A \cdot \rho \cdot u} \tag{3.8}$$

The C_d can be decomposed in two other coefficients as in Equation 3.9, where C_A is the area coefficient and C_V is the velocity coefficient:

$$C_d = C_A \cdot C_V \tag{3.9}$$

$$C_A = \frac{A_{eff}}{A} \tag{3.10}$$

$$C_V = \frac{u_{eff}}{u} \tag{3.11}$$

Based on these assumptions, the momentum flux and the mass flow rate, could be defined as Equation 3.12 and Equation 3.13 respectively:

$$\dot{M} = C_v^2 \cdot C_A \cdot \rho \cdot A \cdot u^2 \tag{3.12}$$

$$\dot{m} = C_v \cdot C_A \cdot \rho \cdot A \cdot u \tag{3.13}$$

Combining Equation 3.12 and Equation 3.13, the injection rate can be expressed as a function of the momentum flux, as is stated in equation 3.14:

$$\dot{m} = \sqrt{C_A \cdot A \cdot \rho} \cdot \sqrt{\dot{M}} \tag{3.14}$$

Therefore, it is possible to calculate the rate of injection based on the experimental data of momentum flux using previous Equation 3.14. Consequently, the injected mass is determined from:

$$m_{inj} = \int_0^t \dot{m} \cdot dt \tag{3.15}$$

Since the injected mass is also measured experimentally, it is possible to compare the calculated injected mass with the measured one (Eq. 3.16) to obtain an adjustment coefficient K. If all assumptions made are correct, the value of the coeffiente K should be a value near one .

$$\int_0^t \dot{m} \cdot dt = K \cdot m_{exp} \tag{3.16}$$

Finally, combining equations 3.14, 3.15 and 3.16, the mass flow can be determined as:

$$\dot{m} = K \cdot \frac{m_{exp}}{\int_o^t \sqrt{\dot{M}} \cdot dt} \cdot \sqrt{\dot{M}} \tag{3.17}$$

3.6 High flow and high temperature installation for UWS spray visualization

The UWS spray development was analyzed experimentally using a novel installation designed in this thesis at the facilities of CMT - Motores Térmicos, which reaches high gas flow and high temperature level. The test rig reproduces realistic operating conditions of flow inside the exhaust line of the engine in a passenger vehicle. It is connected to a chamber with four optical accesses that allow the use of different optical techniques, which are explained in detail in the following subsections.

As mentioned in the literature review in Chapter 2, two different approaches are used for generating the air flow for the visualization of the UWS injection jet in realistic conditions. One method employs a real exhaust gas generated by the operation of a combustion engine. The second procedure uses an installation that provides the air flow at different air temperatures and various mass flow levels, equivalent to the gas condition in the exhaust pipe, for a wide range of engine speeds and loads.

The advantage of performing the measurements directly after the engine is that it allows to carry out the tests in a realistic way. However, this method requires a complex infrastructure for conditioning the system, as well as a dedicated controlling strategy. It also requires a complete exhaust configuration with additional devices, such as a particulate filter and an oxidation catalyst to remove particles and other contaminants. These particles should be avoided in order to have a correct visualization of the spray, without distortion or interference.

The second methodology basically requires a flow generator, such as a blower, and an electrical heater. Controlling this installation is simpler and less costly compared to the previous one. The air flow provided by the blower must be comparable to that of the exhaust gas, so the results obtained can be extrapolated to real operating conditions. The advantage of this type of installation is that the air is cleaner and avoids any optical perturbation during

the spray characterization. Based on this aspect, it was decided to generate the air flow by means of a dedicated installation, using a blower to produce the flow and an electrical heater to reach the desired temperature.

Moreover, for the design of the installation some aspects were considered:

- It must be a flexible test rig that can be relocated to other testing-rooms, since it might be used in other laboratories for different research projects. This restriction means that the installation must be narrower than a single-leaf door and not excessive in length.
- The length of the installation was conditioned by the selection of the air flow measurement system. As will be explained later, a hot-wire flow meter is employed, which requires that the pipe located upstream the sensor has enough length for conditioning the flow. This length is around 10 times the diameter of the flow meter. The pipe length downstream should be between 5 and 10 times the length of the diameter for correct flow measurement. In addition, it should be in horizontal position.
- Several optical tables and breadboards were designed for the positioning of the cameras and the optical material. Therefore, the height of the pipes should match the dimensions of the available optical sets and supports.

3.6.1 Hot-air flow test rig

The installation developed for studying the behavior of the spray in conditions that resemble those of an exhaust line is shown in Figure 3.13.

This test rig is composed of a centrifugal blower, two hot-wire flow meters, a 15-kW electric heater, and a visualization chamber that was used to carry out the experimental measurements. The installation can provide a wide operation range for the study of the spray at conditions of flow and temperature up to 400 kg/h and 400 °C respectively. The test rig aspirates air from its surroundings through the centrifugal compressor, which is then led through pipes, passing the hot-wire flow meter, to the electric heater in which the air is heated to the desired measurement temperature. The heated flow enters the visualization chamber, located after the electric heater, where the UWS is injected into the hot air stream. The flow is continuous and constant during all the tests, allowing the study of the spray under conditions similar to those inside the engine exhaust pipe.

The visualization vessel (Figure 3.14) possesses four optical accesses allowing direct visualization of the UWS spray. The vessel design was performed

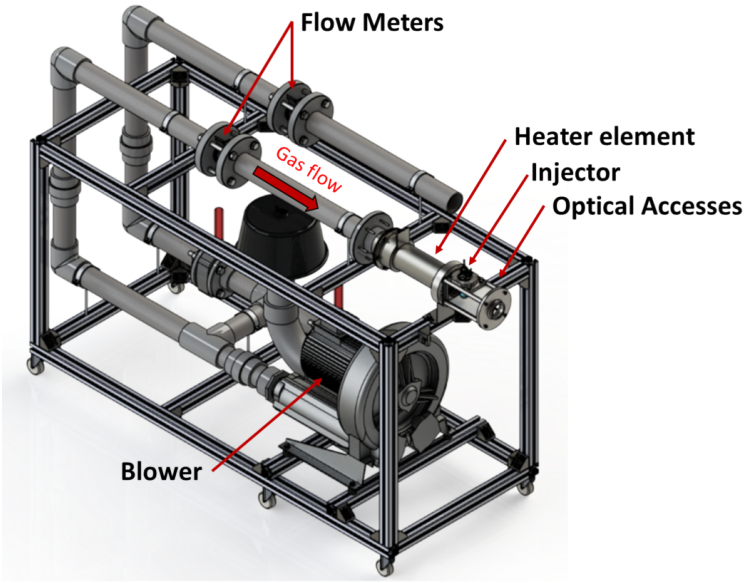

Figure 3.13: Hot-air flow test rig.

based on the dimensions of a standard exhaust pipe for a medium-duty engine. The inlet section has a diameter of 70 mm, and the windows height is 80 mm. It has a modular design and it can be easily rearranged to replicate different configurations of the injector position and the exhaust pipe. The UWS injector is installed in such manner that the whole spray can be registered from the nozzle tip.

Figure 3.15 shows a scheme of the systems and the measurement equipment used. The gas flow inside of the visualization vessel is controlled by a variable frequency driver connected to the centrifugal compressor. The flow passes through a flow meter and a heat resistance before entering the measuring chamber. The temperature of the flow is measured before the flow meter and before entering the chamber. The injector is heated or cooled using the heat exchanger filled with either glycol or oil, depending on the test point and desired temperature.

3.6.2 Control elements and sensors

In addition to the components mentioned in the previous section, there are auxiliary elements that do not create the flow conditions, however, they control the thermodynamic parameters and the main devices. Also, some other

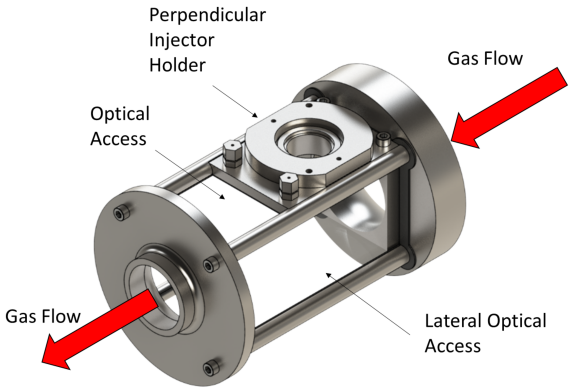

Figure 3.14: Configuration of the optically-accessible section.

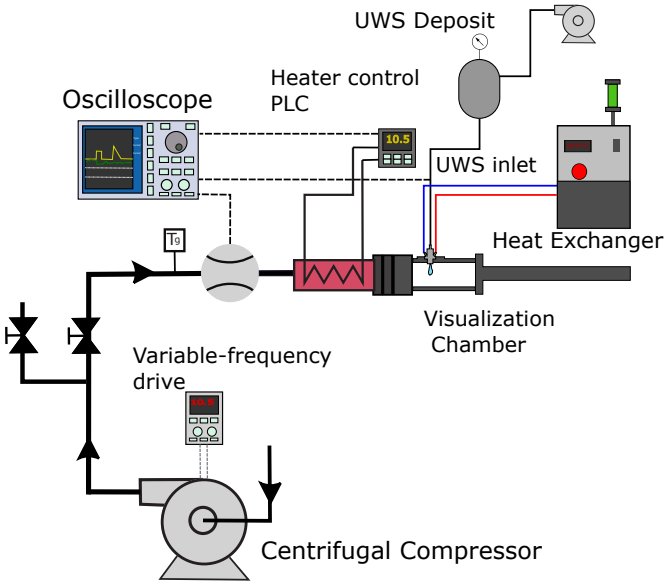

Figure 3.15: Diagram of the visualization test rig setup.

elements register and record the conditions that are obtained in the installation. The variables that are registered and controlled in the flow test rig and in the visualization chamber are the air flow, the temperature and the pressure.

Air mass flow measurement

The air mass flow should be proportional to the blower speed. To control the speed of the blower a frequency inverter of 3.7kW was used.

To ensure a correct operation of the installation, the air mass flow must be measured with accuracy. Then, a flow meter is calibrated and mounted. The flow meter used is a Siemens type 5WK9623. The operation of this instrument is based on the measurement of the output voltage of the transducer, which is formed by the hot wire and a signal conditioning system that depends on the speed of the fluid. The air flow installation used for the calibration of this device was designed for previous research activities at CMT-Motores Térmicos, and is depicted in Figure 3.16. It has a calibrated flow sensor that is used as reference.

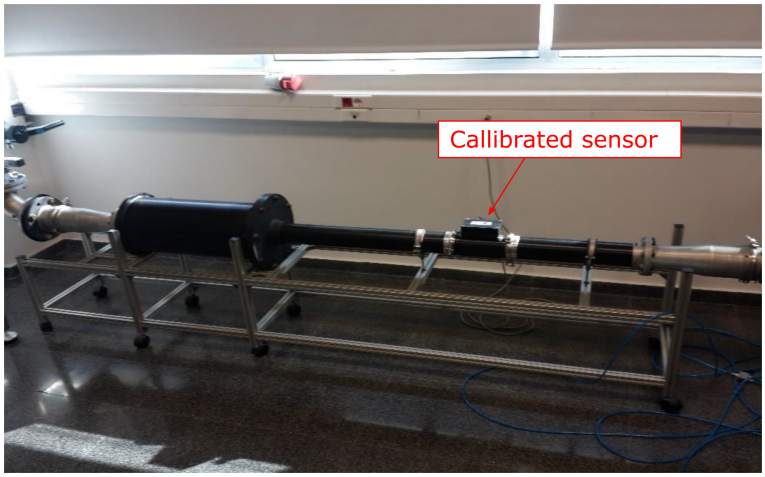

Figure 3.16: Test bench used for the flow meter calibration.

The calibration procedure was performed in a range of [0-450] kg/h, which is the expected operation range of the system. The obtained results are shown in Figure 3.17. As expected, the mass flow is proportional to the frequency, with a linear response. On the other hand, the relationship between the voltage and the mass flow is characterized by means of two equations, a potential function for mass flow values under 185 kg/h, and a linear expression for bigger values. Based on this behaviour, an algorithm was prepared to translate the voltage into mass flow (or vice-versa) using these expressions. This information is sent to the digital oscilloscope and to the system controller.

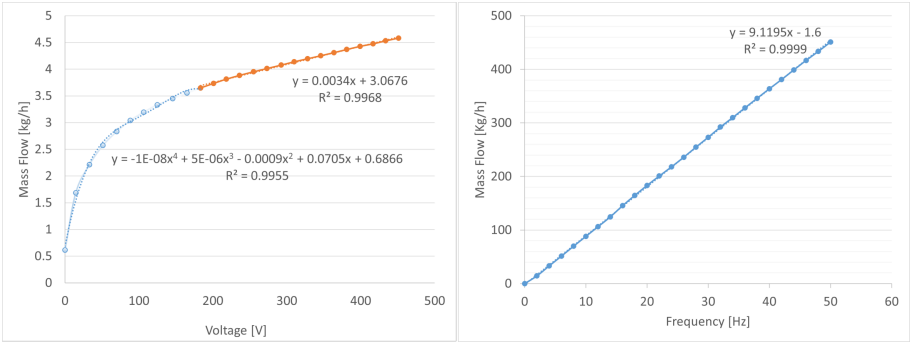

Figure 3.17: Calibration curves of the mass flow meter.

Temperature measurement

Regarding the temperature, there are different points where it was registered. First, the temperature of the air must be measured before the heater. For that purpose, two thermocouples were installed after the flow meters and before the heater, as can be seen in Figure 3.18.

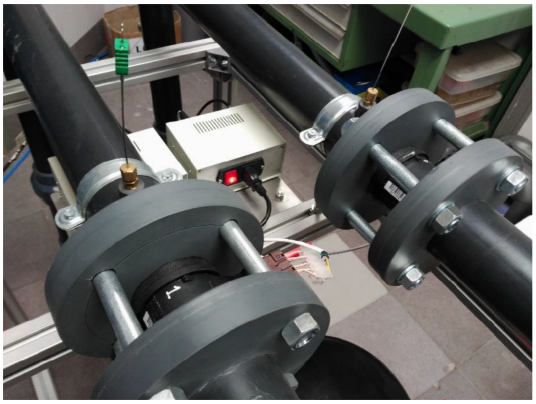

Figure 3.18: Mass flow meter and thermocouples used in the high flow test rig.

Second, the air temperature is registered after passing through the heater, in order to control the current applied to the electric heating element. For this, a temperature control flange was designed, which was placed between the resistor and the visualization chamber, as shown in Figure 3.19. The transducers of the control flange measured the temperature and transformed it to an electrical signal that was sent to a PID from Leister. This device

controlled the resistance power, in order to maintain the air at the desired temperature.

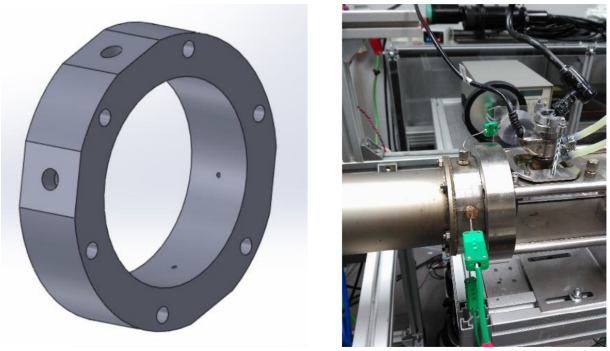

Figure 3.19: Temperature control flange.

Finally, the temperature of the injector tip was also controlled in the visualization test-rig. The temperature controller used for the hydraulic characterization (depicted in Figure 3.8) was employed in this facility as well.

Pressure measurement

Since this dosing unit works with relatively low pressures, it was not necessary to use an external pressure device. As mentioned in previous section, the pressure was supplied by the pressurized line at CMT air system. Then, the pressure was measured using two Bourdon gauges, one located at the main supply line, and the other one measured the pressure at the line upstream the injector. This transducers are depicted in Figure 3.20.

Other electronic components

Finally, in order to control all the electrical elements, an electrical panel has been constructed (Figure 3.21), which consists of the following elements:

- Differential switch: It is responsible for switching the installation on and off. It is a safety element that switches off the system in case of detecting any current leakage.
- Contactor: It is an actuator that can cut off the electrical current of the installation, and can be operated remotely. In this case it is used to cut the current of the relay that supplies the electric resistance in case of emergency (it is controlled with a pushbutton).

Figure 3.20: Pressure gauges employed in the installation.

- Breaker: It is a safety element that is responsible for cutting off the current in case of exceeding maximum current or temperature values that could overload the system and damage the installation.
- Power supply: It is a 24V power supply, whose function is to supply the circuit with the required voltage.
- Transformer: Responsible for transforming the current from 380 to 230 V before the contactor.

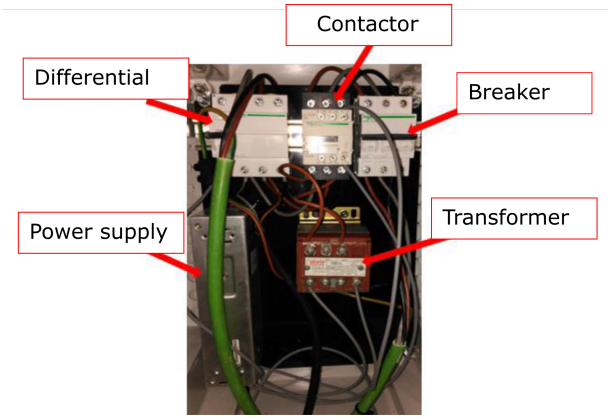

Figure 3.21: Electrical board of the installation.

3.7 Optical techniques

Optical diagnostics are powerful tools that offer a non intrusive method to experimentally measure desired variables. They date back to the nineteen century [6] and have been evolving ever since, with the invention of new technologies and the advances in lasers, high recording speed cameras, optics and illumination. This progress allows a broad range of setups for measuring numerous variables in the UWS spray development such as: spray penetration, opening angle, droplet diameter and velocity, with high recording frequencies, over 120000 frames per second (fps) [7–10].

This section shows the basic principles of the optical arrangements that were used. The penetration of the spray and the spreading angle were measured using a diffused back-illumination (DBI) technique. This technique was also applied to determine the droplet diameter and velocity, exchanging some elements to concentrate the light in the desired region and using a different lens.

3.7.1 Diffused back-illumination

Penetration of the liquid phase of the spray is normally used in the literature to characterize the mixing process of sprays in engine applications [11–13]. The penetration of sprays can be measured through various optical arrangements that use visible-wavelength light as the source of illumination [13–15]. An example of these arrangements are light scattering techniques that capture the rays elastically scattered by the droplets by means of high-speed cameras [14–16]. Diffused back illumination is a method commonly used in measurements that allow line-of-sight visualization, where light is extinct due to the optical depth (τ) of the spray or droplets.

The advances in technology and more specifically, the introduction of fast light emitting diodes (LED) made possible the improvement of the quality of the images obtained throught the DBI technique. The length or duration of the light pulse can be set to low values, reaching the order of nanoseconds and therefore governing the amount of light available in each frame instead of the exposure of the camera. This is an advantage because the images are sharper than those captured with any other continuous light source [8, 13, 14, 17, 18].

This setup was developed by Ghandhi and Heim [19]. It is composed of a high-speed camera, field lens, a diffuser and a light source, as shown in Figure 3.22. A LED unit was equipped with a parabolic reflector to reduce the light aperture angle from 120° to 25° and minimize light loss. Light beams were directed to a 100 mm engineered diffuser with 20.5° of divergence

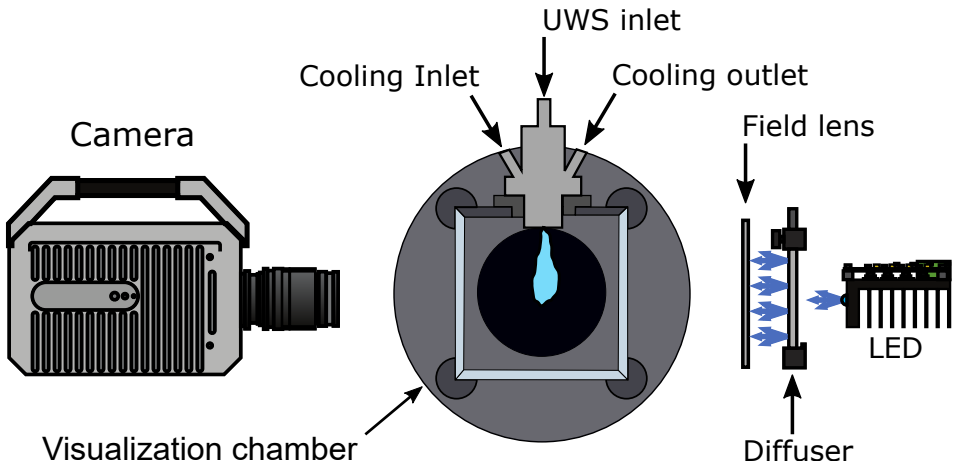

Figure 3.22: Diagram of the diffused back-illumination setup used for the visualization of the spray.

angle. A Fresnel lens with a focal length of 67 mm was located such that the diffused illumination source was reproduced near the optical plane of the spray visualized. The setup is used to determine the spray penetration and spreading angle of the spray.

3.8 Image processing methods

3.8.1 Spray penetration and spreading angle

The Spray penetration and spreading angle are usually measured in diesel and gasoline sprays by finding the contour of the spray and analyzing its geometric properties for each time step. In urea-water solution sprays this approach is not always the best due to the different atomization regimes. This difference results in a bigger gap between the particles of the spray, especially at the beginning of the injection, and thus making difficult the proper detection of the contour using traditional methods as shown in Figure 3.23. In the figure different frames of the same injection event are presented where the detected contour can be observed in red. Meanwhile inside the blue circles a considerable amount of particles of the spray are observed which could not be detected by the classic detecting algorithm employed for other injection systems used in engines.

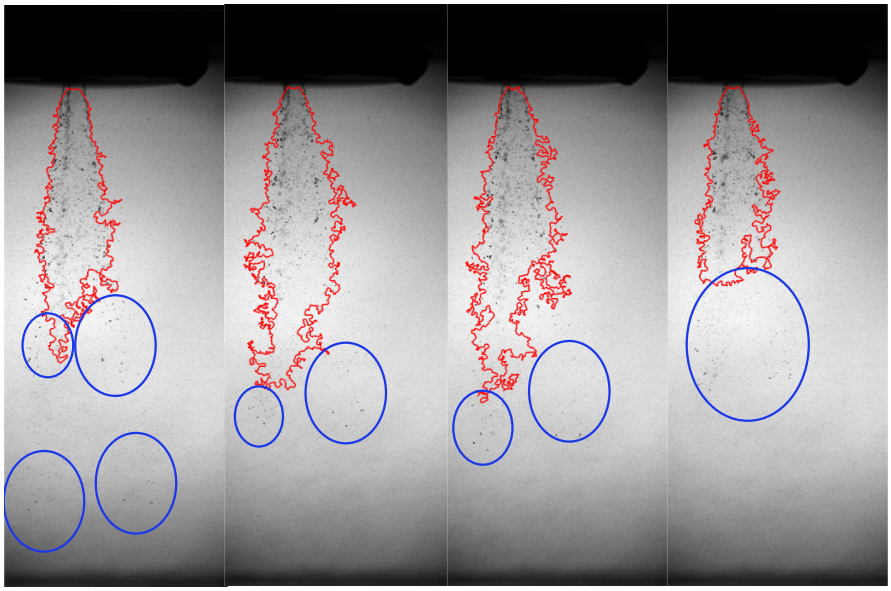

Figure 3.23: Classic contour detecting algorithm (red lines) and region of droplets that are not detected (blue lines).

Furthermore, a characteristic found during the study of these injectors is that the spray is divided in two regions: the initial burst and the body of the spray. In Figure 3.24, the distances and the angle that will be measured from the images are presented.

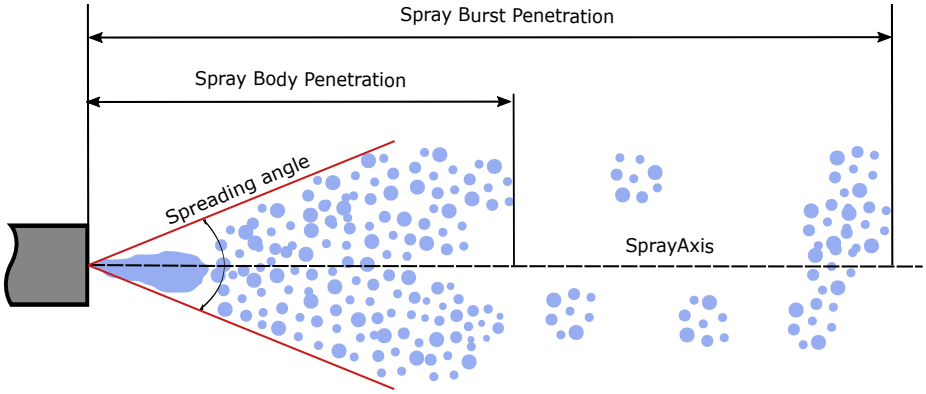

Figure 3.24: Sketch of the UWS spray morphology and burst definition

The main issue with this sprays is separating the small initial burst from

the body to measure both penetrations. In this work a new methodology is developed, where the images are processed following these steps:

- **Background correction:** for removing reflections and back-drop objects that could generate erroneous estimations of the spray. The background is the image acquired before the start of injection and it is subtracted arithmetically from spray images.
- **Image binarization:** a thresholding technique is applied to each frame to transform the gray scale image into a black and white one, where the white pixels indicate the presence of the spray. The binarization threshold is kept high enough to mitigate the noise related to the background, camera sensor noise or beam steering, but low enough to ensure a robust detection of the liquid. This threshold is set accordingly after several iterations, where the best trade off is found for the dynamic range of each image.
- **Intensity curve determination:** the sum of the intensity of each pixel row of the image is then calculated. This results in an intensity curve where it is possible to discern where the presence of liquid is sufficient to be considered part of the spray. In Figure 3.25, four different time steps measured from the start of the energizing are presented, where a binarized image of the spray alongside its respective intensity curve is shown for each one of them.

  In the first two frames, the initial burst of the spray (explained in Figure 3.24) can be observed, and as the spray moves downward the intensity of this burst diminishes and only the intensity of the spray body is then captured in the intensity curves.
- **Separation of Spray burst and body:** after the intensity curves are determined for every time step, the front of the spray is calculated. The penetration of the spray burst is computed based on the furthest row with an intensity value over 5% of the maximum possible intensity. In addition, for the body of the spray the same condition is applied, and the algorithm corroborates that there is a continuous intensity signal from the start of the jet.

For the spray spreading angle, a similar approach used for other automotive sprays was applied. Additionally, since the initial spray burst is not continuous and relatively short, the spray body penetration was the reference in the

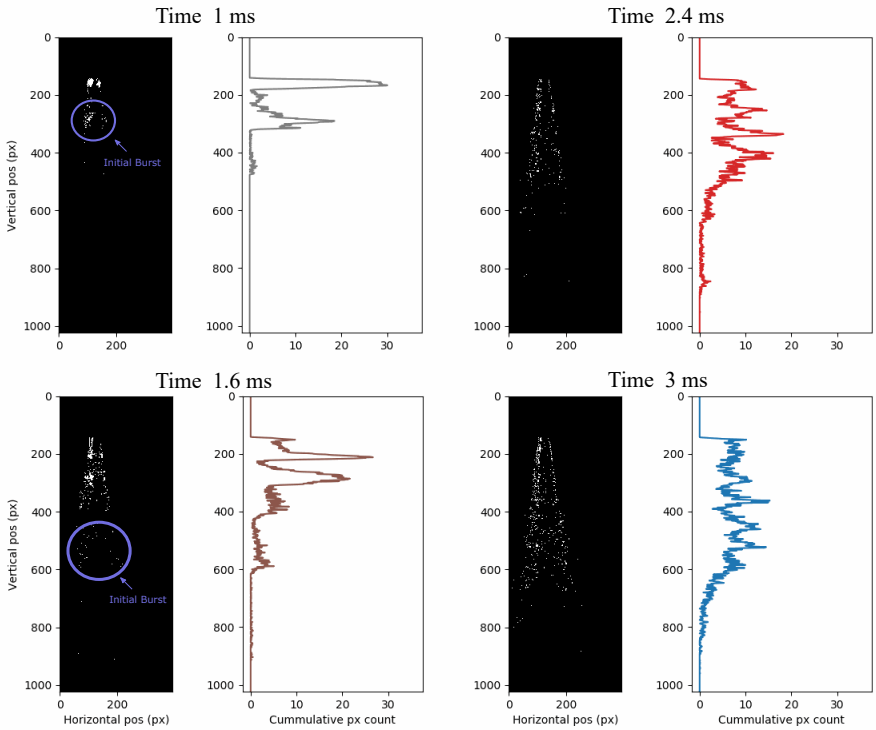

Figure 3.25: Binary image alongside the cumulative pixel count curve for four different time steps.

determination of the distances used for the angle calculations, as shown in Figure 3.26. The opening between the outer boundaries of the spray at the distances of 6% and 12% of the penetration (S) at each time step was obtained. Then, the spreading of the spray is defined as the angle between the lines drawn in each side of the spray.

Droplet size determination

The droplet size determination was based on the methodology presented in [9]. The general configuration presented in Figure 3.22 was used for the near-field visualization. The lens was replaced by the K2 DistaMax microscopic lens that allows a more detailed visualization of the spray. This setup is shown in Figure 3.27

This microscopic lens provided enough magnification, therefore, the droplets of the UWS spray can be captured and measured, allowing the deter-

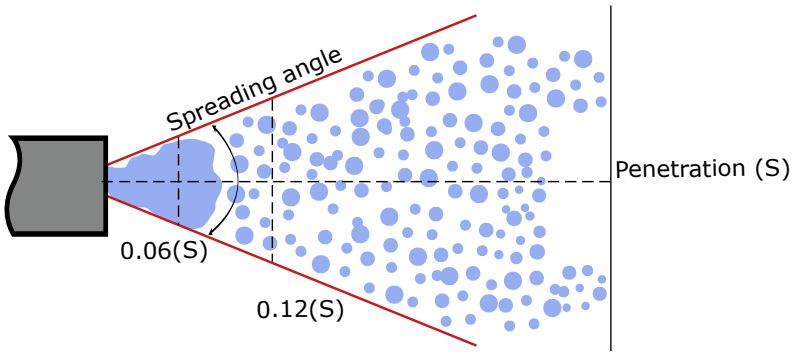

Figure 3.26: Measuring distances for the spray angle determination

mination of their diameter, trajectory, and velocity. The main difficulty of this optical arrangement is the small depth of field of approximately 1 mm, which provokes that some some of the particles appear out of focus. To overcome this issue the images were processed following these steps:

- **Filtering the out of focus droplets:** the unfocused structures on the frame were filtered using a dynamic threshold. Those droplets had low contrast and appeared more blurred the further away they are from the focal plane.

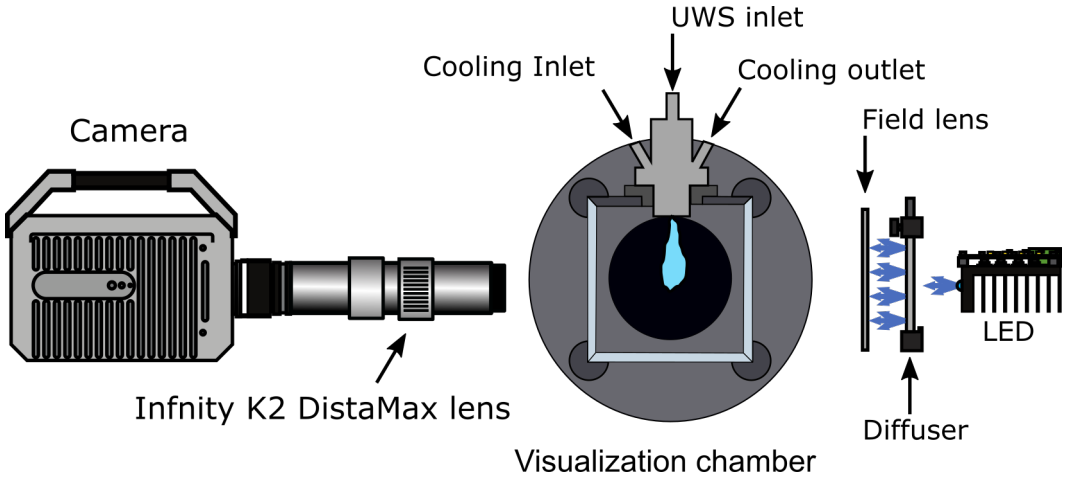

Figure 3.27: Schematic diagram of the diffused back-illumination setup used for the visualization of the droplets.

- **Image binarization:** after the filtering of the droplet out of focus, a binarization of the image takes place. This step simplifies the calculation of the droplet properties.
- **Determination of the properties:** for each detected droplet, several properties were extracted using an image processing tool developed in Matlab. It was focused on obtaining the area of each droplet and its location coordinates for all the time steps.
- **Filtering of the droplet by residence time**: During the measurement, many droplets appear in focus just for a couple of frames. As it is explained in Section 3.8.1, in order to keep only those droplets that could be tracked, the droplets found with this method were cross-referenced with the one used to calculate the velocity of the droplets, and only the matching droplets were kept.

A more detailed explanation of the methods used for the droplet visualization and image processing can be found in the studies of Manin et al. [8], Blaisot and Yon [20], and Payri et al [10].

Droplet velocity

The microscopic visualization was performed using the high-speed cameras, then the droplets can be identified and tracked for each frame. The velocity of each droplet can be determined from the ratio between the particle displacement and the time frame. This procedure was detailed in the work published in [9]. The processing is done considering only those particles that comply with certain parameters, which are:

- Detection of the droplets: After removing the background, the threshold was applied to each image, and the size and location properties were obtained (as showed in Figure 3.28). Then, the resulting filtered image was used for tracking the droplets. This step goes along with the determination of the droplet size.
- Frame to frame position: It was defined a search radius in the algorithm for locating the particles that have similar properties in consecutive frames. Thanks to the high recording speed of 150,000 frames per second, the length of the search radius became smaller, avoiding interferences with other droplet search regions.

- Residence time setting: As mentioned in Section 3.8.1, the volume in which the droplets were detected was small, and some particles might pass through this space, staying in focus for a short period of time. A residence time was set to filter these droplets. Then, the algorithm ignored those drops which did not appear in the images for a certain number of frames.

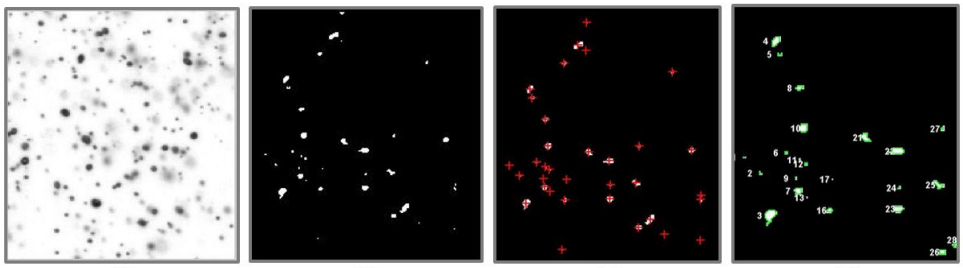

*Figure 3.28: Steps for the detection of the droplets at each frame:(**a**) Image with subtracted background. (**b**) Binarized image. (**c**) Detection of the droplet. (**d**) Tagged droplets.*

The information of the droplet position in each time step was used to track the trajectory, as illustrated in Figure 3.29.

The velocity in each direction of every droplet is calculated by subtracting its position from previous frame and then dividing it by the time step, following the equation:

$$U_i = \frac{X_{t_i} - X_{t_{i-1}}}{\Delta t} \tag{3.18}$$

where U_i is the velocity of the droplet i between two consecutive frames, X_{t_i} and $X_{t_{i-1}}$ are the coordinates of the droplet center of mass in each image and Δt is the time between each frame. The mean velocity of the droplet was estimated as the average of all the values obtained.

3.9 Summary

This chapter presented all the experimental instruments, optical configurations and data processing routines used in the experimental campaigns. First, the fluid injection system and the dosing module have been described. The next section presented the testing facilities, explaining the principles and methods for measuring. The optical diagnostic configurations used to measure

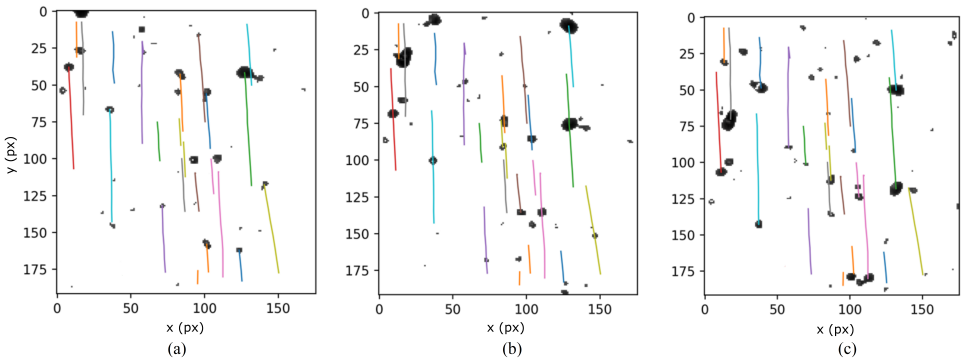

*Figure 3.29: Trajectory of droplets at different frames: (**a**) 1780 µs, (**b**) 1806 µs, and (**c**) 1838 µs After Start of Energizing.*

the macroscopic and microscopic properties of the spray are discussed. Lastly, the image and data processing routines are detailed for each of the acquisition strategies used.

References

[1] Gimeno, Jaime. "Desarrollo y aplicación de la medida de flujo de cantidad de movimiento de un chorro Diesel". PhD thesis. E.T.S. Ingenieros Industriales, Universidad Politécnica de Valencia, 2008. DOI: 10.4995/Thesis/10251/8306.

[2] Payri, R., García, J. M., Salvador, F. J., and Gimeno, J. "Using spray momentum flux measurements to understand the influence of diesel nozzle geometry on spray characteristics". In: *Fuel* 84.5 (2005), pp. 551–561. DOI: 10.1016/j.fuel.2004.10.009.

[3] Payri, Raúl, Bracho, Gabriela, Martí-Aldaraví, Pedro, and Moreno, Armando. "Using momentum flux measurements to determine the injection rate of a commercial Urea Water Solution injector". In: *Flow Measurement and Instrumentation* 80 (2021), p. 101999. DOI: https://doi.org/10.1016/j.flowmeasinst.2021.101999.

[4] Payri, R., Salvador, F. J., Gimeno, J., and Bracho, G. "A new methodology for correcting the signal cumulative phenomenon on injection rate measurements". In: *Experimental Techniques* 32.1 (2008), pp. 46–49. DOI: 10.1111/j.1747-1567.2007.00188.x.

[5] Bracho, Gabriela. "Experimental and theoretical study of the direct diesel injection process at low temperatures". PhD thesis. E.T.S. Ingenieros Industriales, Universidad Politécnica de Valencia, 2011.

[6] Miles, Richard B. "Optical diagnostics for high-speed flows". In: *Progress in Aerospace Sciences* 72 (2015), pp. 30–36. DOI: 10.1016/j.paerosci.2014.09.007.

[7] Payri, Raul, Viera, Juan Pablo, Wang, Hua, and Malbec, Louis-Marie. "Velocity field analysis of the high density, high pressure diesel spray". In: *International Journal of Multiphase Flow* 80 (2016), pp. 69–78. DOI: 10.1016/j.ijmultiphaseflow.2015.10.012.

[8] Manin, Julien, Bardi, Michele, Pickett, Lyle M., Dahms, Rainer N., and Oefelein, Joseph C. "Microscopic investigation of the atomization and mixing processes of diesel sprays injected into high pressure and temperature environments". In: *Fuel* 134 (2014), pp. 531–543. DOI: 10.1016/j.fuel.2014.05.060.

[9] Payri, Raul, Bracho, Gabriela, Gimeno, Jaime, and Moreno, Armando. "Investigation of the urea-water solution atomization process in engine exhaust-like conditions". In: *Experimental Thermal and Fluid Science* 108.June (2019), pp. 75–84. DOI: 10.1016/j.expthermflusci.2019.05.019.

[10] Payri, Raul, Gimeno, Jaime, Bracho, Gabriela, and Moreno, Armando. "Spray characterization of the Urea-Water Solution (UWS) injected in a hot air stream analogous to SCR system operating conditions ." In: *WCX SAE World Congress Experience* 2019-01-0738 (2019), pp. 1–9. DOI: 10.4271/2019-01-0738.Abstract.

[11] Siebers, Dennis L. "Liquid-Phase Fuel Penetration in Diesel Sprays". In: *SAE Technical Paper 980809* (1998), pp. 1–23. DOI: 10.4271/980809.

[12] Hulkkonen, Tuomo, Sarjovaara, Teemu, Kaario, Ossi, Hamalainen, Ismo, and Larmi, Martti. "Experimental Study of Conical Diesel Nozzle Orifice Geometry". In: *Atomization and Sprays* 25.6 (2015), pp. 519–538. DOI: 10.1615/AtomizSpr.2015010383.

[13] Payri, Raul, Bracho, Gabriela, Marti-Aldaravi, Pedro, and Viera, Alberto. "Near field visualization of diesel spray for different nozzle inclination angles in non-vaporizing conditions". In: *Atomization and Sprays* 27.3 (2017), pp. 251–267. DOI: 10.1615/AtomizSpr.2017017949.

[14] Bardi, Michele et al. “Engine Combustion Network: Comparison of Spray Development, Vaporization, and Combustion in Different Combustion Vessels”. In: *Atomization and Sprays* 22.10 (2012), pp. 807–842. DOI: 10.1615/AtomizSpr.2013005837.

[15] Payri, Raul, Garcia-Oliver, Jose Maria, Bardi, Michele, and Manin, Julien. “Fuel temperature influence on diesel sprays in inert and reacting conditions”. In: *Applied Thermal Engineering* 35.1 (2012), pp. 185–195. DOI: 10.1016/j.applthermaleng.2011.10.027.

[16] Payri, Raul, Salvador, Francisco Javier, Gimeno, Jaime, and Viera, Alberto. “10 Tagung Diesel- und Benzindirekteinspritzung 2016-2017”. In: *10. Tagung Diesel- und Benzindirekteinspritzung 2016*. Ed. by Helmut Tschöke and Ralf Marohn. 1. Springer, 2017, pp. 133–152. DOI: 10.1007/978-3-658-15327-4.

[17] Jung, Yongjin, Manin, Julien, Skeen, Scott A, and Pickett, Lyle M. “Measurement of Liquid and Vapor Penetration of Diesel Sprays with a Variation in Spreading Angle”. In: *SAE Technical Paper 2015-01-0946* (2015). DOI: 10.4271/2015-01-0946.

[18] Manin, Julien, Bardi, Michele, and Pickett, Lyle M. “Evaluation of the liquid length via diffused back-illumination imaging in vaporizing diesel sprays”. In: *The Proceedings of the International symposium on diagnostics and modeling of combustion in internal combustion engines*. Vol. 8. Fukuoka, 2012, pp. 665–673. DOI: 10.1299/jmsesdm.2012.8.665.

[19] Ghandhi, J B and Heim, D M. “An optimized optical system for backlit imaging”. In: *Review of Scientific Instruments* 80.5 (2009). DOI: 10.1063/1.3128728.

[20] Blaisot, J. B. and Yon, J. “Droplet size and morphology characterization for dense sprays by image processing: Application to the Diesel spray”. In: *Experiments in Fluids* 39.6 (2005), pp. 977–994. DOI: 10.1007/s00348-005-0026-4.

Chapter 4

UWS Hydraulic performance

4.1 Introduction

This chapter describes the hydraulic characterization of the UWS injector. The first part presents the test plan with the different test conditions. Afterwards the results are presented in this order: first the momentum flux results, then injected mass and calculated rate of injection results, and finally the analysis of the discharge coefficient of the nozzle. Lastly, a summary of the obtained results is listed.

4.2 Hydraulic characterization test plan

The conditions selected for the hydraulic characterization are used to analyze their effect over the injector performance. The test consisted of a single injection event of 5 ms, modifying the injection pressure in three different levels, 4, 6 and 8 bar. The discharge pressure was varied in four different levels, from 0.75 to 2 bar (absolute), covering values below (vacuum) and over atmospheric pressure. Furthermore, the fluid temperature was also controlled to study its effect over the spray, setting this variable at 60 ºC, 90 ºC and 120 ºC. This test plan was applied for the momentum flux and injected mass measurements using two fluids, UWS and water. The test matrix is summarized in Table 4.1

The test plan consisted of 72 experimental points for the hydraulic characterization. Each test condition had two repetitions. Line pressure levels were selected considering normal operating conditions for this kind of injector

Table 4.1: Experimental conditions.

Injection Pressure	4-6-8 bar
Injector cooling temperature	60-90-120 °C
Energizing time	5 ms
Discharge Pressure (absolute)	0.75, 0.90, 1.0, 2.0 bar
Fluids	Water and UWS

and manufacturer guidelines. The discharge pressure levels were selected to resemble conditions from high altitude to high load conditions in the exhaust line.

4.3 Momentum flux results

The first step is to configure the distance between the nozzle exit and the piezoelectric transducer. The separation should be enough to capture the whole spray with the sensor target. Also, the momentum flux in the steady zone of the injection should be independent on the sensor position. For these reasons, different distances of the sensor location were tested. In Figure 4.1, the momentum flux signals acquired for distances of 2, 5, 8 and 11 mm between the nozzle exit and the sensor are depicted.

Some differences were observed in the momentum flux signals for the tested positions. The begining and ending phases of the curve are not in the same time (the horizontal axis represents the time after start of energizing of the solenoid). When the sensor is placed further away from the nozzle tip there is a displacement to the right side of the plot, due to the longer travel time of the spray before hitting the sensor. The signals from 2, 5 and 8 mm distances are similar in the steady phase of the injection curve, meanwhile at 11 mm the signal is lower (on average 8% lower). This can be attributed to a greater cross section of the spray, then the sensor target does not capture the momentum of the whole plume.

Based on the results presented in Figure 4.1, the 5 mm distance was chosen to perform the momentum flux measurements of this work. At this position, the stabilized signal did not differ in a significant amount respect to the signal from 2 and 8 mm. From this point forward, all the results correspond to the measurements carried out with the sensor at 5 mm from the nozzle exit.

Another phenomenon was observed in 4.1 at the begining of the injection event. The initial part of the injection curve had a strong fluctuation. This can be attributed to the packages of fluid leaving the nozzle at the beginning

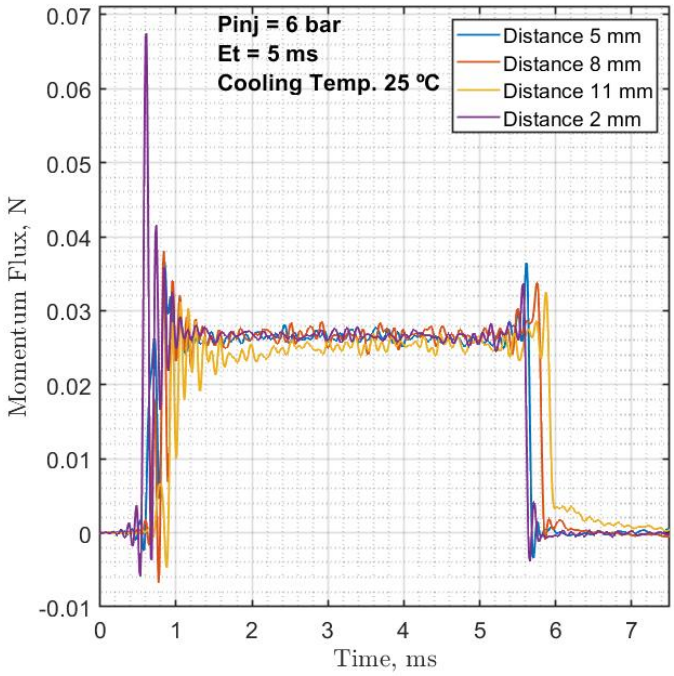

Figure 4.1: Signal of Momentum flux at four distances between nozzle and sensor

of the injection event, where the dynamics of the injector plays an important role. This was confirmed by additional visualization of the spray at the nozzle exit, during the start of injection. The test images were reported in the work of Payri et al. [1] and are shown in Figure 4.2. In the first four frames (A, B, C and D), packages of fluid that leave the nozzle unsteadily can be seen. The droplet quantity and shape vary in the first moments of the injection event, and the initial bursts present ligaments and blobs. Afterwards, the density of packages seems smaller for a few moments (E and F), until a new burst of packages appears showing different morphology of ligaments and bigger blobs (G and H) than those observed in the first instant. Later, after 0.8 ms approximately, the injection stabilizes and the fluid delivery is more uniform.

Effect of the pressure on the momentum flux

This section presents the effect of the injection pressure and the discharge pressure on the momentum flux for water and UWS. In order to compare

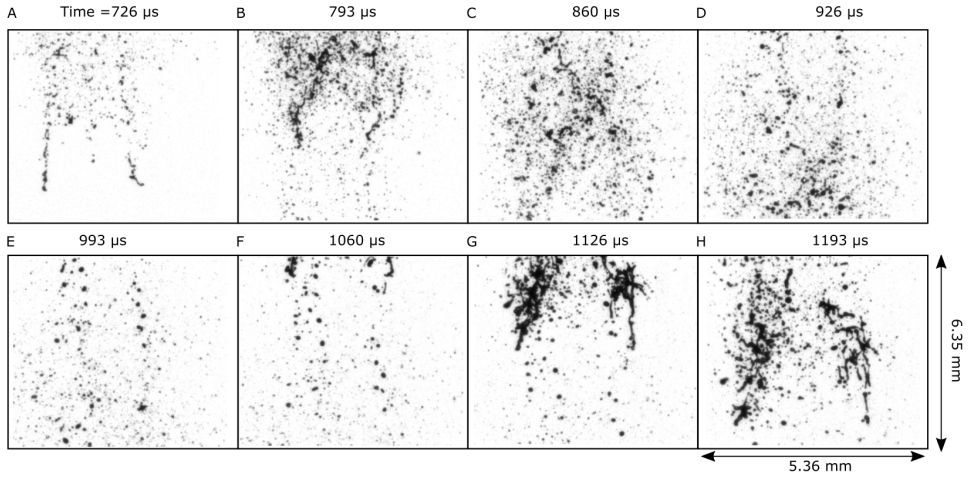

Figure 4.2: Images of the spray at 4 mm from the hole exit. Time is measured After Start Of Energizing (ASOE).

the effects of the different conditions on the spray momentum, an average of the steady region of the signal was calculated in the time window from 2.5 ms to 5 ms after the start of energizing. Figure 4.3 shows an example of the momentum flux signal. The time interval used for the averaging is represented with red dashed vertical lines. The reason for selecting this time window is because the signal is not affected by the transient effects evidenced at the beginning of the injection.

The average momentum flux versus the injection pressure is presented in Figure 4.4, for both fluids water and UWS, and all the tested injection pressures and discharge pressure condition. In these plots the pressure is indicated in absolute values.

As expected, the higher the discharge pressure, the lower the momentum flux. This behaviour is logical considering Equation 3.12, where the momentum flux is proportional to the square of the velocity. From the Bernoulli equation, the velocity is also proportional to the square root of the pressure difference between the injection pressure and the discharge pressure. This trend is observed for both fluids, water and UWS. This is important when the engine is operating at high altitudes (where the ambient pressure is lower), then the differential pressure has to be taken into account to inject the proper amount of fluid into the exhaust stream.

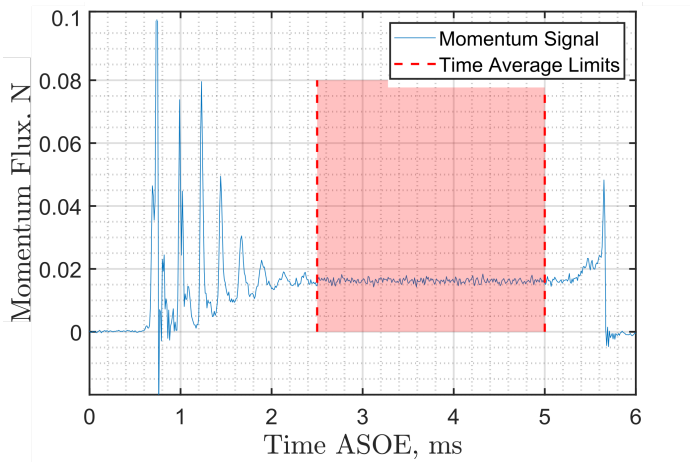

Figure 4.3: Momentum flux signal. Injection pressure: 5 bar (absolute). Discharge pressure: 0.75 bar (absolute). Cooling temperature: 60 °C. (Time ASOE).

Effect of the cooling temperature on the momentum flux

The cooling temperature of the injector regulates the temperature of the injection fluid, and consequently has an influence on the properties of the fluid such as viscosity, density and surface tension. It also affects the performance of the spray and the dynamics of the injector [2].

The effect of the cooling temperatures on the average momentum flux is shown in Figure 4.5. This plot presents the results for the three pressure levels. For the UWS at the operating condition of 5 bar the momentum flux decreases when the cooling temperature is higher. However, for the higher injection pressures (7 and 9 bar) the influence of the temperature on the momentum flux is not clear, since the tendency has an opposite behaviour for the highest cooling temperature.

The water results showed that there is little difference at the lowest injection pressure, meanwhile as the pressure upstream is increased the effect of the cooling temperature is more evident.

This results are in agreement with previous works. Brizi et al. [3] reported results for UWS, and Kapusta et al. [4] did experiments for water and UWS. They concluded that increasing the cooling temperature and the injection pressure promotes the atomization of the spray. Furthermore, the structure of the spray changes significantly when the fluid reaches fully developed flash boiling conditions.

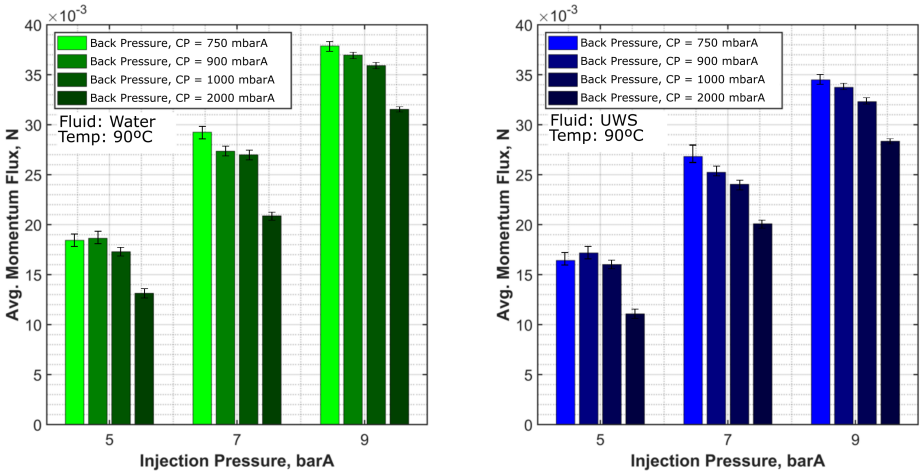

Figure 4.4: Momentum flux for water (left) and UWS (right). Influence of the injection pressure and discharge pressure.

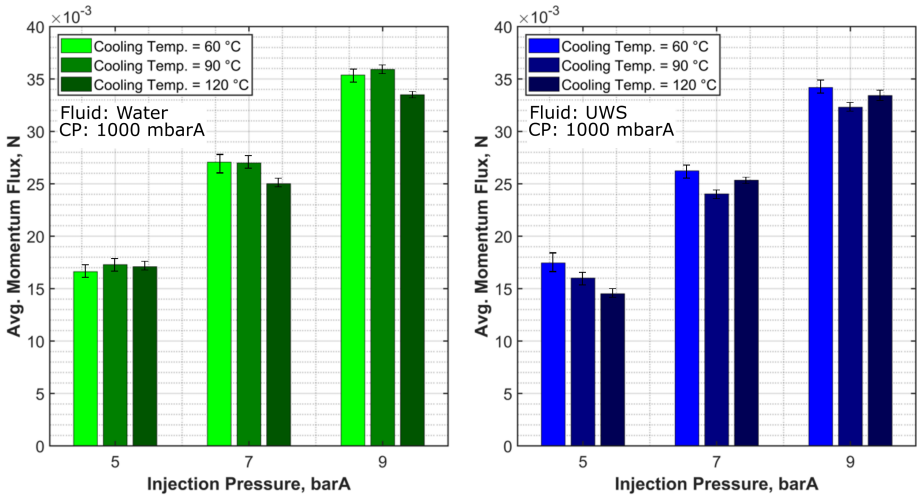

Figure 4.5: Momentum flux for water (left) and UWS (right). Influence of the cooling temperature.

They also reported that flash boiling conditions increases the spreading of the spray cone, decreasing the penetration length for the same pressure condi-

tions. Also, it promotes a better atomization, enhancing the air entrainment in the spray and evaporation. All these factors may have an effect on the spray momentum, possibly stopping part of the spray from hitting the target or slowing the spray and thus affecting the measurement.

Effect of the fluid on the momentum flux

The average momentum flux for the two tested fluids with a cooling temperature of 90 °C and a discharge pressure of 1 bar, for the three tested injection pressures is shown in Figure 4.6.

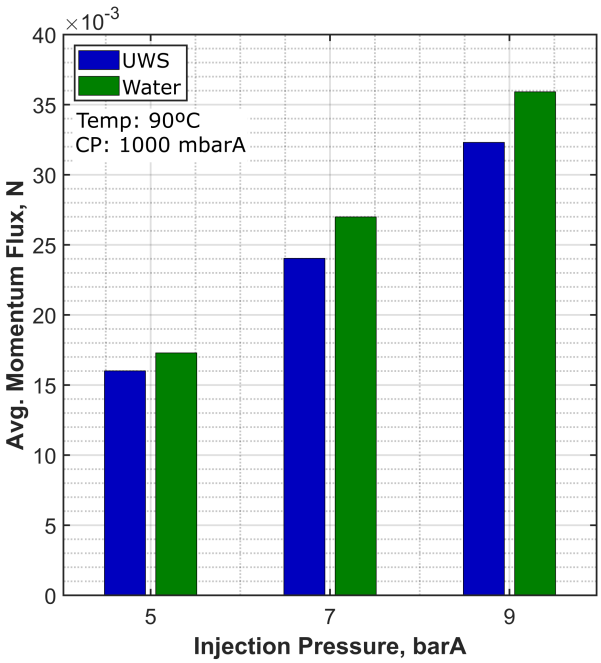

Figure 4.6: Comparison of the spray momentum flux for both fluids.

Results show that when water is injected the momentum flux is always higher than for the UWS. It is consistent with the theory and previous works in the literature. As shown in Equation 3.12, the spray momentum is proportional to the square of the velocity [5].

This sugests that when UWS is replaced by water in the measurements, some corrections should be done in terms of the momentum quantity. These results are of especial importance due to the common use of water as a substitute for UWS for experiments.

Therefore, a summary of the average value of momentum flux is presented in Figure 4.7. It can be seen that the average momentum flux is linearly proportional to the pressure difference (ΔP).

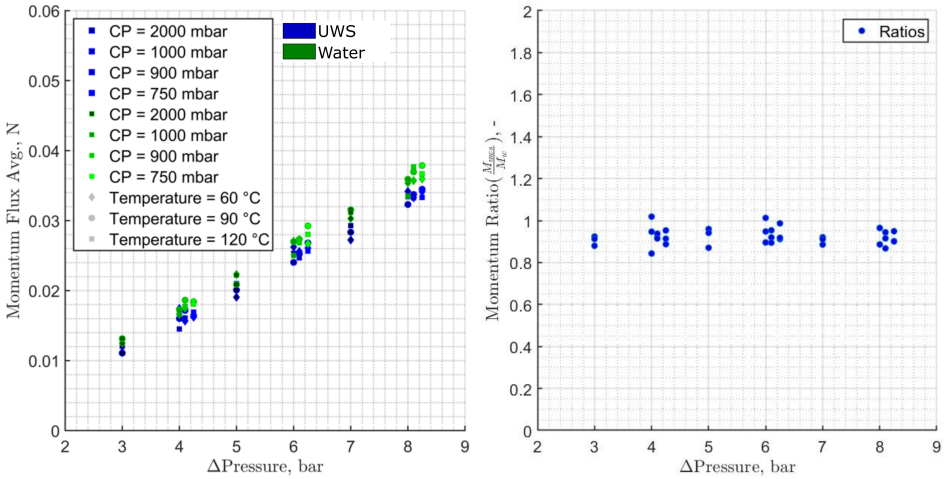

Figure 4.7: (left) Average momentum flux for all tested conditions. (right) Ratio of the average momentum flux between water and UWS.

The image in the right side presents the ratio R between the momentum flux of the UWS and the water for each test condition. The ratio is calculated using Equation 4.1.

$$R = \frac{\dot{M}_{UWS}}{\dot{M}_{water}} \tag{4.1}$$

The value of the ratio R for each testd condition is shown in the right side of Figure 4.7. It has an almost constant value, and is independent on the injection pressure, cooling temperature or ambient pressure. Based on this tendency, a coefficient R for correcting the momentum flux values is proposed. This will be valid when water is used as a substitute of UWS in experiments. The average ratio between all the measurements has a value of $\overline{R} = 0.92$, with a standard deviation of $s = 0.038$. The ratio is a consequence of the differences in the properties of the fluids, as will be discussed later in Section 4.6.

4.4 Injected mass results

The determination of the injected mass per pulse was carried out by collecting the injected liquid after 500 shots. The mass was delivered inside of the test vessel at the same test conditions used for spray momentum. The total mass was measured using a weight. The system was designed to ensure that the fluid delivered by the dosing unit remains inside vessel, minimizing the possibility of leakages or losses due to evaporation during the measurement process. In Figure 4.8, the injected mass per pulse is shown. It summarizes the results for all the cooling temperatures, discharge pressure and injection pressure, for UWS (right side) and for water (left side).

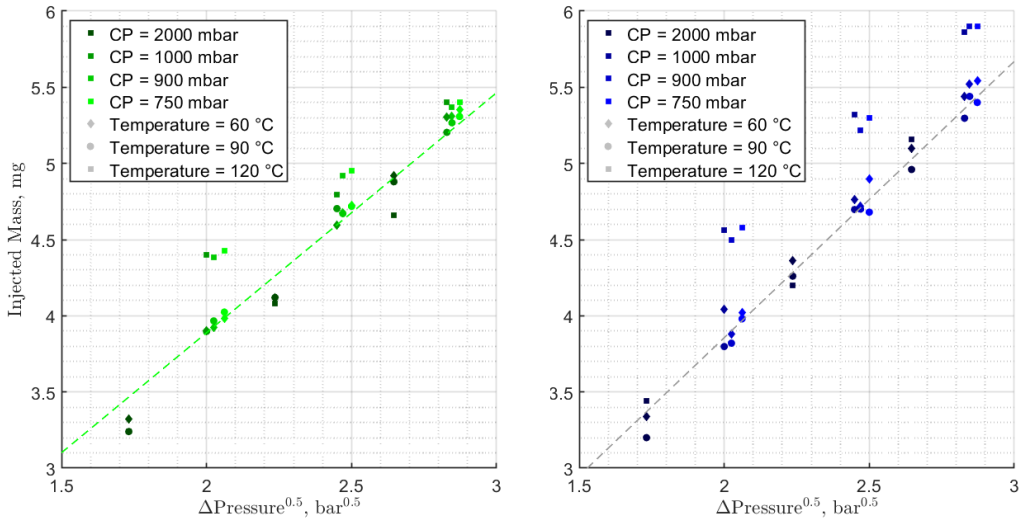

Figure 4.8: Comparison of the injected mass. (Left) Water. (Right) UWS.

As expected, the injected mass is proportional to the square root of the pressure difference. Moreover, the behavior is similar for both fluids.

The most remarkable injected mass results were seen at the higher cooling temperature level of 120 °C. At those operating conditions the injected mass was around 15% higher than for the lower cooling temperature. This behaviour could be attributed to changes in the physical properties of the fluid like the viscosity, which increases the discharge coefficient of the nozzle, together with the flash boiling conditions. To verify this hypothesis an additional

investigation is proposed, using modelling tools as CFD to analyze the internal flow at those temperatures, which is being performed in a separated Thesis.

Besides, Brizi et al. [3] detected that under flash boiling conditions some UWS fluid was still coming out of the injector after the end of the injection event. This effect can also explain the increment in the injected mass.

4.5 Rate of injection results

The rate of injection (ROI) curves were calculated from the measurements of injected mass and momentum flux. The Equations 3.15, 3.16 and 3.17 were used for this purpose. The rate of injection signals calculated from the previous equations are presented in Figure 4.9. The plots in the right side summarize the results for UWS and the plots in the left side shows the curves for water. They depict the ROI for the three cooling temperatures, the three injection pressures, at discharge pressure of 1 bar.

In agreement with the theory and with previous works reported in the literature, the ROI increased for higher injection pressure levels.

Futhermore, the shape of the curves are similar for the fluid temperatures of 60 °C and 90 °C, meanwhile for the 120 °C curves a different and longer opening transient is observed [6]. This change in the curve could indicate changes in the internal flow of the nozzle due to the change of density of the fluid or the internal dynamic behaviour of the injector.

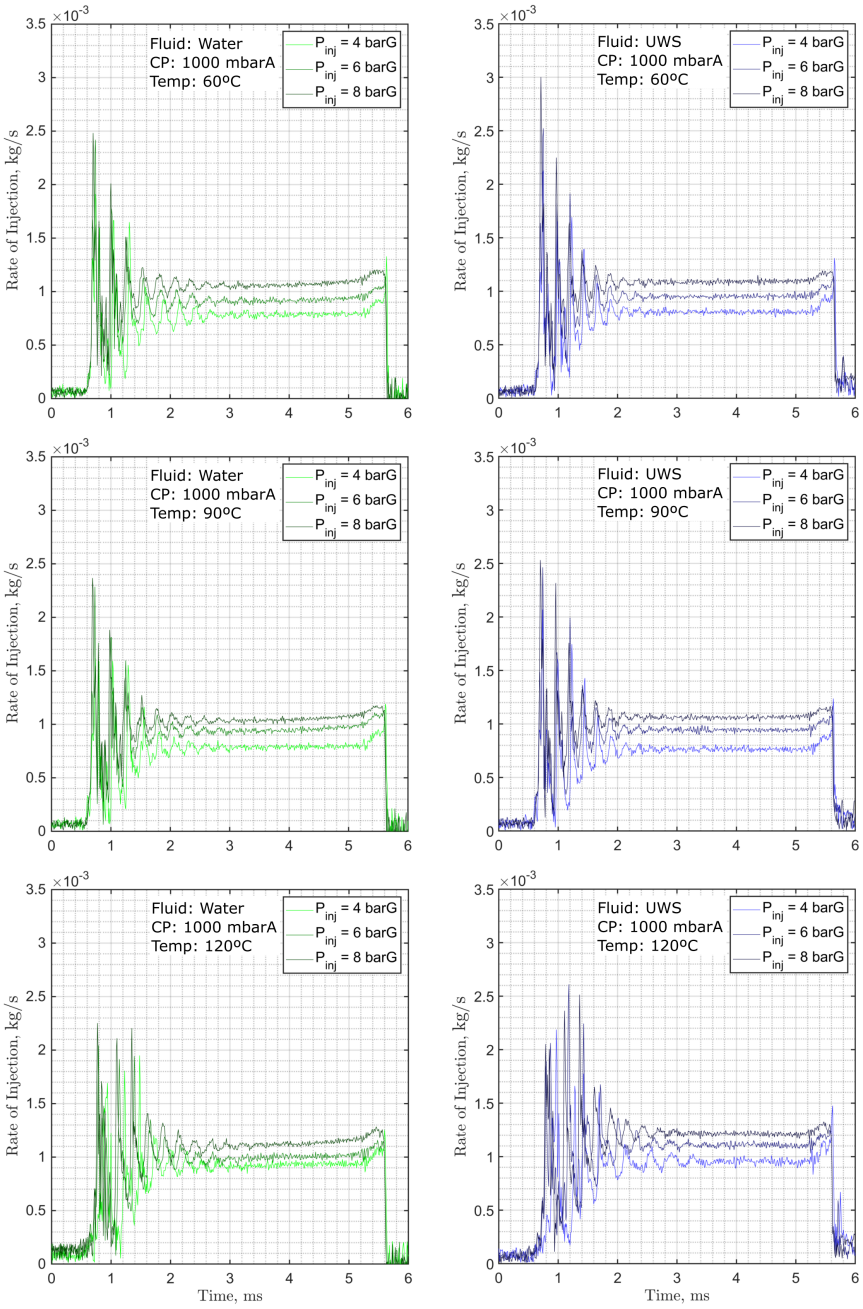

Figure 4.9: Rate of injection curves. Comparison of injection pressure effect at three cooling temperatures and 1 bar of discharge pressure.

Analogous to the momentum flux curves, an average of the ROI value was calculated using the values comprehended between 2.5 ms and 5 ms, where the injection is in stabilized conditions. Figure 4.10 shows the average value for all the tested points, indicating a consistency with the injected mass trends.

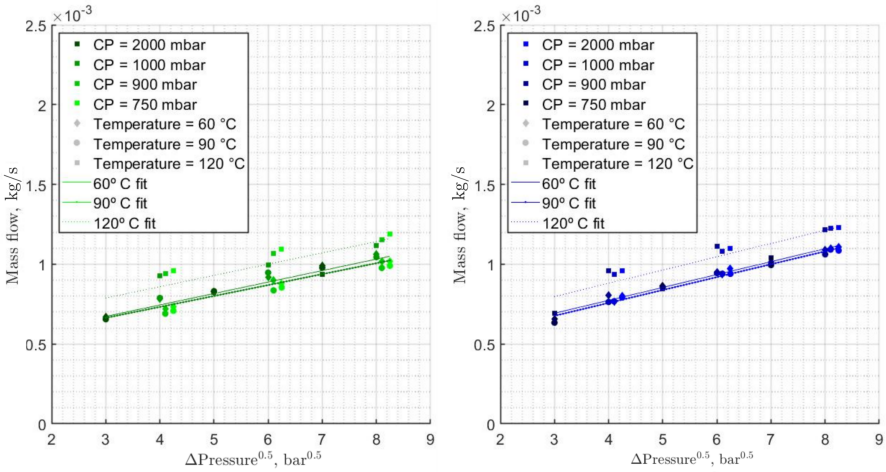

Figure 4.10: Averaged rate of injection as a function of $\Delta P^{0.5}$. (Left) Water. (Right) UWS.

The ROI values follow a linear trend with the square root of the pressure difference. As seen before with the injected mass, when the conditions for flash boiling of the spray are set, the rate of injection is considerable higher (around 20%).

The ROI curves have been employed in a parallel study done by Payri et al in [7]. It has been used as an input for CFD modelling. It has been demonstrated that this is a convenient method to characterize the injector when other techniques are difficult or impossible to apply.

4.6 Discharge Coefficient

Once the ROI has been calculated from the momentum flux data, it is possible to estimate the discharge coefficient C_d of the nozzle. It is calculated by using the ROI combining Equation 3.8 and the Bernoulli equation $u_b = \sqrt{2\Delta P \rho_f}$ as follows:

$$C_d = \frac{\dot{m}}{A\sqrt{2\Delta P \rho_f}} \tag{4.2}$$

Then, the evolution of the discharge coefficient of the nozzle can be characterized in terms of the Reynolds number, which is defined as:

$$Re = \frac{\rho_f u_0 D_0}{\mu_f} \tag{4.3}$$

Where D_0 is the diameter of the orifice, ρ_f is the density of the fluid, u_0 the velocity at the nozzle exit and μ_f the dynamic viscosity of the fluid.

To determine the Reynolds number it is required to know the properties of the fluid at the corresponding conditions. The density used for Equations 3.12, 3.13 and 3.14 was calculated using the information from [8].

The viscosity of the fluid varies widely with the temperature, therefore it was calculated using an exponential decay fit with the data available in the work of Halonen et al [9]. Figure 4.11 shows the viscosity of water and the data points and fit used to determine this property at different temperatures for UWS.

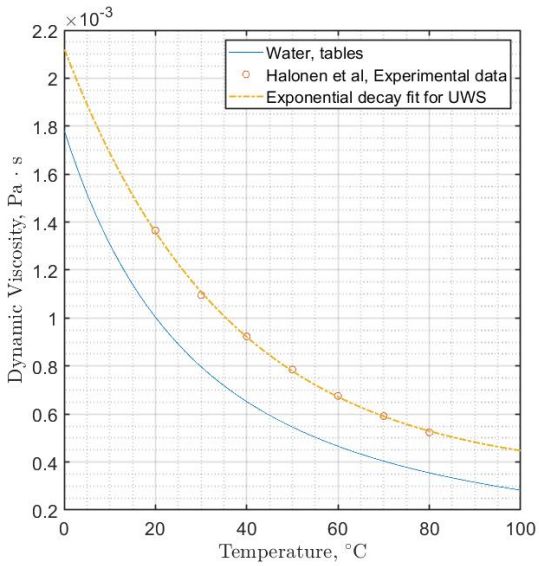

Figure 4.11: Viscosity of the UWS and water at different temperatures.

Figure 4.12 shows the discharge coefficient C_d versus the Reynolds number Re for the tested conditions, on the left image the C_d of the water and on the right side for UWS.

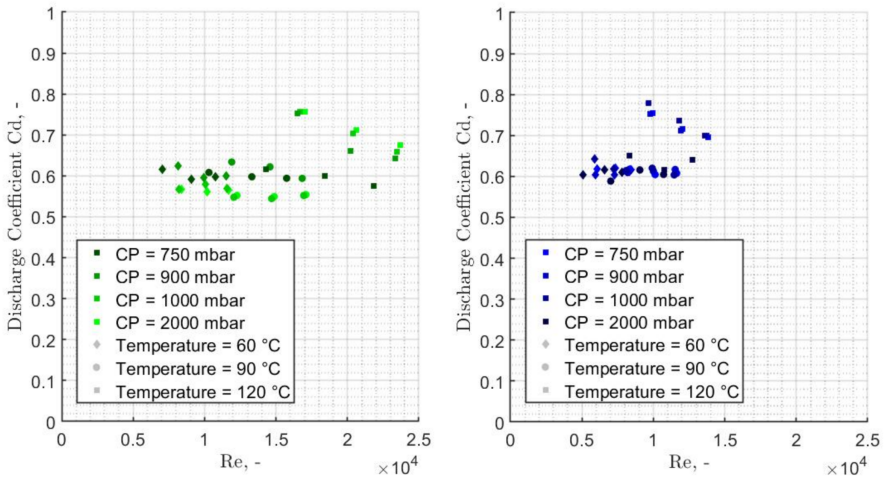

Figure 4.12: Discharge coefficient vs Reynolds number for water (left side) and UWS (right side).

In the images we can observe how the discharge coefficient of both fluids is near 0.6 for the temperatures of 60 °C and 90 °C. Comparing the obtained value for the SCR dosing unit with other applications in engines, it is similar to the C_d of GDI injectors with a value near 0.55, but lower than diesel injectors which usually have a C_d value around 0.8 [10].

The differences can be attributed to a combination of facts. On one side, the pressures involved in the injection process of the current application is low compared to those used in gasoline or diesel injection. On the other hand, Figure 4.13 shows the internal geometry of the nozzle, showing a short L/d ratio, combined with a deflection of the flow at the inlet of the orifices, which can generate some perturbations in the fluid motion.

Once the fluid temperature is above the flash boiling condition and the ambient pressure is below 2 bar, a strange behavior is observed where the discharge coefficient rises nearly to 0.8, and then decreases towards 0.65 as the Reynolds number is higher (higher ΔP).

These outlier points take higher value due to the difficulty measuring its momentum flux at flash boiling conditions, where the values are considerably

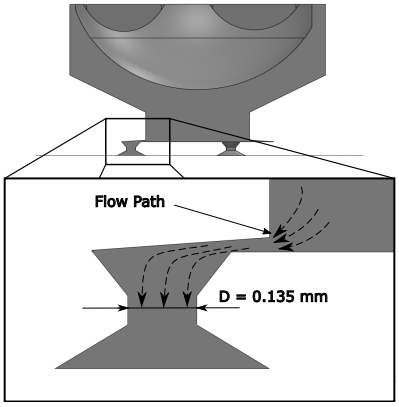

Figure 4.13: Section view of the internal geometry of the studied injector.

smaller than the values for lower temperatures at the same ΔP, resulting in higher injected mass and ROI as shown in Figures 4.8 and 4.10.

Another notable difference in Figure 4.12 is the higher range of Reynolds numbers for water, which can be attributed to the higher exit velocity (higher momentum flux) than for UWS and to the lower viscosity of the fluid.

4.7 Summary and conclusions

A methodology to determine the rate of injection in a SCR dosing unit was employed obtaining remarking results. Normally an Injection Rate Discharge Curve indicator device based on the Bosch long tube method would be used to determine the rate of injection, but the low ΔP and the small amount of injected mass makes hard to employ this kind of system. In this case, a methodology to determine the rate of injection using momentum flux measurements under different conditions of temperature and ambient pressure becomes useful.

The momentum flux of the SCR system injector was measured using water and UWS as fluids. The results shows that the water has higher momentum flux than the UWS for the same testing conditions due to higher velocity of water at the exit of the nozzle.

The momentum was affected by the cooling temperature of the fluid and the ambient pressure, showing lower momentum flux as the temperature of the spray was higher and lower momentum for higher ambient pressures.

A ratio R between the momentum flux of water and UWS was determined, finding that on average the momentum flux of UWS is 0.924 times the momentum of water.

The injected mass was also determined for all the tested conditions, increasing linearly with the square root of ΔP. Also finding that under cooling temperatures of 120° C where flash boiling conditions are set, the amount of mass injected was nearly 15% higher for both fluids. This can be attributed to the changes in the physical properties of the fluids, which increases the discharge coefficient of the nozzle, due to the high temperatures combined with the effects of the flash boiling.

The injected mass and momentum flux were used to determine the rate of injection using Equations 3.15, 3.16 and 3.17. The ROI also followed a linear behaviour with the square root of ΔP.

With the ROI, the discharge coefficients of the nozzle were calculated finding a steady value as the Reynolds number increased for most testing points, except for the points that reached flash boiling conditions.

When the injector cooling temperature is at 120° C and flash boiling conditions for the spray are set, a higher ROI and Cd were determined for both fluids. The reason behind this increase can be attributed to two factors: the internal behaviour of the nozzle and the changes in the structure of the spray (higher spreading angle) at high temperatures, leading to higher injected mass and probably not capturing the whole spray with the piezoelectric sensor (and thus leading to lower measured momentum flux).

Finally, the measuring technique is a useful tool for the hydraulic characterization of the spray, providing a valid method to accurately determine the ROI relying on the momentum flux measurements and the total injected mass. This is of importance due to the need to determine the ROI, especially when other methodologies cannot be applied, to validate CFD models and accurately dose the UWS, allowing proper reduction of emissions (NOx or Ammonia slip) and minimizing the deposit formation in the exhaust line.

References

[1] Payri, Raul, Bracho, Gabriela, Gimeno, Jaime, and Moreno, Armando. "A Methodology for the hydraulic characterization of a Urea-Water Solution injector by means of Spray Momentum Measurement". In: *ILASS - Europe 2019, 29th Conference on Liquid Atomization and Spray Systems* September (2019), pp. 2–4.

[2] Carreres, Marcos. "Thermal effects influence on the Diesel injector performance through a combined 1D modelling and experimental approach". PhD thesis. Universitat Politècnica de València, 2016. DOI: 10.4995/Thesis/10251/73066.

[3] Brizi, Gabriele, Postrioti, Lucio, and Vuuren, Nic van. "Experimental analysis of SCR spray evolution and sizing in high-temperature and flash boiling conditions". In: *SAE International Journal of Fuels and Lubricants* 12.2 (2019), pp. 87–107. DOI: 10.4271/04-12-02-0006.

[4] Kapusta, Łukasz Jan et al. "Low-Pressure Injection of Water and Urea-Water Solution in Flash-Boiling Conditions". In: *SAE Powertrains, Fuels & Lubricants Meeting*. SAE International, 2020.

[5] Kapusta, Łukasz Jan, Sutkowski, Marek, Rogóż, Rafał, Zommara, Mohamed, and Teodorczyk, Andrzej. "Characteristics of Water and Urea–Water Solution Sprays". In: *Catalysts* 9.9 (2019), p. 750. DOI: 10.3390/catal9090750.

[6] Payri, Raúl, Bracho, Gabriela, Martí-Aldaraví, Pedro, and Moreno, Armando. "Using momentum flux measurements to determine the injection rate of a commercial Urea Water Solution injector". In: *Flow Measurement and Instrumentation* 80 (2021), p. 101999. DOI: https://doi.org/10.1016/j.flowmeasinst.2021.101999.

[7] Payri, Raul et al. "Computational study of urea-water solution sprays for the analysis of the injection process in SCR-like conditions". In: *Industrial & Engineering Chemistry Research* (2020). DOI: 10.1021/acs.iecr.0c02494.

[8] BASF. "AdBlue® Technical Leaflet". In: November (2006), pp. 1–6.

[9] Halonen, Sauli, Kangas, Teija, Haataja, Mauri, and Lassi, Ulla. "Urea-Water-Solution Properties: Density, Viscosity, and Surface Tension in an Under-Saturated Solution". In: *Emission Control Science and Technology* 3.2 (2017), pp. 161–170. DOI: 10.1007/s40825-016-0051-1.

[10] Payri, R., Bracho, G., Soriano, J. A., Fernández-Yáñez, P., and Armas, O. "Nozzle rate of injection estimation from hole to hole momentum flux data with different fossil and renewable fuels". In: *Fuel* 279.March (2020), p. 118404. DOI: 10.1016/j.fuel.2020.118404.

Chapter 5

Spray penetration and spreading angle of UWS injection systems

5.1 Introduction

This chapter presents the results of the experimental campaign performed in the optically accessible facility. These tests were carried out in conditions of flow and temperature that resemble those of the exhaust line. First, the test plan is shown, then results are analysed in two parts: spray tip penetration and spreading angle. Lastly, the chapter ends with a summary and conclusions.

5.2 Spray characterization test plan

The test conditions for the UWS spray visualization were selected to resemble those of a light duty vehicle exhaust pipe and normal operating conditions for the dosing unit. Boundary conditions include three feeding line pressures, cooling temperatures, air temperatures and mass flow, using the same conditions and injector energizing time applied in the hydraulic characterization. The test conditions are presented in Table 5.1.

The test matrix consists of 113 test point. Ten repetitions were done per each condition. Injection pressures, air temperatures, air mass flow and cooling temperatures were selected considering exhaust-like operating conditions

Table 5.1: Test plan for the macroscopic spray visualization campaign.

Parameter	**Value**	**Units**
Injection Pressure (P_{inj})	4 - 6 - 8	bar
Coolant Temperature (T_{ref})	60 - 90 - 120(*)	°C
Air Mass Flow ($\dot{m}_{air}$)	40 - 180 - 300	$\mathrm{kg\,h^{-1}}$
Flow Temperature (T_{flow})	100 - 250 - 400(**)	°C
Injector Angles	90 - 45	°
Injection duration	5	ms
Injection frequency	1	Hz
Tested Fluid	Adblue	-
Repetitions	10	-

* Only for the 90° position
** Only for 40kg $\mathrm{h^{-1}}$ $\dot{m}_{air}$

found in literature for similar injectors. For each test point a moving average was performed on the data to obtain the spray penetration and spreading angle curves.

The injection frequency and pulse duration for these type of dosing units can vary according to the amount of UWS mass needed to achieve the proper mixture of fluids, up to 3.33 Hz (injector manufacturer set limit), but it was set to 1 Hz to keep a similar arrangement through the different experimental tests. The dosing system (Subsection 3.2.1), cooling system and operating pulses used are the same ones that were utilized previously for the hydraulic characterization.

Injector position

The effect of the injector position with respect to the flow direction was also studied. In Figure 5.1, the two dispositions of the injector with respect to the flow are shown. The spray penetration was measured from the nozzle exit and in the direction parallel to the injector axis.

5.3 Spray penetration

The spray penetration is an important parameter for many sprays inside the automotive industry [1–3], and the Urea water solution used in exhaust after-treatment is one of those [4–8]. The ambient conditions and injection settings

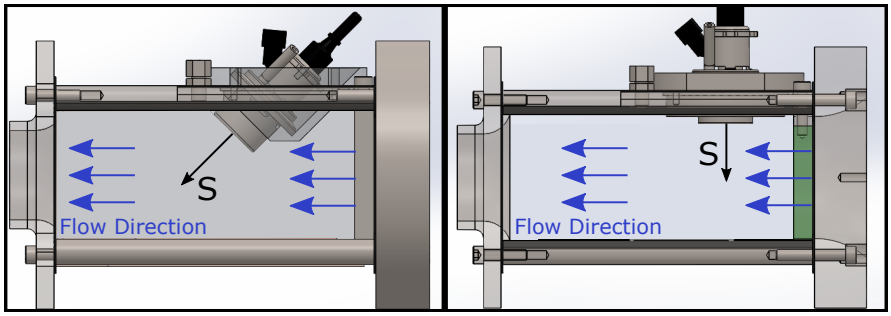

Figure 5.1: Injector positioning inside of the visualization chamber at 45° (left) and 90° (right) inclination angles regarding the air mass flow.

inside of the exhaust line differ from those of the cylinder of an engine, nevertheless the analysis of spray penetration for both environments is similar. The purpose it to understand the mixing of the fluids [8], performance and improvements [4, 9, 10], and to prevent spray impingement and deposit formation in the exhaust walls [10–13]. Furthermore, these results are often employed in CFD modelling [14, 15], aiding in the design and validation of future UWS dosing equipment.

5.3.1 Spray Segmentation of burst and spray body

As explained in subsection 3.8.1, the initial phase of the injection process in low pressure atomizers such as the UWS injector, is characterized by small bursts or packages of droplets that exit the injector nozzle in pulses before the full spray plume is formed. Therefore, the initial part of the analysis consists of the segmentation of these initial packages from the main spray body and to understand the differences between them.

In Figure 5.2, three frames representing the times of 1.1, 1.6 and 2.2 ms are presented for the injection pressures of 4 (top row) and 8 bar (bottom row). In these images, the burst and body of the spray are enclosed inside orange and blue squares respectively, indicating their position and evolution through the injection event. In the 4 bar images, one can notice how the first burst separates from the rest of the spray at the beginning of the injection event. There is an increasing gap between the two parts of the spray and the burst scatters considerably as the spray develops. When the injection pressure is increased up to 8 bar, the gap between the burst and the main spray still exists, but the separation between them is less noticeable compared to the low pressure case. Based on the penetration definition presented in chapter 3,

the spray length for the burst and main spray is computed and presented hereafter.

Figures 5.3, 5.4 and 5.5 present a comparison of the burst and spray penetration behaviour for the three injection pressures levels and the three cooling temperatures of the injector.

The curves of the burst are shown in yellow while the spray body is depicted in blue. The initial burst does not appear to be affected significantly by the injection pressure, given the similar slope of the curves for all the three levels of pressure. Nevertheless, as the injected fluid temperature is increased, the slope of the penetration curves decreases, in particular for the 120^{o}C test condition. This indicates that at higher temperatures, the internal mechanics of injector and the fluid properties have a more pronoun effect on the injector behavior.

Another factor that can be observed is the effect of the injection pressure, which reduces the difference between the spray burst and the body indicating a more continuous injection evolution from the initial stage. This gap between the two parts of the spray becomes smaller due to the higher momentum of the spray at higher injection pressures as shown in chapter 4. Furthermore, the effect of the cooling temperature can also be observed, where the behavior of the spray body curves become more similar to the burst curves as the temperature increases, specially when the spray is developed (between 2 and 4 ms after the start of energizing).

At the lowest injection pressure (4 bar), oscillations in the penetration curve show that the spray is not being ejected evenly out of the nozzles, i.e.., other bursts with smaller gaps between them are exiting the nozzle in the initial stages of the injection event, which are later combined with the spray body. This behaviour can be attributed to the bounce of the needle inside of the nozzle and is reduced as the injection pressure increases.

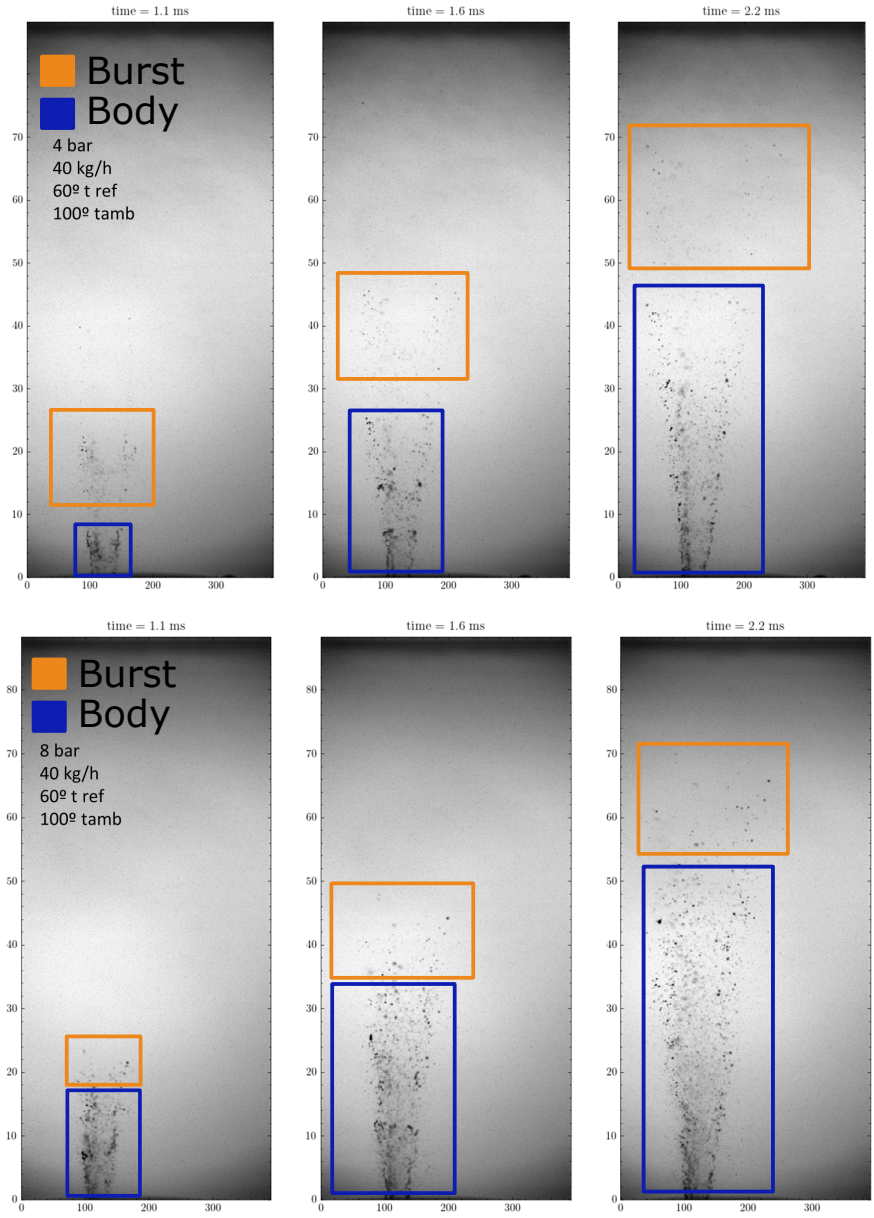

Figure 5.2: Spray burst and body evolution at 1.1, 1.6 and 2.2 ms measured from the start of energizing. The upper row represents the injection pressure of 4 bar and the lower 8 bar.

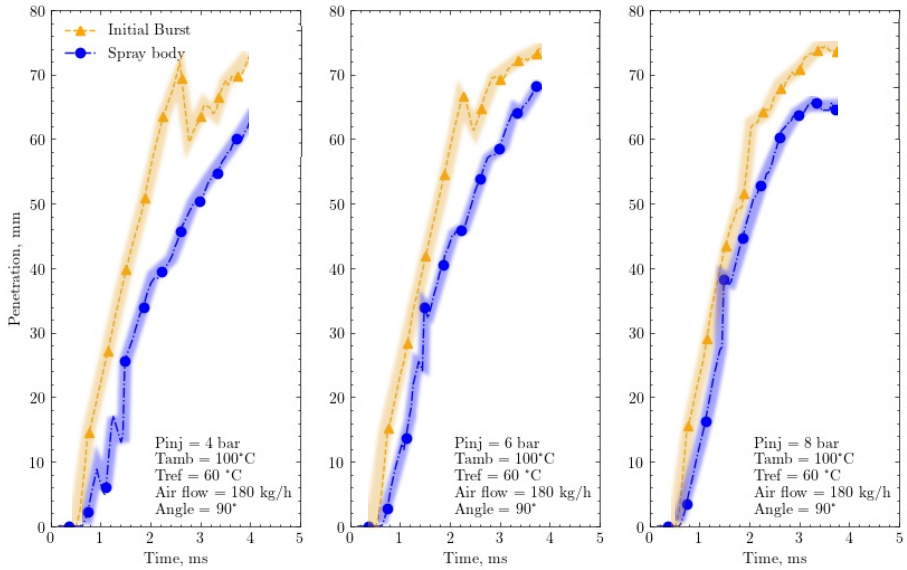

Figure 5.3: Spray burst and body comparison for all injection pressures and cooling temperature of 60°C, time after start of energizing.

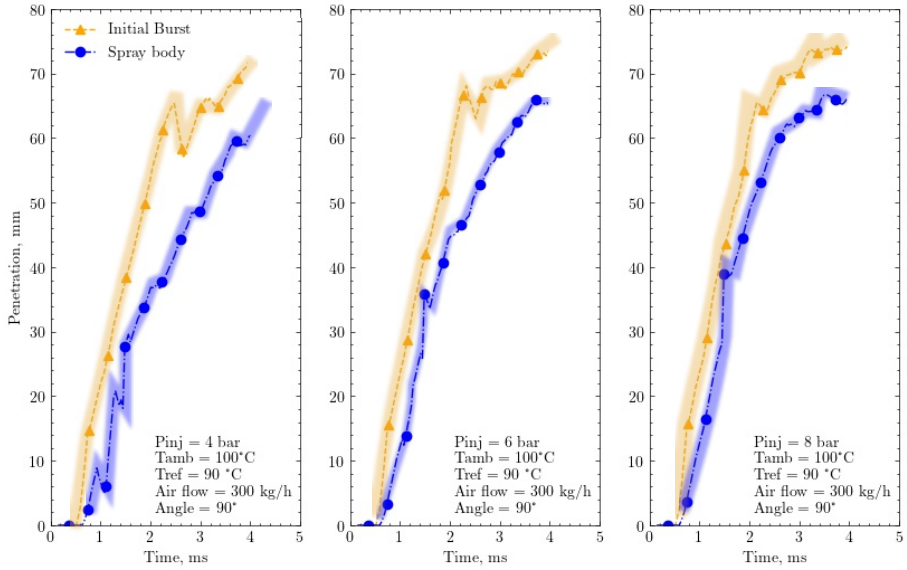

Figure 5.4: Spray burst and body comparison for all injection pressures and cooling temperature of 90°C

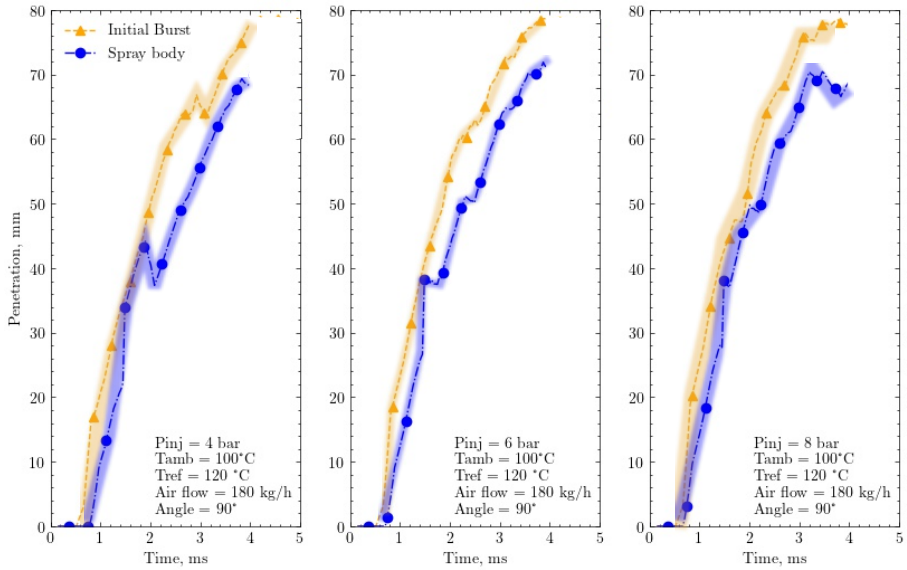

Figure 5.5: Spray burst and body comparison for all injection pressures and cooling temperature of 120°C

5.3.2 Spray penetration behaviour at 90 degree position.

Several conditions were tested during the measuring campaign. To analyze the effect that each condition has over the spray, the different levels of injection pressure, cooling temperature, ambient temperature, air mass flow and injector angle disposition are presented in the following subsections.

Effect of air mass flow

Exhaust flow differs depending on the working regime of the engine. As explained in Table 5.1 three different gas flows have been studied during the measuring campaigns. In Figures 5.6, 5.7 and 5.8 the comparison of the different air mass flows for the spray burst (left) and body (right) is shown for the three cooling temperatures used in the tests.

At 60 °C the air flow has negligible influence the penetrations curves. When the cooling temperature of the injected liquid is at 90 °C the influence over the spray burst is also barely noticeable. On the other hand, a difference begins to appear in the spray body as the spray develops, however, the difference between them is within the experimental dispersion. Finally, some influence of the air mass flow is observed when the cooling temperature is at

the higher level of 120 °C, in which the increase in air flow leads to a shorter penetration for the body and the burst of the spray.

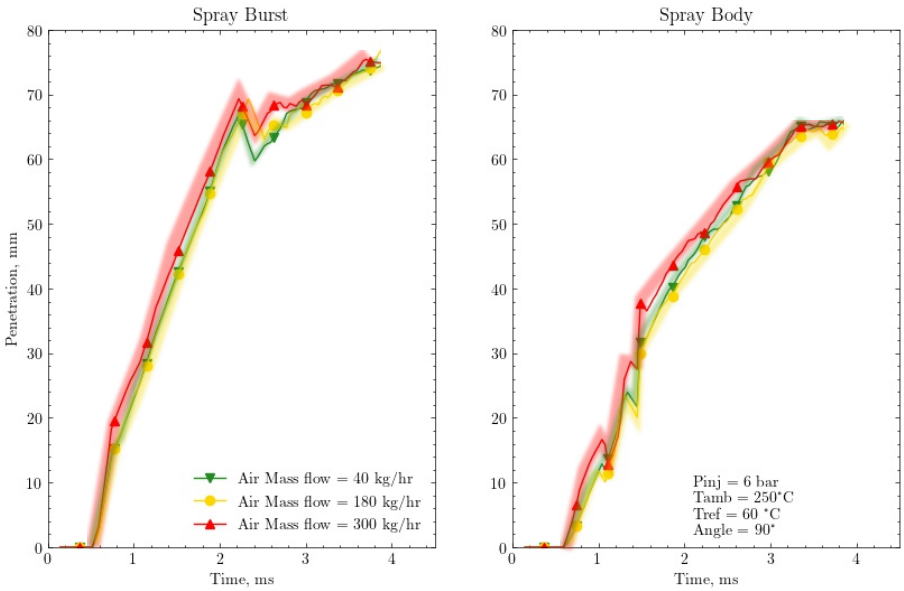

Figure 5.6: Comparison of the spray Burst and Body for different air mass flows and injector cooling temperature of 60 °C

The effect seen at higher air mass flows and higher fluid temperatures can be attributed to a reduction in the diameter of the droplets, shortening the liquid penetration, which is due to the effect of high temperatures on the properties of the UWS (lower surface tension and viscosity). These changes in the fluid improve the evaporation of the fluid, decreasing the liquid phase penetration. This could be a good combination of parameters to reduce the risk of wall impingement.

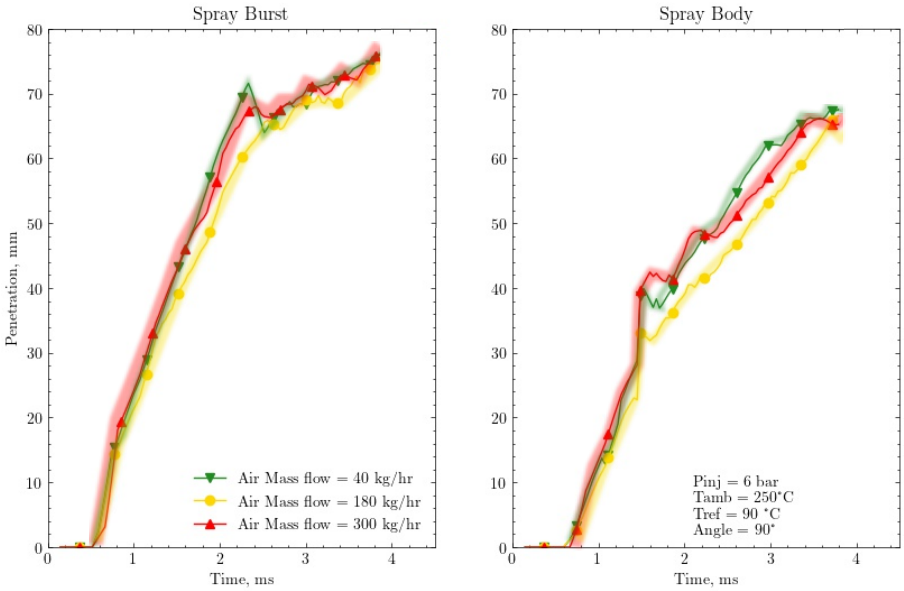

Figure 5.7: Comparison of the spray Burst and Body for different air mass flows and injector cooling temperature of 90 °C

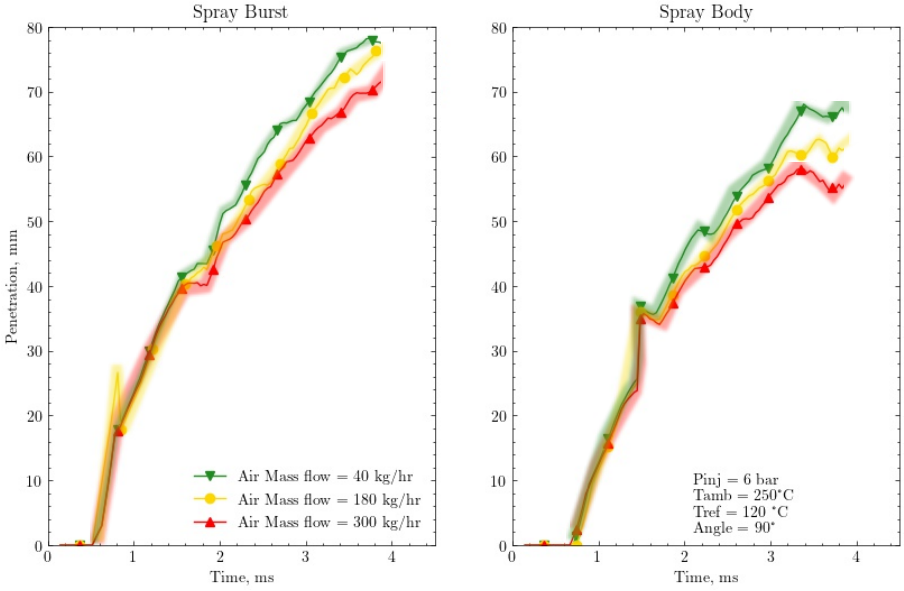

Figure 5.8: Comparison of the spray Burst and Body for different air mass flows and injector cooling temperature of 120°C

5.3.3 Spray penetration behaviour at 45 degree position.

Spray Segmentation of burst and spray body at 45°

The same approach used for the 90° positioning of the injector was applied for the 45° one. In Figures 5.9 and 5.10, the penetration of the burst and the body of spray is presented in yellow and blue, respectively.

In this case, the difference between the two parts of the spray is smaller than the behavior observed previously for the 90° positioning of the injector. The two cooling temperatures shown in Figures 5.9 and 5.10 present a higher separation in the 4 bar curves, meanwhile for the 90°C, the separation of the burst and body of the spray is larger than for the 60°C curve.

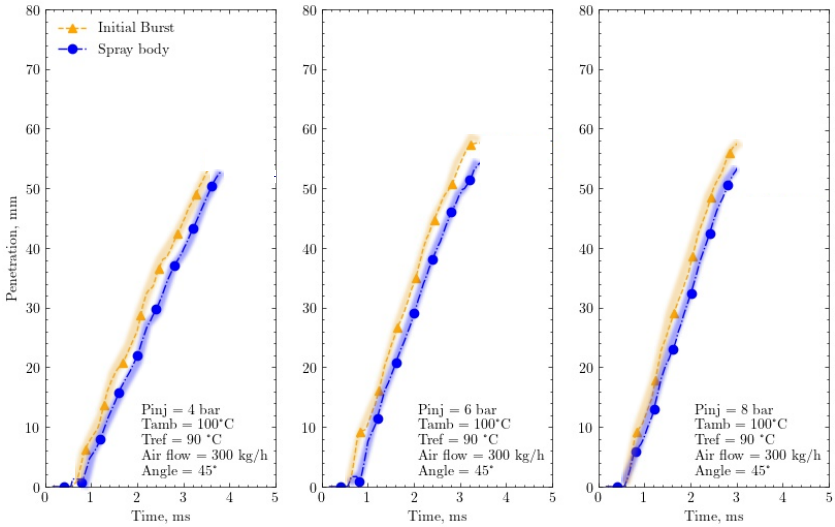

Figure 5.9: Spray burst and body comparison for all injection pressures and cooling temperature of 60°C

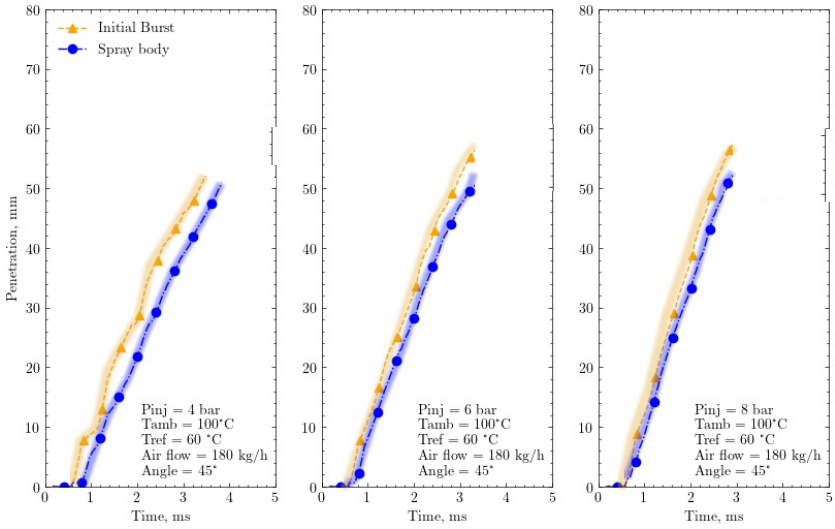

Figure 5.10: Spray burst and body comparison for all injection pressures and cooling temperature of 90°C

Effect of injection pressure and cooling temperature

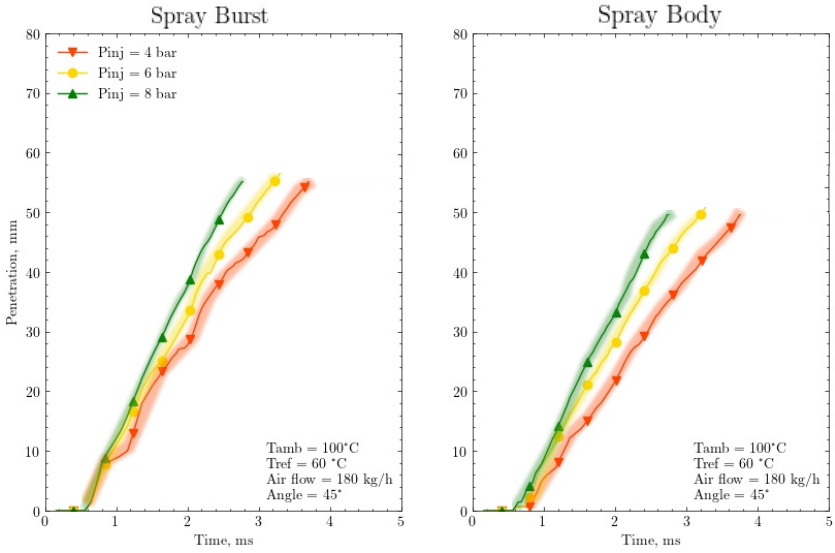

Figure 5.11: Effect of injection pressure at a UWS cooling temperature of 60°C

In Figures 5.11 and 5.12, the effect of the injection pressure on the penetration of the spray burst and body is presented for the temperatures of 60 and 90°C, respectively. Note that the air flow in 5.11 is 180kg h^{-1} and in 5.12 the air flow is 300kg h^{-1}. Although the air flows are different, they worth for comparison purposes and for trend evaluation, since the air flow has very little influence as was shown in Section 5.3.2.

The slope of the curve increases as the injection pressure level goes from 4 to 8 bar. This effect is expected due to the higher momentum flux of the spray. The main difference observed for the case of lower cooling temperature (60°C) is that there is a clear influence of the injection pressure over the spray development due to higher velocity of the fluid flow. However, when the cooling temperature is higher (90°C), closer to the boiling point of the fluid, the injection pressure plays a minor role on the liquid fluid evolution. This would be related to the vaporization of the fluid in the initial stages of the plume and will be corroborated in the following chapter. Moreover, a noticeable characteristic observed in the curves when the injector is tilted at an angle of 45° with respect to the air flow, is that the spray penetration evolution is more linear rather than parabolic potential obtained in the penetration curves at 90°. This change of behaviour can be attributed to a reduced resistance of the flow (a component of the spray now travels in the same direction of the flow), reducing the drag that the air exerts on the particles of the spray.

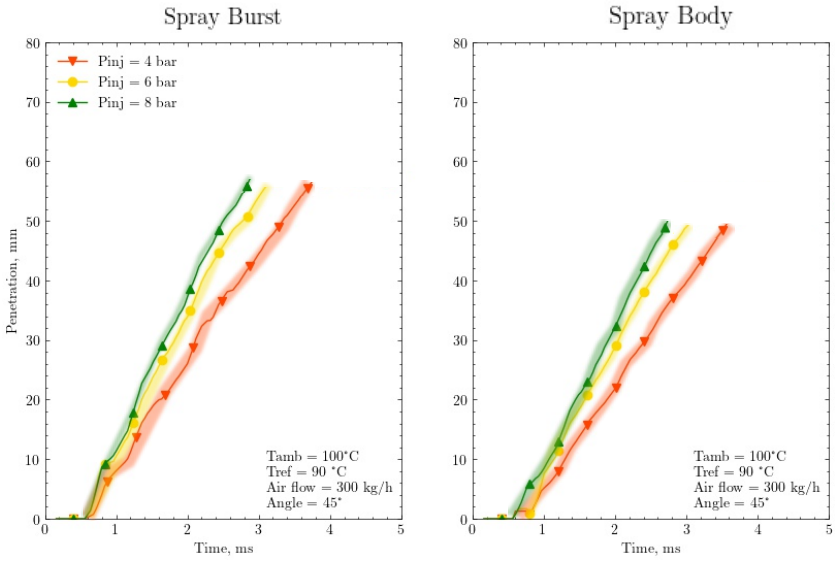

Figure 5.12: Effect of injection pressure at a UWS cooling temperature of 90°C

5.4 Spray spreading angle

The spreading angle of the spray has been studied before for UWS dosing modules, but the characteristics of each injector differ greatly, from number of holes and diameters to working conditions [5, 7, 14, 16–18]. Therefore, there is no single agreement on how to measure it. Hence, an approach similar to those commonly used in diesel and gasoline injectors was selected for this work. This section presents the results of the spray spreading angle. The criteria for the angle calculation was explained in chapter 3.

The spreading angle time evolution is depicted in Figure 5.13. It summarizes all the tested conditions: the two injector positions respect to the gas flow, the three air mass flows and the three injection pressures. In the left side column of the figure, the curves for the three mass flows are presented for the 90° position. Regarding the injection pressure, there is no clear trend that can be observed in the figure. The influence of the injection pressure on the spray angle depends on the gas mass flow. At lower mass flow, a clear trend was not found regarding the injection pressure influence, perhaps because other factors are interacting as well, like the evaporation of the droplets, the turbulence inside the hole injector and the interaction between the gas and the droplets. However, for the highest air mass flow, the spreading angle converges to a value of nearly 14° indicating that the aerodynamics or the gas flow has a higher effect on the spray opening rather than the injection velocity, which is related to the pressure difference upstream and downstream the orifice. Also, it can be attributed to the effect that the air flow motion causes on the spray evolution since at 90° the flow travels perpendicularly to the injector axis, then the air pushes the left side of the spray narrowing the angle.

In the right side column, the curves representing the position of 45 degrees are depicted. The angle of the spray is wider for the lower injection pressure and it is reduced as the injection pressure is increased. The effect of the air mass flow is opposite of what was observed for the 90 degree position, showing that for the air mass flow of $40\,\mathrm{kg\,h^{-1}}$ the spray angle converges to a value of around 14 degrees as the spray evolves over time, meanwhile for higher air flows the opening of the spray angle has not a clear trend regarding the injection pressure.

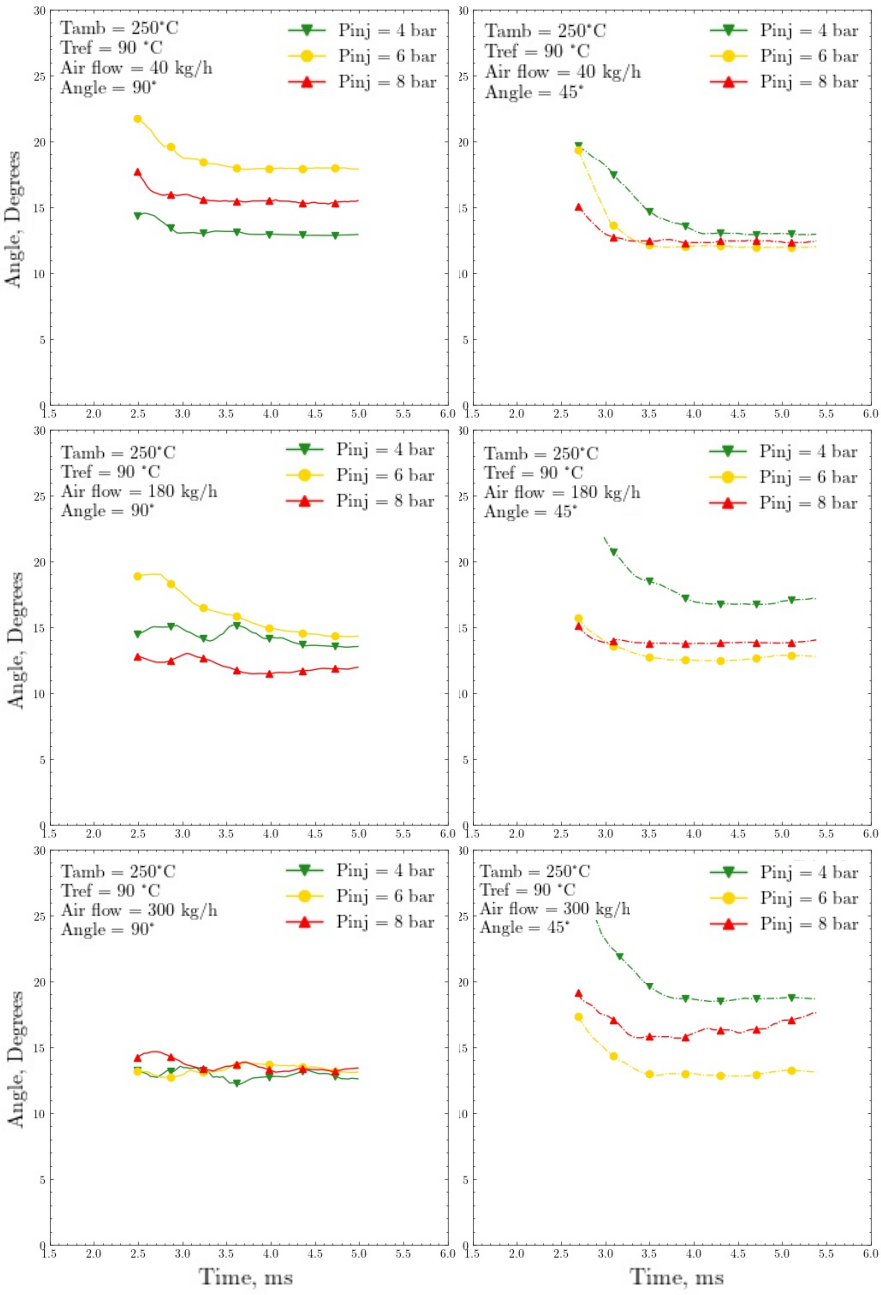

Figure 5.13: Effect of the injection pressure, air mass flow, and injector positioning on the spray spreading angle.

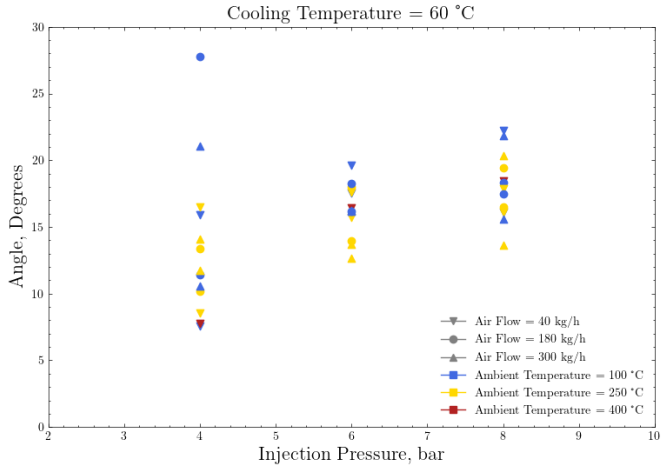

Figure 5.14: Average angles from the steady part of the spray at a cooling temperature of 60°C

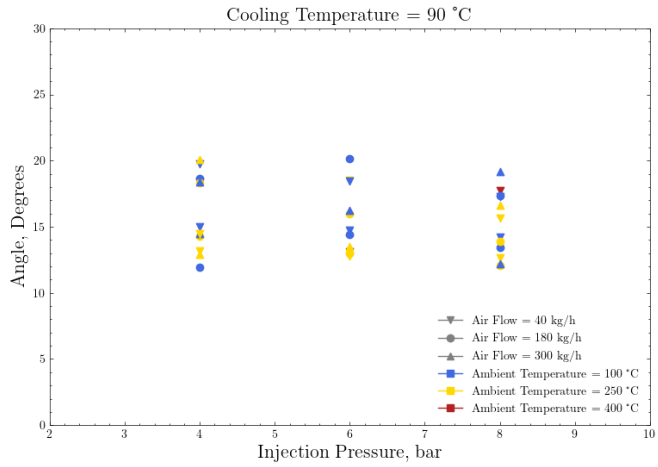

Figure 5.15: Average angles from the steady part of the spray at a cooling temperature of 90°C

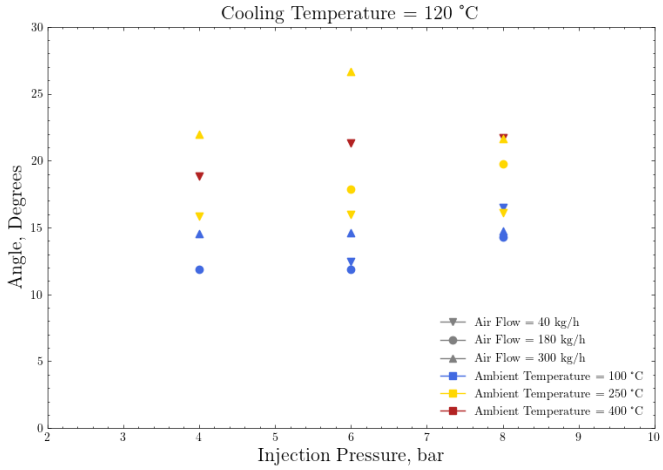

Figure 5.16: Average angles from the steady part of the spray at a cooling temperature of 120°C

Figures 5.14, 5.15 and 5.16 summarize an average of the spreading angle of all test points. The averaging is done considering the time window where the spray angle is stable. In each of the figures a different trend can be observed. In Figure 5.14, the spreading angle of the spray has higher values as the injection pressure increases. Meanwhile in Figure 5.15, the value of the angles remains in the same range for all injection pressures. Finally, a wider range of spreading angles is observed for the temperature of 120C which could be a result of the enhanced atomization process.

5.5 Summary and conclusions

The spray penetration and spreading angle were determined for several conditions of air mass flow, air temperature, injector cooling temperature, injection pressure and injector position for a UWS dosing unit. The penetration was divided in two sections, the spray burst and the body, where it was observed that the initial part of the injected spray is not particularly affected by the injection pressure but was rather influenced by the cooling temperature of the injector.

Concerning the spray body, the effect of the injection pressure was the most important of all parameters evaluated. As expected, higher injection pressures led to an increase in spray penetration, where multiple bursts were shown most likely due to the bouncing of the needle in the injector.

The effect of the air mass flow was not noticeable for most conditions. The penetration curves are fairly similar for all injection pressures and for the cooling temperatures of 60°C and 90°C, but for the 120°C curves a trend of lower penetration at higher injection pressures was observed, suggesting an enhancement of the atomization process caused by the change of the properties of the fluid (lower surface tension and viscosity). This result is particularly important due to the need of better atomization inside the exhaust gas line, therefore, a deeper study of the evaporation and flash boiling of the urea water solution is suggested.

Furthermore, the effect of the inclination of the injector in the visualization chamber was also studied. The injector was placed at two different inclination angles with respect to the flow directions, at 90° and 45°, with the aim of evaluating the behaviour of the spray penetration of the liquid phase. Regarding the spray burst and body, the differences were less noticeable at 45° than at 90° reducing the separation of both parts of the spray in most conditions. As for the cooling temperature of the injector, there was not noticeable difference in most test points, except for the 4 bar injection pressure curves, where at 90°C the gap between the burst and the body of the spray was more evident.

The effect of the injection pressure was similar to what was observed at the 90° position, showing higher slopes for higher pressure levels. The most noticeable difference observed in the curves is that compared to the penetration at 90°, when the injector is tilted at an angle of 45° with respect to the air flow, the spray penetration evolution is more linear rather than parabolic potential. This change of behaviour can be attributed to a reduced resistance of the flow (a component of the spray now travels in the same direction of the flow), reducing the drag that the air exerts on the particles of the spray.

The spreading angle of the spray did not show continuous trends regarding the injection pressure for the 90° position of the injector. But as the air mass flow increased from 40 $\mathrm{kg\,h^{-1}}$ to 300 $\mathrm{kg\,h^{-1}}$ the angle of the spray converged towards 14 °. On the other hand, for the 45° position, an opposite effect was seen where the three injection pressures converged towards 14° as the spray developed at 40$\mathrm{kg\,h^{-1}}$. As the flow rate was increased to 300$\mathrm{kg\,h^{-1}}$, the spray widened due to the low momentum at 4 bar of pressure and the finer particles being easily dragged at 8 bar of pressure. Finally, the range of angles at 60°C and 90°C were similar, whereas the average angle value increased at 120°C.

References

[1] Payri, Raul, Garcia-Oliver, Jose Maria, Xuan, Tiemin, and Bardi, Michele. "A study on diesel spray tip penetration and radial expansion under reacting conditions". In: *Applied Thermal Engineering* 90 (2015), pp. 619–629. DOI: 10.1016/j.applthermaleng.2015.07.042.

[2] Bardi, Michele et al. "Engine Combustion Network: Comparison of Spray Development, Vaporization, and Combustion in Different Combustion Vessels". In: *Atomization and Sprays* 22.10 (2012), pp. 807–842. DOI: 10.1615/AtomizSpr.2013005837.

[3] Payri, Raul, Salvador, Francisco Javier, Marti-Aldaravi, Pedro, and Vaquerizo, Daniel. "ECN Spray G external spray visualization and spray collapse description through penetration and morphology analysis". In: *Applied Thermal Engineering* 112 (2017), pp. 304–316. DOI: 10.1016/j.applthermaleng.2016.10.023.

[4] Kapusta, Łukasz Jan et al. "Low-Pressure Injection of Water and Urea-Water Solution in Flash-Boiling Conditions". In: *SAE Powertrains, Fuels & Lubricants Meeting*. SAE International, 2020.

[5] Payri, Raul, Bracho, Gabriela, Gimeno, Jaime, and Moreno, Armando. "Investigation of the urea-water solution atomization process in engine exhaust-like conditions". In: *Experimental Thermal and Fluid Science* 108.June (2019), pp. 75–84. DOI: 10.1016/j.expthermflusci.2019.05.019.

[6] Payri, Raul, Gimeno, Jaime, Bracho, Gabriela, and Moreno, Armando. "Spray characterization of the Urea-Water Solution (UWS) injected in a hot air stream analogous to SCR system operating conditions ." In: *WCX SAE World Congress Experience* 2019-01-0738 (2019), pp. 1–9. DOI: 10.4271/2019-01-0738.Abstract.

[7] Vuuren, Nic van, Postrioti, Lucio, Brizi, Gabriele, Ungaro, Carmine, and Buitoni, Giacomo. "Experimental Analysis of the Urea-Water Solution Temperature Effect on the Spray Characteristics in SCR Systems". In: *SAE Technical Paper Series* 1 (2015). DOI: 10.4271/2015-24-2500.

[8] Oh, Jungmo and Lee, Kihyung. "Spray characteristics of a urea solution injector and optimal mixer location to improve droplet uniformity and NOx conversion efficiency for selective catalytic reduction". In: *Fuel* 119 (2014), pp. 90–97. DOI: 10.1016/j.fuel.2013.11.032.

[9] Zheng, Guanyu. "Development of Air-Assisted Urea Injection Systems for Medium Duty Trucks". In: *SAE Technical Papers* 2017-Septe.September (2017). DOI: 10.4271/2017-24-0112.

[10] Munnannur, Achuth, Chiruta, Mihai, and Liu, Z Gerald. "Thermal and Fluid Dynamic Considerations in Aftertreatment System Design for SCR Solid Deposit Mitigation". In: *SAE Technical Paper Series* 1.1 (2012). DOI: 10.4271/2012-01-1287.

[11] Shahariar, G. M.Hasan and Lim, Ock Taeck. "A study on urea-water solution spray-wall impingement process and solid deposit formation in urea-scr de-nox system". In: *Energies* 12.1 (2019). DOI: 10.3390/en12010125.

[12] Montenegro, G. et al. "CFD analysis applied to the design of aqueous urea SCR dosing system with reduced risk of solid deposit formation". In: *THIESEL 2018 Conference on Thermo- and Fluid Dynamic Processes in Direct Injection Engines High-pressure*. 2018.

[13] Strots, Vadim O., Santhanam, Shyam, Adelman, Brad J., Griffin, Gregory A., and Derybowski, Edward M. "Deposit formation in urea-scr systems". In: *SAE International Journal of Fuels and Lubricants* 2.2 (2010), pp. 283–289. DOI: 10.4271/2009-01-2780.

[14] Kim, Chang Su and Park, Sung Young. "A design-variable-based computational study on the unsteady internal-flow characteristics of the urea-SCR injector for commercial vehicles". In: *Defect and Diffusion Forum* 379 (2017), pp. 64–72. DOI: 10.4028/www.scientific.net/DDF.379.64.

[15] De Rudder, Korneel and Chauvin, Corine. "Close coupled DOC - mixer - SCR for Tier 4 final". In: *7th AVL International Commercial Powertrain Conference* (2013), pp. 1–10.

[16] Kapusta, Łukasz Jan. "LIF/Mie Droplet Sizing of Water Sprays from SCR System Injector using Structured Illumination". In: *Proceedings of ILASS2017 - 28th European Conference on Liquid Atomization and Spray Systems* September (2017), pp. 580–587. DOI: 10.4995/ilass2017.2017.5031.

[17] Varna, Achinta, Spiteri, Alexander C., Wright, Yuri M., Dimopoulos Eggenschwiler, Panayotis, and Boulouchos, Konstantinos. "Experimental and numerical assessment of impingement and mixing of urea-water sprays for nitric oxide reduction in diesel exhaust". In: *Applied Energy* 157 (2015), pp. 824–837. DOI: 10.1016/j.apenergy.2015.03.015.

[18] Spiteri, Alexander and Dimopoulos Eggenschwiler, Panayotis. "Experimental fluid dynamic investigation of urea-water sprays for diesel selective catalytic reduction-denox applications". In: *Industrial and Engineering Chemistry Research* 53.8 (2014), pp. 3047–3055. DOI: 10.1021/ie404037h.

Chapter 6

Droplet Characterization

6.1 Introduction

This chapter covers all the results related to the spray droplet characterization. The experimental tests were performed in the optically accessible facility detailed in chapter 3. The first part describes the experimental test conditions of pressure, mass flow, and temperature that resemble those of the exhaust line in a real engine. The chosen values for the tests are in accordance with the test points of the macroscopic spray characterization presented in previous chapter 5, which cover the general operating conditions range. Then, results are discussed in two main parts: droplet diameter distribution and droplet velocity at different regions of the spray. As previously underlined in chapter 2, the spray atomization is crucial for the mixture preparation and the effective decomposition process of the UWS injected into ammonia. Finally, the chapter lists a summary and the main conclusions.

6.2 Test plan

This section focuses on the description of the test plan employed in the experimental campaign. The droplet characterization was performed at the same conditions used for the spray visualization measurements in order to be consistent and to complement the analysis. The selected operating points were chosen with the aim to cover different conditions that resemble a real exhaust pipe in standard operation. The test plan is presented in Table 6.1.

Table 6.1: Test plan for the droplet characterization.

Parameter	**Value**	**Units**
Injection Pressure (P_{inj})	4 - 6 - 8	bar
Coolant Temperature (T_{ref})	90	°C
Air Mass Flow ($\dot{m}_{air}$)	40	$kg\,h^{-1}$
Flow Temperature (T_{flow})	180 - 350	°C
Injection frequency	1	Hz
Tested Fluid	Adblue	-
Repetitions	10	-

For the droplet characterization, the near field visualization set up was employed (detailed in section 3.8.1). The optical configuration used was presented in Figure 3.27, where the Nikon Sigma lens used for the macroscopic spray was replaced with the K2 DistaMax microscopic lens (about 40.2 pix/mm), providing a more detailed visualization of the spray. With the magnification captured by this lens, droplets of the UWS spray can be seen and measured, allowing the determination of their diameter, trajectory, and velocity. Based on the preliminary results of global spray penetration and angle, three representative measuring positions were selected for the droplet size imaging:

- Position 1 (P1): at 4 mm below the nozzle exit to understand the droplet morphology near the injector, at the beginning of the atomization process.
- Position 2 (P2): placed on the axis of the injector and located 30 mm far from the nozzle exit. This position was chosen to understand what is happening in the central region of the spray (note that from previous results the 3 orifices form a single global spray) where the droplets should be already formed.
- Position 3 (P3): located as far from the nozzle as P2, but 7 mm off-axis in the direction of the flow (see Figure 6.1). This position will provide information about the droplet distribution in the region near to the border of the spray.

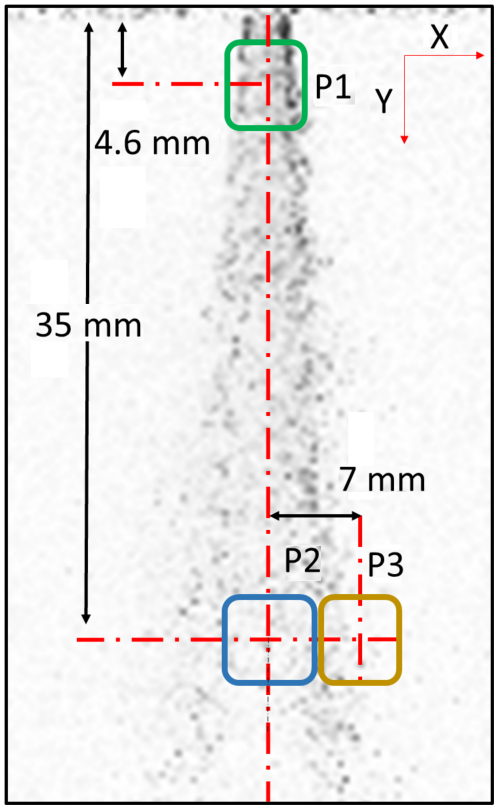

Figure 6.1: Location of the windows used for the near-field visualization (not to scale). P1: Position 1, P2: Position 2, P3: Position 3.

All measurement positions were recorded in an optical window of 4.1 mm in height and 3.8 mm in width (not to scale in the drawing) and can be seen in Figure 6.1. The axis of the injector coincides with the Y-axis of the reference system. The field of view lies on the XY plane, and the size of the window was considered an adequate compromise to obtain a proper image resolution while preserving the possibility to get a significant number of droplets recognized by the system. The characteristics of the optical configuration are detailed in Table 6.2. Current method is analogous to the DBI technique used in previous chapter, however since in this optical arrangement the long-distance microscope is used, the optical technique in this chapter is called "High-Speed Microscopic Imaging" (HSMI).

The experiments were performed using the same three-hole injector employed for the hydraulic characterization and the macroscopic spray measure-

Table 6.2: Details of the optical setup for the DBI: Near field spray measurements.

	DBI: Near-Field Spray
Camera	Photron SA5
Lens	K2 DistaMax
LED	200 ns
Frame Rate	150.000 fps
Resolution	256 x 216 pixels
Pixel/mm	40.2

ments presented in previous chapters. The fluid used was AdBlue, which properties are also described in section 4.6. The tests were performed in accordance with the conditions summarized in Table 6.1, with 10 repetitions per test point.

6.3 Droplet size distribution

The understanding of the spray evolution and the droplet sizing is of particular importance for a proper mixing in the exhaust after-treatment line. An adequate spray atomization quality should be obtained to exploit the potential of the UWS system. Therefore, this section shows the results of the droplet evolution in terms of droplet size distribution in a wide range of injection pressure levels, gas mass flow, and temperature conditions to assess the effect of each variable. In order to investigate the droplet characteristics in realistic operating conditions, the test rig described in 3.6 is employed together with the optical set up detailed in section 3.7. The quantitative and qualitative results obtained are useful information that can be directly employed for validation or as a boundary condition in CFD modelling, to improve the design and performance of UWS dosing equipment [1, 2].

6.3.1 Droplet size determination

Figure 6.2 shows three images at position P1 near to the nozzle exit (top row) and three frames at position P2 downstream in the center axis of the spray (bottom row), for the three pressure levels tested at a gas temperature of 180 °C. Those images correspond to the time step of 3 ms after start of energizing (ASOE). The injection event is stabilized at this time step, with no influence of the movement of the needle during the opening or closing stages.

From these images, it can be seen that in position P2 (frames D, E and F) most of the droplets were spheres with small size. However, at location P1 (frames A, B and C) there were some other regions of liquid with non-spherical droplets, with more elongated structures, like blobs or ligaments, that were still breaking up [3, 4]. A similar observation was previously reported by Brizi et al [5], where they also registered the appearance of some non-spherical blobs at different positions of the plume.

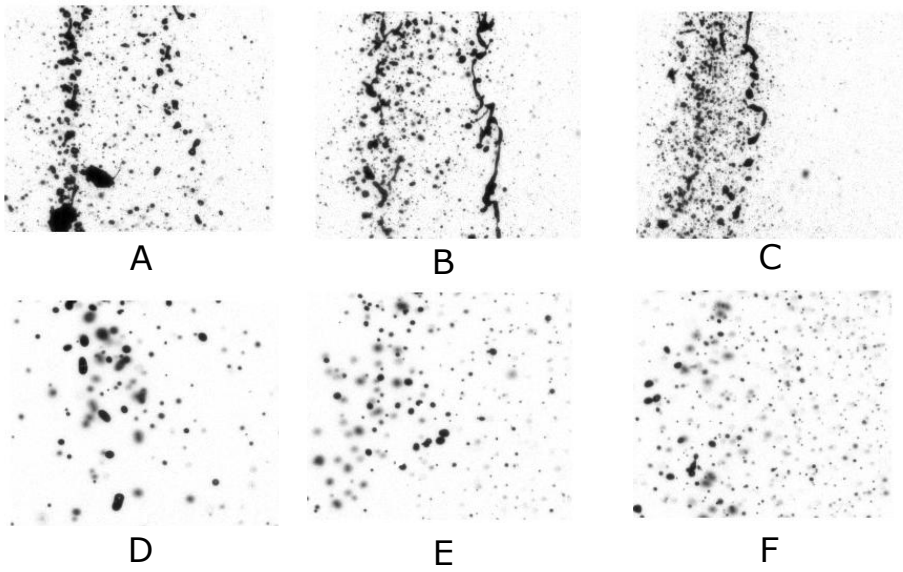

Figure 6.2: Images of the UWS droplets at two positions of the spray. Top row: Position P1. Bottom row: P2. For three injection pressures: 4 bar (A and D), 6 bar (B and E), and 8 bar (C and F). Gas temperature: 180 °C.

Since the liquid structures in the UWS spray can have different morphologies (spheres, blobs, ligaments, etc.), it was decided to standardize all the non-spherical and ligament shapes, calculating an equivalent diameter of all the contours detected using the following relationship:

$$D_{eq} = \sqrt{\frac{4A}{\pi}} \tag{6.1}$$

Where D_{eq} is the equivalent diameter and A is the area of the droplet. This calculation was applied to each time step of the injection event during the stabilized phase of the injection (not considering the opening and closing

transient) and for all 10 repetitions. At the end, around 6000 frames were analyzed per each test condition.

Validation of the diameter measurements:

An important activity that should be done before going into detail of the analysis of the droplet diameter distribution is a validation of the High Speed Microscopic Imaging (HSMI) method that is employed. The characterization of the droplets can vary depending on the experimental technique used. This section compares and analyzes the similarities and differences of the methodology implemented in the current study against two more optical techniques available, such as the Phase Doppler Anemometry (PDA) and the High Resolution Laser Backlight imaging (HRLBI).

Those optical techniques were configured and implemented during a research stay of the author at Universitat degli Studi di Perugia, where the similarities and differences of the three optical techniques for the droplet diameter detection were explored. The details of the optical arrangement employed and the image processing procedure for the PDA and the HRLBI are explained in [4]. The reason for choosing those techniques is justified as follows: From one side, PDA has the most robust data acquisition, but it could become a challenge due to the high precision in the alignment needed in the equipment to measure accurately, especially for the complexity of the test chamber geometries used to reproduce existing SCR systems. The other imaging technique, the HRLBI, is also a viable option to capture the microscopic characteristics of the spray, since that techniques acquire data in a fast manner and capture relatively large areas of the spray in each position. On the contrary, the PDA system can only make local measurements and require a high number of samples in each test point.

Position P2 (located 30 mm away from the nozzle exit in the spray axis) was chosen to compare the data obtained from the three techniques. For this purpose, the corresponding position for PDA was analysed individually. The data obtained from the HRLBI was filtered to characterize only the droplets located inside a region of 4 by 4 mm in that position, which is approximately the same window used for the HSMI used in this Thesis. The results of the three techniques are illustrated in Figure 6.3. It presents the Probability Density Function curves (PDF curves) at an injection pressure of 6 bar, which was the pressure level chosen for the comparison. This figure simultaneously presents the Cumulative Volume Fraction (CVF) curves in the right side axis, where the location of the characteristic diameters Dv10, SMD, Dv50 and Dv90 are indicated with symbols for each case.

The curves represented in the figure show a similar behaviour. In general, it indicates that the three techniques are comparable and provide equivalent results for the droplet diameter distribution. Nevertheless, it should be noted that the PDA system available for the validation campaign is limited in terms of maximum droplet dimension, specifically a diameter value of approximately 400 μm can not be captured properly. However, big size droplets (above 400 μm) can be observed in this low-pressure type of atomizer, particularly at the beginning of the spray. Then, the use of PDA would provide an imprecise characterization of the spray.

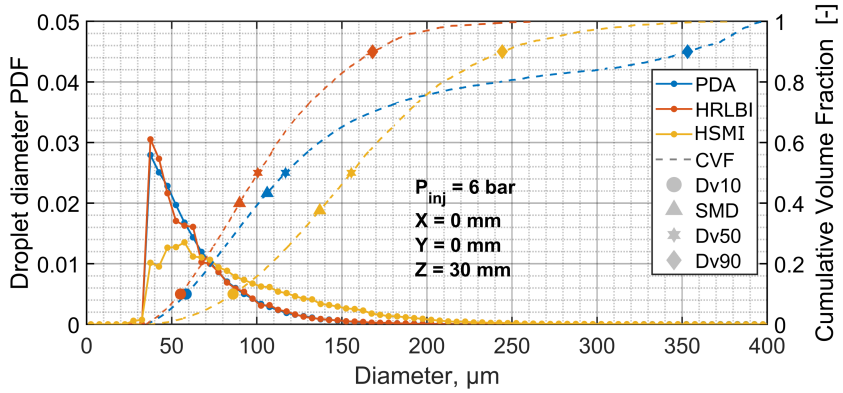

Figure 6.3: Droplet diameter PDF for three different techniques at position P2. Injection pressure: 6 bar.

The main difference between the HSMI and the other two techniques is observed in the lower probability curve for droplet diameters in the range between 35 and 50 μm. This difference could be attributed to the criteria applied to keep the droplets during the image processing step, which required that the droplets remained in the focus plane for at least 4 consecutive frames for this technique.

On the other hand, the confidence of the data obtained in this work is also based on references found in the literature that compared the DBI technique versus the PDA, finding good agreement in the results [5, 6]. Those reports were done at spray positions far from the nozzle exit, where most of the particles are spherical. In the near nozzle region, the spray is denser and the droplets are not spherical and could have any other shape, as ligaments or blobs. Here the validation is more restricted, and from the knowledge of the author there is very limited information available in the literature.

Although there are some differences between the HSMI and the other two techniques in the determination of the smallest droplet diameter, this is the chosen one for the current thesis, since this optical technique provides reasonable results comparable to those obtained from a direct measurement of spray drop size like PDA. Moreover, it can identify liquid ligaments and non-spherical droplets (as seen in Figure 6.2) which are present in low pressure injector sprays, especially in the region near the nozzle exit. Therefore, from now on the results that are analysed in subsequent sections correspond to those obtained with this technique.

6.3.2 Effect of injection pressure on the droplet size distribution

As stated in Table 6.1, three different levels of injection pressure were used in the test plan. It is expected that the total number of droplets for each injection pressure should be proportional to this parameter. This is based on the results presented in previous chapter, which corroborated that the injected mass is proportional to the square root of the pressure difference between the injector line and the discharge vessel. In fact, the number of droplets found were on average 10% and 25% higher with the increase of the injection pressure from 4 to 6 and 6 to 8 bar, respectively. To be able to draw comparisons between measurement points, a normalized probability distribution [7] was calculated and is depicted in Figure 6.4, for the position P1 and the three injection pressures. Even though a wide range of diameter size distribution was captured, the minimum diameter detected with this setup was limited to 21.7 μm, due to the optical zoom restriction and pix/mm relation. However, as Varna et al [8] and Postrioti [9] reported for similar conditions, the number of droplets with a diameter below 25 μm could be considered negligible.

In the position near the nozzle exit (position P1), the injection pressure influenced the droplet quantity and size distribution. For the smaller droplets (21 μm to 45 μm) the three curves behave similarly. The injection pressure of 8 bar has a higher droplet probability in the range between 80 μm and 180 μm. For droplets with diameters above 200 μm, the tendency reverts and depicts a higher droplet probability for the injection pressure of 4 bar. This result is consistent with the worse atomization generated at 4 bar, where more blobs and particles with bigger area could be observed and was also visible in the images of Figure 6.2 (A, B, and C). This technique detects that most of the volume of the droplets is concentrated in diameters above 150 μm. The overall values obtained in this work were in the same order of magnitude as those found by other authors [8–11].

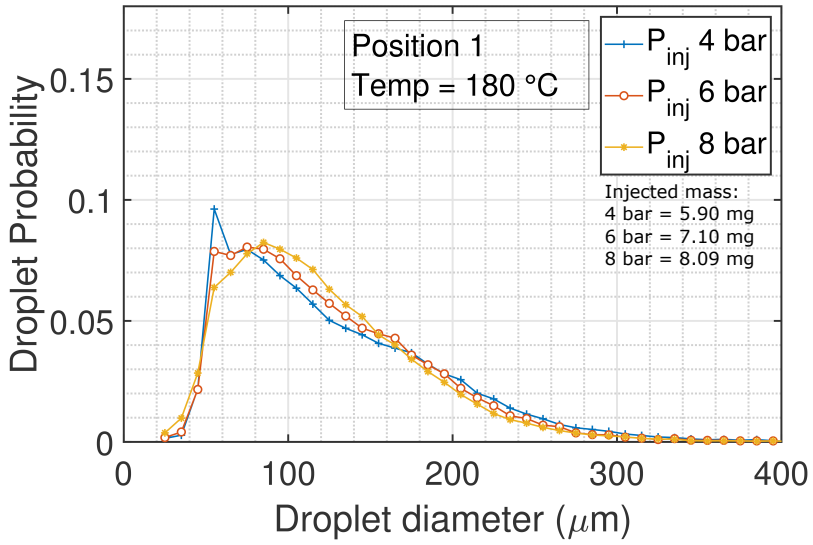

Figure 6.4: Distribution of the droplet diameter at position P1 (near the nozzle exit) for the three injection pressures.

Figure 6.5 shows the distribution of the droplet size at the region of interest in position P2, far from the nozzle exit. Injection pressures of 6 and 8 bar have a higher proportion of droplets with diameter below 50 μm than the one of 4 bar. The mode of the three distributions is at 50 μm, and between this diameter and 110 μm the 8 bar curve has a higher probability than the rest. For diameter values greater than 110 μm, the 4 bar curve has higher probability than the 6 and 8 bar curves as was observed in Position P1.

In Figure 6.6, the trends of the distributions at position P3 are shown. The behaviour observed is similar to the position P2. The 8 bar curve has a higher proportion of droplets with sizes between 55 and 110 μm, whereas the 4 bar curve has greater probability for diameters bigger than 110 μm. The difference in the distribution curves is small compared to what was observed in Figure 6.5, meaning that as the region of interest is moved away from the spray axis, the effect of the injection pressure is less noticeable in terms of droplet distribution. This can be related to the fact that there is more aerodynamic interaction with the surrounding cross-flow circulating through the test facility.

Comparing the droplet distribution in the three positions of the spray it can be seen that in regions further away from the nozzle, the proportion of big

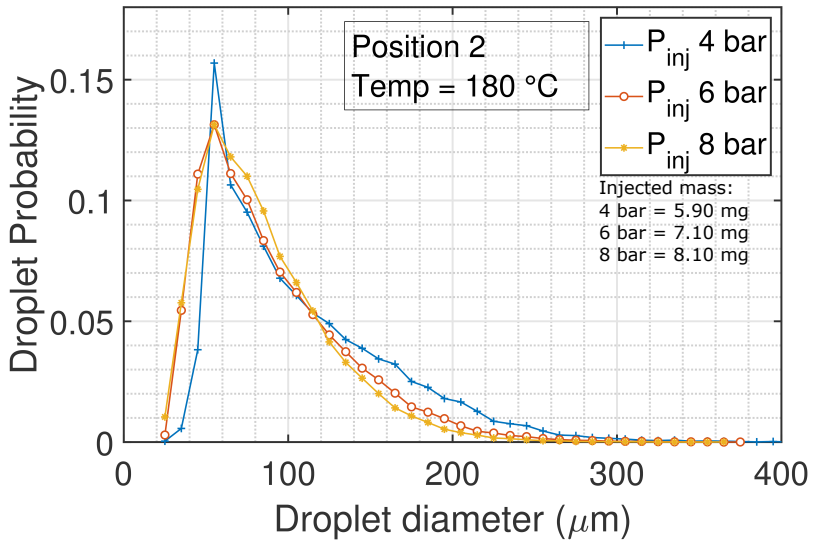

Figure 6.5: Distribution of the droplet diameter at position P2, for the three injection pressures.

droplets with a diameter above 100 μm decreased, evidencing that atomization process or evaporation took place at the developed zone of the spray.

Effect of the pressure on the morphology of the droplet during the opening and closing stages

Although the main part of the work focuses on the study of the stable region of the injection event (when the injector is completely open), an interesting aspect of the optical technique used is the possibility to analyse the behaviour of droplets during the opening and closing of the needle. In Figure 6.7, a sequence of images obtained with the HSMI technique is presented. The frames were obtained at position P2, where the columns represent the evolution of the injection. From left to right: the start of injection, the stable part of the spray and the end of injection, respectively. Meanwhile, the rows indicate the injection pressures of 4, 6, and 8 bar (upper row, intermediate and lower row, respectively).

Droplets and ligaments of big dimensions can be observed at the beginning of the injection event. The biggest structures appears for the lower injection pressure. The images corresponding to the 8 bar pressure have a greater number of droplets and qualitatively are smaller than the particles present in the

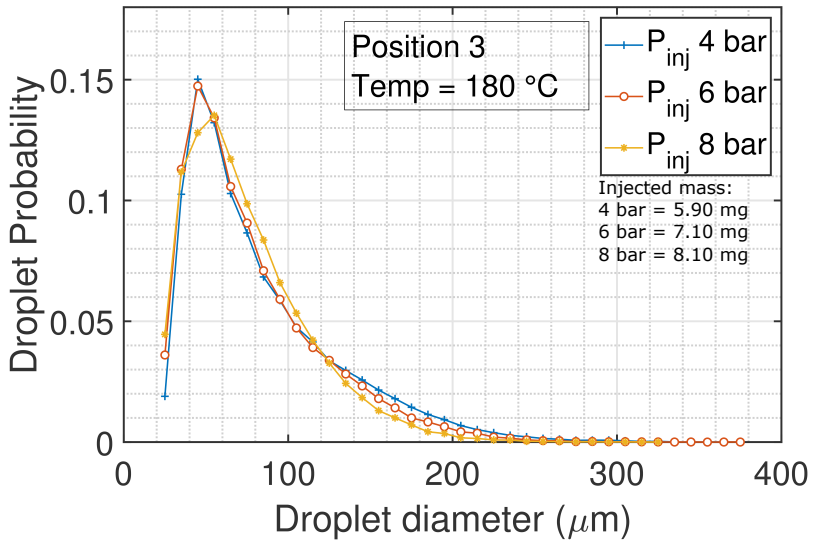

Figure 6.6: Distribution of the droplet diameter at position P3, for the three injection pressures.

images of 4 and 6 bar. This is an indication of better atomization of the spray. As the injection event ends, droplets and blobs with big dimensions appear again. These variations on the droplet sizes are also reflected in the Figure 6.8, which illustrates the evolution of the Sauter Mean Diameter (SMD) over time, showing similar behaviour for all injection pressures during the injection event. Two particular peaks can be observed, around 2.5 ms and 7.5 ms. The first peak at 2.5 ms denotes the initial packages of big droplets and ligaments due to the opening of the injector (in agreement with the fluctuations observed in the momentum flux curves). Meanwhile, at 7.5 ms there is an increase of the diameter that can be attributed to the final bobbles and big drops formed when the needle of the injector closes.

6.4 Droplet velocity distribution

A similar approach as the one shown in the previous section was used to compare the velocity of the droplets in the injector axis (Y component) and in the gas flow direction axis (X component).

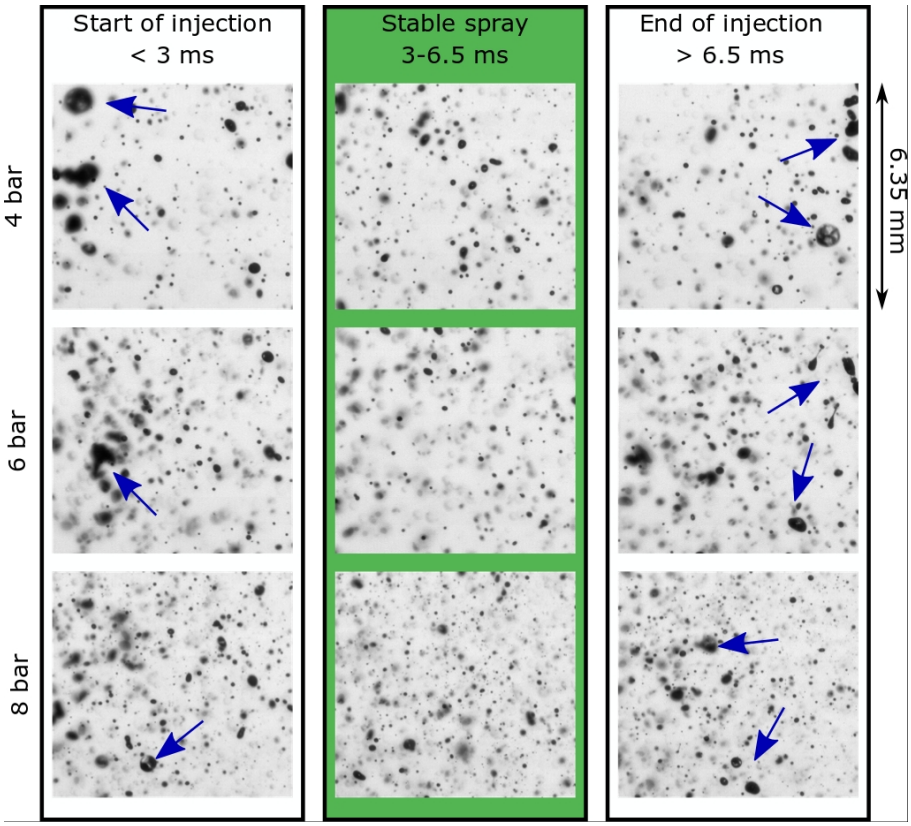

Figure 6.7: Droplet morphology identification in position P2 (Y = 30 mm) at different time steps. Injection pressure: 4, 6 and 8 bar. Technique: HSMI

6.5 Velocity determination and validation of the measurement technique

The velocity of the droplets in the X and Y directions are calculated following the methodology explained in section 3.8.1 and also presented by Payri et al. [12]. Note that the X direction is perpendicular to the spray axis, and the Y component is in the vertical direction parallel to the injector axis. Analogous to the procedure followed for the droplet diameter characterization, the first step was to validate the methodology for the droplet velocity determination. This work was also performed during the international visiting stage at Universitat degli Studi di Perugia. For the droplet velocity validation, only the PDA technique was employed since the HRLBI method does not allow to determine this parameter.

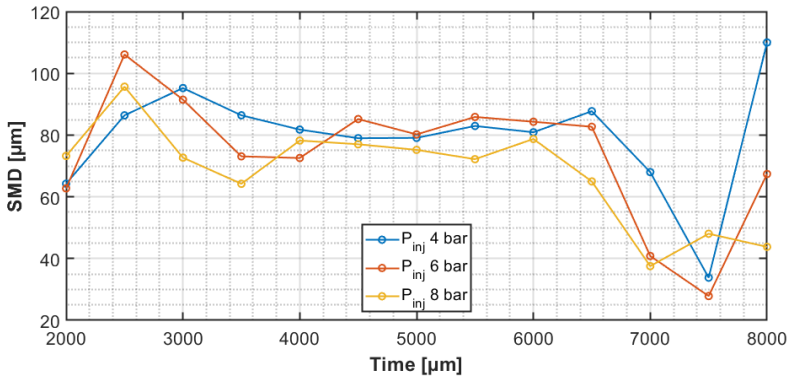

Figure 6.8: Sauter Mean Diameter (SMD) evolution over injction time. Injection pressure: 4, 6 and 8 bar.

For the initial comparison, the velocity in the Y direction obtained with the PDA and HSMI techniques in position P2 (30 mm away from the nozzle exit) are compared in the range of diameters from 35 to 350 μm. Figure 6.9 illustrates a scatter of the droplet velocity versus its correspondent diameter where similar trends can be observed in both techniques. In a previous study [4] it was evidenced that smaller droplets have a wide range of velocities ranging from 0 m/s to 40 m/s. Meanwhile, as the diameter of the droplets increases, most droplets travel at the same velocity, converging towards 30 m/s. This behaviour is observed with both techniques.

An average velocity of the droplets was then calculated for the three injection pressures and is presented in Figure 6.10 . This figure does not contain droplets from all distances from the nozzle exit (Y axis), just those at Y = 30 mm in the center of the spray. Therefore, the mean velocity is calculated for the droplets contained in the region of interest for the HSMI and the corresponding traverse points for the PDA to make a suitable comparison. The figure shows that the average velocity increases almost linearly with the pressure (within the tested injection pressure range), presenting a similar slope for both techniques, with a narrow difference of nearly 2 m/s between the averages of the measured velocity for each technique in every tested injection pressure.

The gap between the blue and the red lines can be attributed to the intrinsic differences between both techniques (PDA measures in a small volume, whereas the HSMI measures a wider region), and to the fact that the HSMI has difficulties tracking the tiny droplets, which are the ones with lower velocities.

Based on these results, and despite the small differences commented above, it can be concluded that for the droplet velocity in the Y direction, there is good agreement between the PDA and the HSMI, showing that the trend of the captured droplet velocity distribution and the average velocity are similar in both techniques. Therefore, the HSMI and the corresponding methodology is going to be implemented for further parametric analysis due to its versatility for the setup and also because it has the capability to capture the movement of the droplets in the X and Y direction of the spray simultaneously.

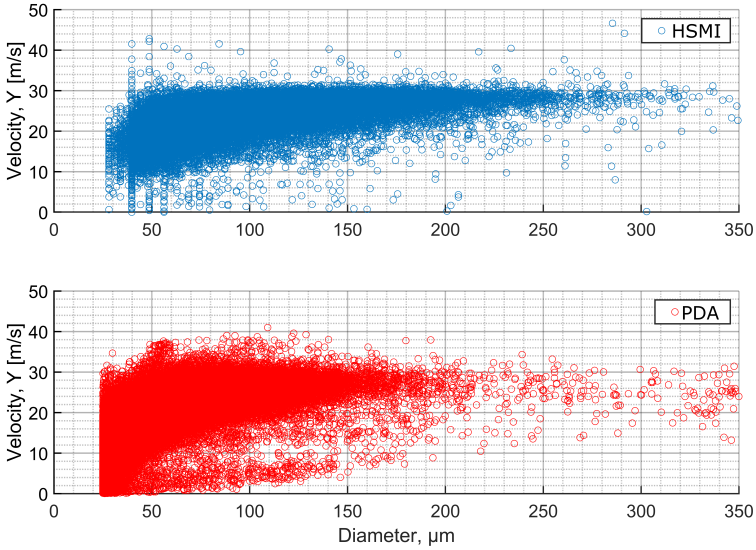

Figure 6.9: Droplet velocity versus diameter comparison for both measuring techniques.

6.5.1 Effect of injection pressure on droplet velocity

Droplet Velocity: Y axis component

Figure 6.11 depicts the curves of the droplet velocity distribution in the region near to the nozzle exit (position P1). Higher injection pressure means more energy present in the fluid, and then the droplets have a faster velocity. Moreover, an increase in the pressure results in an asymmetric distribution of the droplet velocity. The peak of the velocity distribution is shifted towards the right side of the graph at the highest injection pressure of 8 bar. The behaviour is different at 4 bar, where the values have a narrower normal

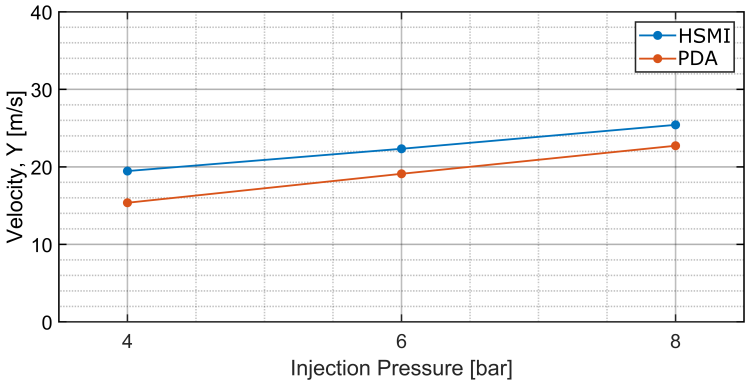

Figure 6.10: Droplet average velocity in Y direction measured by PDA and HSMV for three pressure levels.

distribution with a mean of 23m/s, comparable to the theoretical Bernoulli velocity at those conditions in the nozzle exit (approximately 24.4 m/s).

Figure 6.12 shows the velocity distribution curves for position P2. The behaviour with the injection pressure is similar to what was observed in position P1, finding a higher velocity of the droplets when the pressure increased. Unlike the previous position P1, in this part of the spray the shape of the velocity curves are similar and more uniform, which is reasonable since the particles tend to decelerate when they exchange momentum with the surrounding gas. The homogenization of the curves can be attributed to atomization processes happening between both positions and to the drag generated by the gas.

Finally, the droplet distribution for position P3 is shown in Figure 6.13. It can be seen that the curves for the three cases had a uniform distribution for this off-axis position. An increment in the injection pressure shifted the distribution curves toward faster velocities. In comparison with position 2, the distributions have a wider range, especially for the 4 bar curve, meaning that there are more droplets with heterogeneous velocities in this position.

If velocity values are compared between the three positions for the same injection pressure, a general deceleration is observed as the droplets move far from the nozzle due to the momentum exchange with its surroundings and to the interaction of the UWS with the flow (that tends to deflect the spray in the direction of the gasses) [13].

The results obtained for this component of the velocity are in concordance with the ones found in other studies [14]. As a summary, the injection pressure

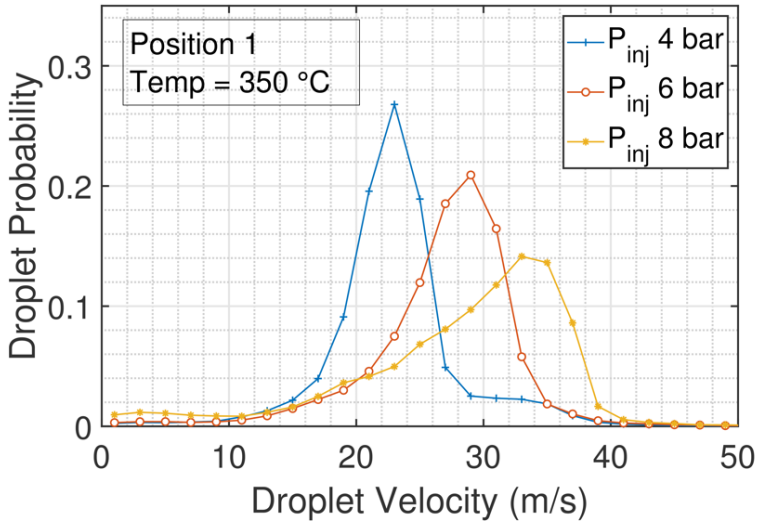

Figure 6.11: Droplet velocity distribution in the Y axis at prosition P1, for the three injection pressures.

plays an important role in the observed values as expected for the Y component of the velocity. Higher injection pressure causes a higher exit velocity of the fluid from the nozzle and it is reflected on the droplets velocity downstream.

Droplet Velocity: X axis component

The following figures present the results for the X component of the velocity. Figure 6.14 shows that the velocity in the X direction is faster when the injection pressure is increased, and could be an indication of the tangential movement of the droplets due to higher turbulence of the fluid as it exits the nozzle of the injector. In the X direction, the velocity has negative and positive values in an almost symmetrical way due to the spray opening in the radial direction (in both directions left and right), nevertheless there is a significant amount of droplets where the $Vx = 0m/s$ that only move in the Y component [15].

Figure 6.15 illustrates the distribution of the droplets velocity at position P2. It is noticeable that at this position the distribution is narrow and symmetric. In this region most of the droplets observed are those that travelled straight down from the nozzle, mainly in the vertical component of the velocity, not being deflected by the air flow.

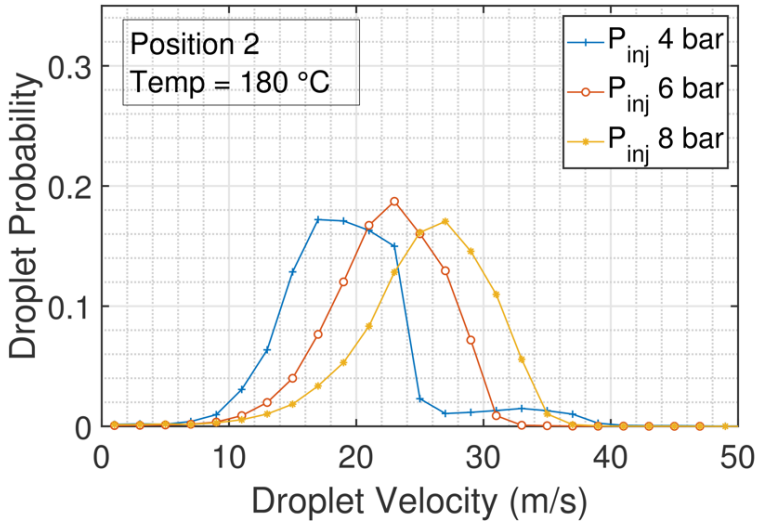

Figure 6.12: Droplet velocity distribution in the Y axis at prosition P2, for the three injection pressures.

Figure 6.16 presents the results of the X component of the velocity at P3 for the three injection pressures, showing a similar behaviour in terms of distribution range and shape for the three levels. The mode is on the positive side of the chart, indicating that the majority of the droplets in the periphery of the spray are traveling in the gas flow direction. Also, the velocity values are shifted to the right side of the chart for the highest injection pressure.

6.5.2 Effect of the flow temperature on droplet velocity

In Figures 6.17 and 6.18, the influence of the temperature of the flow on the velocity of the droplets is presented. In the closest position to the nozzle, there was not a relevant effect on the droplet velocity distribution shape for both components due to the short distance from the exit orifices and the short exposure of the spray to the flow. Nevertheless, the curves representing the flow temperature of 350 °C are slightly displaced towards a higher velocity. When the temperature of the gas is increased, its density becomes smaller and since the gas flow is set to 40 kg/h and the section area is constant for all test points, its velocity increases due to mass flow conservation ($\dot{m} = \rho v A$). This could explain the increase of velocity observed in Figure 6.18 at positions P2 (spray axis) and P3 (periphery of the spray). Additionally, the effect of

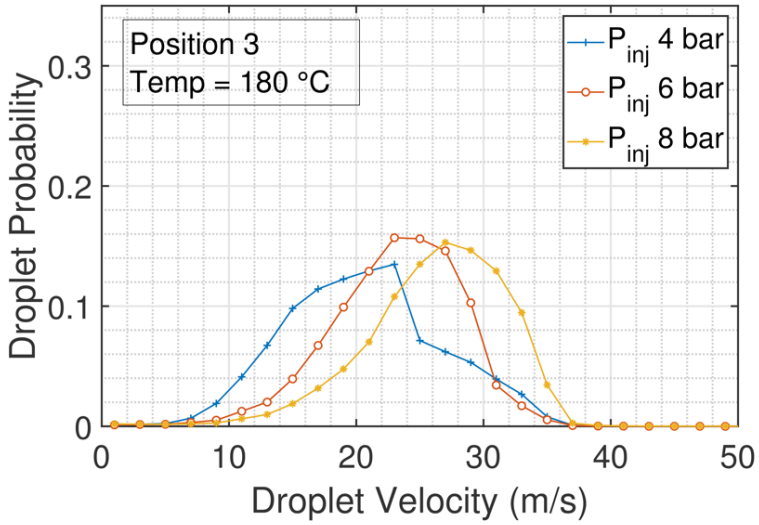

Figure 6.13: Droplet velocity distribution in the Y axis at prosition P3, for the three injection pressures.

increasing the temperature of the gas flow affects its viscosity facilitating the penetration of the fluid in the chamber, in agreement with the results of the macroscopic spray characterization of the same injector studied by Payri et al [13].

6.5.3 Droplet diameter - velocity relationship

As a summary of the results presented above, Figure 6.19 shows the relationship that exists between the velocity of the droplets and their size, corresponding to the injection pressure of 4, 6, and 8 bar and 180 °C at position P1. The upper part of Figure 6.19 shows a three-dimensional plot of the normalized droplet size and velocity distributions. In the case of the velocity of the droplets, the normalization is done considering the theoretical exit velocity from the nozzle as $U_o = \sqrt{2\Delta P/(\rho L)}$. For the droplet size, the normalization takes into account the mass median diameter (MDD), which is obtained by calculating the volume in each interval of the distributions as $\Delta Q_i = \Delta N_i(\pi/6)[1/2(D_{i1} + D_{i2}]^3$, where ΔN_i is the number of droplets in each interval and D_{i1} and D_{i2} the boundary diameters of the mentioned interval, then the MMD is the diameter where the cumulative sum of the volume in the intervals equals 50% of the total liquid volume [15].

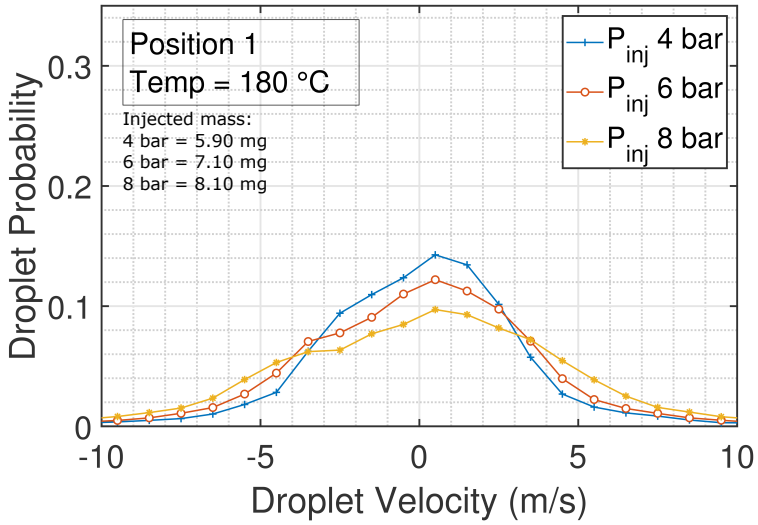

Figure 6.14: Distribution of the droplet velocity in the X axis at P1, for the three injection pressures.

The bottom part of Figure 6.19 shows three projections from the top view, which gives a good idea of the diameter-velocity trend. In general, from the three plots, the majority of the droplets are smaller than the MMD and travel at a lower velocity than the theoretical U_o. From a practical point of view this could have some implications when the boundary conditions are imposed for CFD calculations. This scattered distribution could be important when the evaporation rate wants to be determined because, as Birkhold suggested in [16], small droplets do not penetrate as much as bigger droplets and evaporate and decompose faster, resulting in a temperature drop and an increase of the concentration of water vapour and NH_3 far from the nozzle where this phenomenon occurs, affecting the de-NOx process in the catalytic converter.

6.5.4 Dimensionless numbers and atomization regimes

As a final stage of this work, a brief analysis of the regimes of the UWS spray is done in two stages: first, the primary breakup, considering the influence of the internal flow regime (inertial forces and viscous forces), and in the second step, considering the second breakup. In general, several authors have described the disintegration of liquid jets by two main mechanisms. The first mechanism is the breakup of the intact liquid core into droplets (primary atomization).

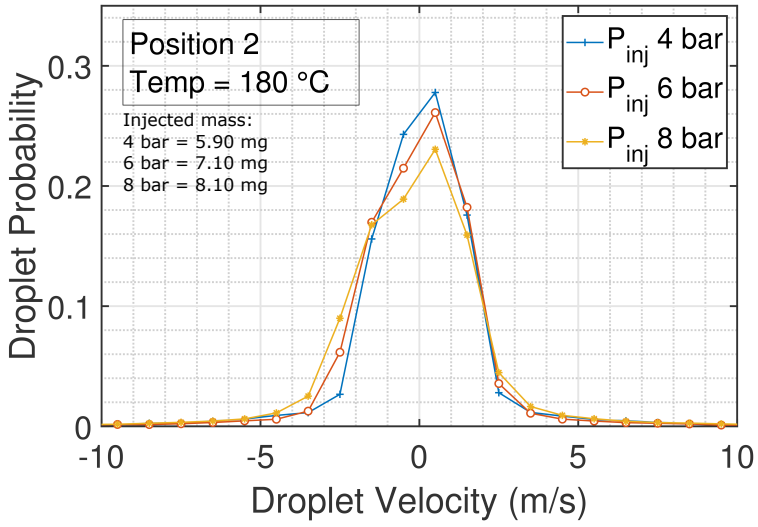

Figure 6.15: Distribution of the droplet velocity in the X axis at P2, for the three injection pressures.

The second mechanism is the breakup of droplets into smaller ones (secondary atomization). Both mechanisms are dependent on the properties of the liquid and the surrounding gas. Equally important is the relative velocity between the liquid and the surrounding gas.

Specifically, the primary breakup mechanism concerns the breakup of the intact liquid core, and perhaps the most commonly used criteria for classifying spray disintegration is that proposed by Ohnesorge, who classified the jets according to the relative importance of gravitational, inertial, surface tension and viscous forces. He used dimensionless analysis to show that the breakup mechanism of a jet could be expressed in three stages, characterized by the magnitudes of the Reynolds number and a non-dimensional number Oh,

The Oh number is the relation of viscous to surface tension and inertial forces and is generally expressed as shown in equation 6.2, where μ_l is the liquid dynamic viscosity, ρ_l is the density, σ is the surface tension and L is a characteristic length. The subscript l denotes the properties of the liquid.

$$Oh = \frac{\mu_l}{\sqrt{\rho_l \sigma L}} \tag{6.2}$$

For the analysis of the primary breakup, the Ohnesorge chart is used, which relates the Oh and the Re, as is also explained in Section 2.4. For this step,

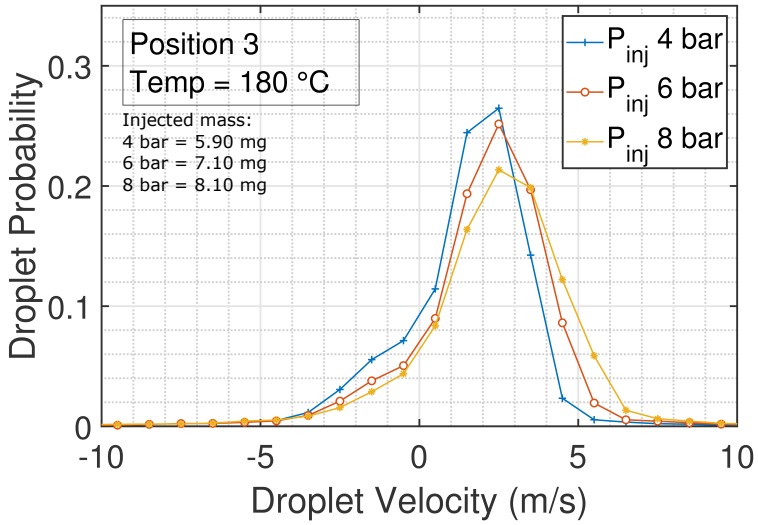

Figure 6.16: Distribution of the droplet velocity in the X axis at P3, for the three injection pressures.

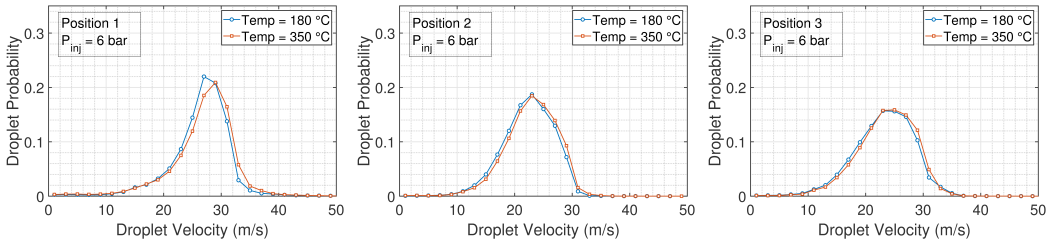

Figure 6.17: Droplet velocity distribution in the Y axis. Position P1 (left), Position P2 (center), and Position P3 (right), Gas-flow temperatures: 180 and 350 ºC.

both non-dimensional numbers are calculated assuming the fluid properties at the pressure and temperature at the nozzle conditions, and the characteristic length is the exit hole diameter. The result is presented in Figure 6.20, where the three pressure conditions are depicted, for the temperature condition of 180ºC. All the conditions are in the second-wind induced regime, and the lower the injection pressure, the closer it is to the first-wind induced zone. This result is in agreement to what is reported in previous studies [17].

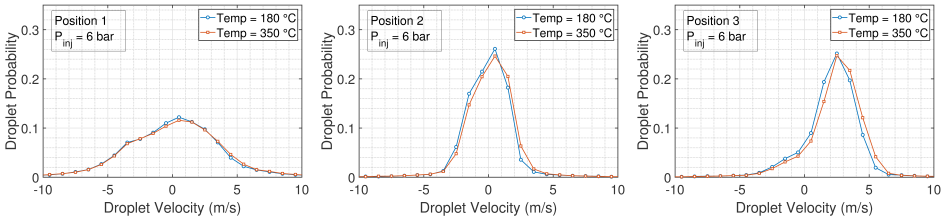

Figure 6.18: Droplet velocity distribution in the X axis. Position P1 (left), Position P2 (center), and Position P3 (right), Gas-flow temperatures: 180 and 350 ºC.

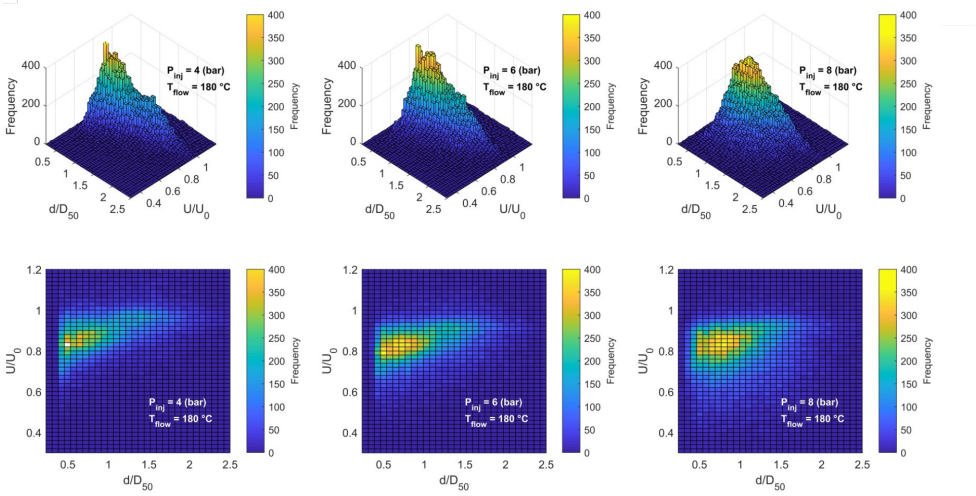

Figure 6.19: Normalized droplet and velocity relationship.

For analyzing the secondary atomization of droplets, the information obtained from position P3 is used. The secondary atomization indicates the breakup of liquid drops into smaller fragments. The most used parameters to evaluate the regimes of the breakup are the Droplet Weber Number $We = \rho_g(U_d)^2 D_d/\sigma$ and the Oh, where now the characteristic length is the droplet diameter D_d.

Figure 6.21 shows the results in the $We - Oh$ chart for the three injection pressure levels tested. It can be seen that all the points have an Oh number below 0.1, indicating that the effects of the fluid viscosity are negligible, and the Weber number governs the transition from one regime to another. At the same time, the Weber number obtained at this location of the spray, is very small and they fall within the non-oscillatory deformation region (for the

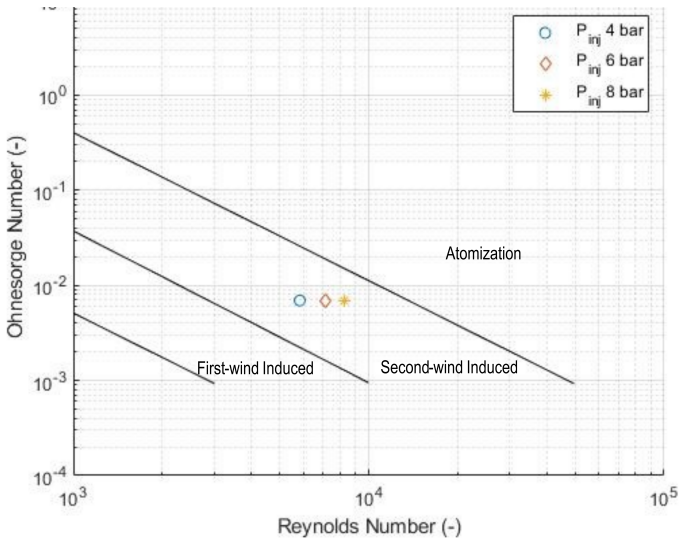

Figure 6.20: Primary breakup regime for the three pressure levels tested.

lowest injection pressure some of the droplets are also in the no-breakup side of the diagram).

The literature refers that the surface tension can resist the breakup if $We < 6$. When the Weber number is slightly higher (around $We < 12$) vibrational breakup is expected, where the external flow leads to oscillations of the drop, promoting the breakup of it into a few fragments (the droplets move towards this direction for the higher injection pressure case). The droplet only vibrates at low speeds and does not disintegrate since it does not reach the relative velocity that defines the critical Weber. All the evaluated points are bellow the critical Weber number (generally agreed upon in the literature to lie between 10 and 12), which is the minimum Weber number required for the liquid droplet to undergo breakup. This means that there are very little probabilities that the droplets would disintegrate more from this position on.

These results shed light on the quantification of the effect of some parameters on the droplet dimensions and evolution. Certainly, there is room for improvement in the disintegration process of the UWS. A proper combination of injection pressure and flow temperature would promote the atomization and the further mixing in the SCR system.

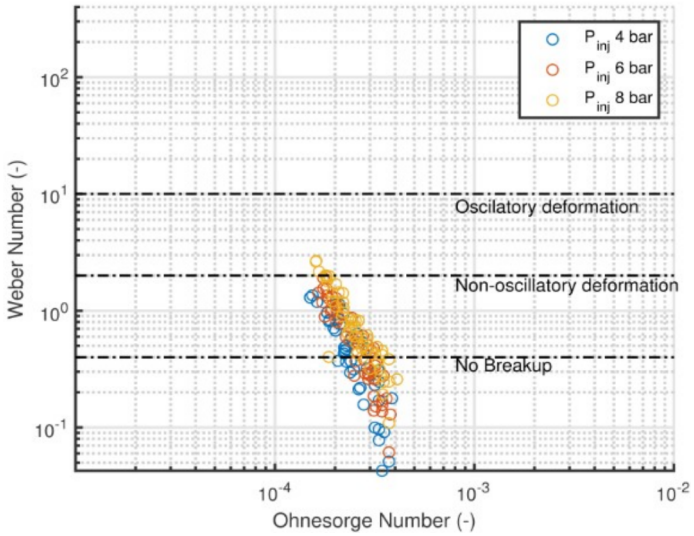

Figure 6.21: Second Atomization regime for the three pressure levels tested.

6.6 Summary and conclusions

This chapter presented and discussed several results related with the droplet characterization. A new test rig was built to carry out the experimental test plan, which is capable of reaching high temperatures and gas mass flow, resembling the conditions of a real exhaust pipe of an engine. The optical accesses of the facility allowed the measurement of the microscopic properties of the spray using the DBI technique at high imaging speed. Three measuring windows were selected for the characterization: one very close to the nozzle exit, and the other two in the developed region of the spray (in the axis of the plume and in the periphery of the spray in the direction of the flow). The first part of the chapter provides the insights of the of the effect of different parameters on the diameter of the droplets. The second part exposes the results of the droplet velocity determination in the three regions of interest of the spray.

The first section is focused on the droplet size determination, and provides the results of the droplet diameter distribution under different conditions of injection pressure and gas temperature. Differences were seen at the three positions of the spray. Near the nozzle exit, higher injection pressure produced more number of droplets with a smaller diameter. Also, at the developed zone of the spray, the particle size distribution showed a higher concentration of

droplets with a small diameter, evidencing that some atomization process took place. The fact of a decrease in the droplet size is an indication of enhanced evaporation as well.

In regions further away from the nozzle, the proportion of big droplets with a diameter above 100 μm decreased, evidencing that some atomization process or evaporation took place at the developed zone of the spray. The confidence of the data obtained is based on references found in the literature and on supplementary measurements that compared the DBI technique versus the PDA, finding good agreement in the results.

The second part of the chapter presents the results of the droplet velocity, which was calculated using a droplet tracking algorithm. The interest in the technique is that the setup is relatively easy and that the velocity can be determined in two components at the same time. I general, it can be stated that the droplet velocity is affected by injection pressure.

The droplet velocity distribution in the injector axis (Y component) showed a wider range of velocity as the injection pressure rose. As the region of interest was set in the developed zone of the spray, the velocity distribution became similar in shape, but still with higher values for higher pressures as expected. The velocity distribution in the flow direction (X component) depended on injection pressure in the region near to the nozzle exit, with a wider shape (negative and positive values) at high pressure that can be related to some degree of turbulence inside the nozzle, moving the flow in the radial component.

The gas temperature influences the velocity distribution in the developed spray zone. The increase of velocity at high flow temperature could be attributed to the change of properties in the gas mass flow, allowing the droplets to penetrate the chamber faster in both directions. From a qualitative point of view, the raw images showed that in locations near the nozzle exit there were regions of liquid with non-spherical structures, like blobs or ligaments, that were still breaking up. On the other hand, in the frames registered in the developed zone of the spray, most of the droplets were spherical, more uniform and smaller than in the first position.

References

[1] Kim, Chang Su and Park, Sung Young. “A design-variable-based computational study on the unsteady internal-flow characteristics of the urea-SCR injector for commercial vehicles”. In: *Defect and Diffusion*

Forum 379 (2017), pp. 64–72. DOI: 10.4028/www.scientific.net/DDF.379.64.

[2] De Rudder, Korneel and Chauvin, Corine. "Close coupled DOC - mixer - SCR for Tier 4 final". In: *7th AVL International Commercial Powertrain Conference* (2013), pp. 1–10.

[3] Payri, Raúl, Bracho, Gabriela, Martí-Aldaraví, Pedro, and Moreno, Armando. "Using momentum flux measurements to determine the injection rate of a commercial Urea Water Solution injector". In: *Flow Measurement and Instrumentation* 80 (2021), p. 101999. DOI: https://doi.org/10.1016/j.flowmeasinst.2021.101999.

[4] Bracho, G., Postrioti, L., Moreno, A., and Brizi, G. "Experimental study of the droplet characteristics of a SCR injector spray through optical techniques". In: *International Journal of Multiphase Flow* 135 (2021), p. 103531.

[5] Brizi, Gabriele, Postrioti, Lucio, and Vuuren, Nic van. "Experimental analysis of SCR spray evolution and sizing in high-temperature and flash boiling conditions". In: *SAE International Journal of Fuels and Lubricants* 12.2 (2019), pp. 87–107. DOI: 10.4271/04-12-02-0006.

[6] Blaisot, J. B. and Yon, J. "Droplet size and morphology characterization for dense sprays by image processing: Application to the Diesel spray". In: *Experiments in Fluids* 39.6 (2005), pp. 977–994. DOI: 10.1007/s00348-005-0026-4.

[7] Tang, Chenglong, Feng, Zehao, Zhan, Cheng, Ma, Wen'an, and Huang, Zuohua. "Experimental study on the effect of injector nozzle K factor on the spray characteristics in a constant volume chamber: Near nozzle spray initiation, the macroscopic and the droplet statistics". In: *Fuel* 202 (2017), pp. 583–594. DOI: https://doi.org/10.1016/j.fuel.2017.04.078.

[8] Varna, Achinta, Spiteri, Alexander C., Wright, Yuri M., Dimopoulos Eggenschwiler, Panayotis, and Boulouchos, Konstantinos. "Experimental and numerical assessment of impingement and mixing of urea-water sprays for nitric oxide reduction in diesel exhaust". In: *Applied Energy* 157 (2015), pp. 824–837. DOI: 10.1016/j.apenergy.2015.03.015.

[9] Postrioti, Lucio, Brizi, Gabriele, Ungaro, Carmine, Mosser, Mark, and Bianconi, Francesco. "A methodology to investigate the behaviour of urea-water sprays in high temperature air flow for SCR de-NOx applications". In: *Fuel* 150.x (2015), pp. 548–557. DOI: 10.1016/j.fuel.2015.02.067.

[10] Kapusta, Łukasz Jan and Teodorczyk, Andrzej. "Laser diagnostics for urea-water solution spray characterization". In: *MATEC Web of Conferences* 118.00029 (2017), p. 00029. DOI: 10.1051/matecconf/201711800029.

[11] Kapusta, Łukasz Jan. "LIF/Mie Droplet Sizing of Water Sprays from SCR System Injector using Structured Illumination". In: *Proceedings of ILASS2017 - 28th European Conference on Liquid Atomization and Spray Systems* September (2017), pp. 580–587. DOI: 10.4995/ilass2017.2017.5031.

[12] Payri, Raul, Bracho, Gabriela, Gimeno, Jaime, and Moreno, Armando. "Investigation of the urea-water solution atomization process in engine exhaust-like conditions". In: *Experimental Thermal and Fluid Science* 108.June (2019), pp. 75–84. DOI: 10.1016/j.expthermflusci.2019.05.019.

[13] Payri, Raul, Gimeno, Jaime, Bracho, Gabriela, and Moreno, Armando. "Spray characterization of the Urea-Water Solution (UWS) injected in a hot air stream analogous to SCR system operating conditions ." In: *WCX SAE World Congress Experience* 2019-01-0738 (2019), pp. 1–9. DOI: 10.4271/2019-01-0738.Abstract.

[14] Zhao, Le et al. "Evaluation of Diesel Spray-Wall Interaction and Morphology around Impingement Location". In: *SAE Technical Paper 2018-01-0276* (2018). DOI: 10.4271/2018-01-0276.

[15] Chen, SK, Lefebvre, AH, and Rollbuhler, J. "Influence of geometric features on the performance of pressure-swirl atomizers". In: (1990).

[16] Birkhold, Felix, Meingast, Ulrich, Wassermann, Peter, and Deutschmann, Olaf. "Modeling and simulation of the injection of urea-water-solution for automotive SCR DeNOx-systems". In: *Applied Catalysis B: Environmental* 70.1-4 (2007), pp. 119–127.

[17] Kapusta, Łukasz Jan, Sutkowski, Marek, Rogóż, Rafał, Zommara, Mohamed, and Teodorczyk, Andrzej. "Characteristics of Water and Urea–Water Solution Sprays". In: *Catalysts* 9.9 (2019), p. 750. DOI: 10.3390/catal9090750.

Chapter 7

Conclusions and future works

The main objective of this chapter is to point out the conclusions achieved along this research work. The accomplishments of this study are discussed according to the findings obtained during the different phases of development and their application in a larger context.

From the knowledge gathered, some potential ideas are presented, pointing towards new research paths and enhancements of the techniques employed.

7.1 Summary

The implementation of the Selective Catalytic Reduction (SCR) technology in diesel engines has been one of the keys for the reduction of NO_x emissions. To improve the performance of this deNOx system it is necessary to extend the comprehension of the different phenomena that take place in the NO_x abatement. In this context, the current work aimed to develop experimental techniques and methodologies to perform a complete characterization of the urea-water injection process, which is an important element for the correct operation of the SCR.

The main part of this research was the development of novel experimental devices that could be useful to investigate and analyse the injection system under realistic operating conditions. Non-intrusive optical techniques were used to determine the global characteristics of the jet (penetration and angle) and microscopic properties of the spray (droplet diameter and velocity). The internal flow characterization of the injector was also performed using the

equipment and technology available at CMT - Motores Térmicos, with suitable modifications in order to capture the injection event of this low-pressure atomizer. Each experimental activity was complemented by the development of post-processing tools, imaging processing algorithms, and scripts to classify and evaluate big databases systematically.

The first two chapters of this manuscript provided an overview of the current situation regarding the technology for NO_x reduction and the status of emission regulations. Besides, a review of previous methods used for urea-water injection investigation is presented.

In chapter 3, all the experimental instruments, optical configurations and data processing routines were detailed. First, the fluid injection system and the dosing module were described. The experimental test plans were performed on a commercial Bosch deNOxtronic injector with a three-orifice configuration. Boundary conditions included three levels of injection pressure and different levels of injector cooling temperature, reaching flash boiling conditions in some of them.

For the visualization of the spray, different levels of air flow temperature and air mass flow were contemplated. The dedicated experimental facility for the spray visualization was built to cover conditions needed to resemble the mass flow and temperature of a real exhaust pipe of an engine. There was not a facility in the CMT capable of reaching high temperatures and gas mass flow before. The new test rig possesses four optical accesses that allowed the measurement of the macroscopic and microscopic properties of the spray. Moreover, the vessel had to meet other requirements for future studies, such as the possibility to install the injector at different positions, versatility in the location of instrumentation and for the implementation of other diagnosis techniques like PDA.

The results of the work were divided into three chapters based on each specific field of study of the injection process. In particular, the aspects evaluated were: first, the internal flow characterization, which combined the momentum flux measurements with the injected mass to determine the rate of injection. Second, measurements of the global spray development, quantifying the plume penetration and angle. And third, the microscopic properties of the spray using the DBI technique with a microscopic lens at high imaging speed.

The hydraulic characterization of the dosing unit provided an insight of the flow performance. Usually, for the rate of injection determination a device based on the Bosch long tube method would be used. However, since this dosing unit operates at low discharge pressure, the use of this type of instrument is not recommended. Therefore, a new methodology was proposed based

on the momentum flux measurements combined with the total injected mass quantification. The characterization was performed for two fluids: water and UWS to recall the differences and similarities between them. The following remarks can be drawn from this study:

- For the same testing conditions, results showed that the water has higher momentum flux than the UWS due to higher velocity of water at the exit of the nozzle. Then, a ratio R between the momentum flux of water and UWS was determined, finding that on average the momentum flux of UWS is 0.924 times the momentum of water.
- Regarding the effect of the cooling temperature, lower momentum flux was registered for higher temperatures. Moreover, the injected mass was influenced by the cooling temperature, finding that at 120 ^{o}C, where flash boiling conditions are set, the amount of injected mass was nearly 15% higher for both fluids. This was attributed to the changes in the physical properties of the fluids, due to the high temperatures combined with the effects of the flash boiling conditions, which also increased the discharge coefficient of the nozzle.
- The injected mass and momentum flux were used to determine the rate of injection using the proposed methodology. The ROI followed a linear behaviour with the square root of ΔP.
- The measuring technique is a useful tool for the hydraulic characterization of UWS dosing units, and can be implemented for other types of low-pressure atomizers. This is of importance due to the need to determine the ROI, especially when other methodologies cannot be applied, to validate CFD models and accurately dose those liquid fluids.

Measurements of the global spray development were carried out in the new facility that reproduces the engine exhaust pipe conditions. A DBI optical setup was employed to visualize the liquid phase. The spray penetration and spreading angle were determined for several conditions of air mass flow, air temperature, injector cooling temperature, injection pressure and injector position for a UWS dosing unit. A novel image processing method was used to identify the contour of the plume at each time frame. The analysis of the penetration was done for two regions of the spray: the spray burst and the spray body. From this study, the following conclusions were obtained:

- The initial part of the injected spray was denoted as the burst. It was observed that this zone of the jet is not particularly affected by the injection pressure but was rather influenced by the cooling temperature of the injector. When the injection pressure was increased, multiple bursts appeared due to the bouncing of the needle with the injector seat.

- The main part of the jet was denoted as the spray body. As expected, higher injection pressures led to an increase in the spray body penetration. The effect of the injection pressure was the most relevant of all parameters evaluated.

- Concerning the influence of the cooling temperature in the spray development, the penetration curves were fairly similar for temperatures of 60°C and 90°C. Meanwhile, a lower liquid penetration was found for the 120°C condition. This suggested an enhancement of the atomization process caused by the change of the properties of the fluid, in particular lower surface tension and viscosity.

- The effect of the air mass flow was not noticeable for most conditions, which is in agreement with previous studies from the literature.

- An additional study was performed to evaluate the influence of the injector pressure and cooling temperature when the dosing unit is placed at a different inclination angle with respect to the flow direction, specifically at 45º. The influence of the cooling temperature on the penetration at this position was negligible, similarly to the result obtained in the initial position of the injector. Only a slight difference was registered at the injection pressure of 4 bar, where at 90°C the gap between the burst and the body of the spray was more significant. Regarding the effect of the injection pressure, the most visible difference in the curves is that the spray penetration evolution is more linear rather than potential trend obtained at the angle of 90° with respect to the air flow.

- The spreading angle of the spray did not show continuous trends regarding the injection pressure for the 90° position of the injector. When the air mass flow was increased, the spray angle reached a constant value of 14°.

Measurements of the microscopic properties of the spray were carried out in the same optically accessible high-flow and high-temperature test rig. A dedicated microscope lens was added to the previous optical setup to visualize

the droplet morphology and position. A novel image processing methodology was developed to quantify the droplet diameter and velocity. The method was successfully verified comparing results from other optical procedures at the same conditions. The microscopic properties were determined at three regions of the spray: The first one very close to the nozzle exit, the second one in the developed region of the spray (in the axis of the plume), and the third one in the periphery of the spray in the direction of the flow. The results from the experiments leaded to the following conclusions:

- From a qualitative point of view, the raw images showed regions of liquid with non-spherical structures, like blobs or ligaments in the measurement window close to the nozzle exit. On the other hand, in the developed zone of the spray, most of the droplets were spherical, more uniform and smaller than in the first position.
- In the region of the spray near the nozzle exit, the effect of the injection pressure was observed, registering more number of droplets with smaller diameter when the pressure was higher. In the zones of the spray further away from the injector nozzle, the influence of the pressure was less notorious.
- The atomization process along the spray was examined. The particle size distribution showed a higher concentration of small droplets at the developed zone of the spray. The fact of a decrease in the droplet size is an indication of enhanced evaporation as well.
- Moreover, in both regions further away from the nozzle, the proportion of big droplets with a diameter above 100 μm decreased, corroborating the previous remark.
- Regarding the velocity, it was calculated using a droplet tracking algorithm. The interest in the technique is that the setup is relatively easy and that the velocity can be determined in two components at the same time.
- As expected, the injection pressure had an evident influence on the droplet velocity, affecting the magnitude and also the distribution. The velocity distribution in the injector axis component showed a wider range of velocity values as the injection pressure rose. The velocity distribution in the flow direction component depended on the injection pressure in the region near to the nozzle exit, with a wider shape at high pressure levels that can be attributed to some degree of turbulence inside the nozzle.

- The air flow temperature also had an effect on the droplet velocity, increasing the motion of the particles when the temperature is higher. This is related with the change of properties in the gas mass flow, allowing the droplets to penetrate the chamber faster in both directions.

As observed throughout the document, the injection process of this low-pressure atomizer is influenced by several parameters that well combined could improve the mixing in the exhaust line and the performance of the deNOx technology. Moreover, the experimental approaches described in the present document could be useful to support the propulsion industry in the design and development of the SCR system components. Finally, the experimental data gathered could be used as boundary conditions and for validation of CFD codes and numerical methods.

7.2 Future Works

This work is the first formal research study for the comprehension of the urea-water injection process in the CMT. The spray development of these low-pressure atomizers is very complex, due to the many physical and chemical mechanisms involved in a transitory event. It has been seen that optical techniques are suitable tools for non-intrusive analysis of the spray behaviour. Additionally, there are some operating conditions that promote flash boiling, which influences the atomization and the evolution of the jet, and although this work had shed some light on this phenomenon, the presented analysis was not enough to explain all the details involved in the flash boiling characteristics. Therefore, there are still many possible research fields to extend the knowledge on this topic.

The list below enumerates some potential activities that can be done in the future to contribute to the development of the experimental facilities, and the improvement of the analysis of the data:

- The determination of the real inner geometry of the injector was a difficult task due to the complexity of the nozzle and because the covering material used as cooling jacket restricted to perform direct measurements of the interior of the holes. Therefore, a more detailed characterization of the inner geometry using X-ray or disassembling the unit is recommended.
- Deeper study of the urea deposits formation in the nozzle tip. This is one of the biggest problems of SRC systems as when the water present

in the UWS evaporates, the urea solidifies forming crystals that obstruct the nozzle, the feeding system, and the exhaust components, as can be seen in Figure 7.1. The proposed task would help on the understanding of the effect of deposits on the hydraulic performance.

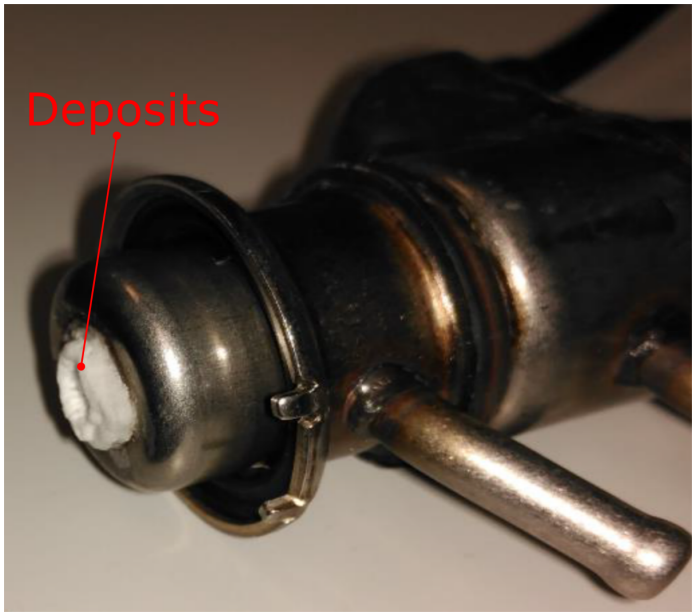

Figure 7.1: Urea deposits in the injector nozzle tip

- Regarding the installation design, some improvements are proposed. In the future, it would be convenient to change the resistor for a new one with higher power. Another possibility would be to add another with the same specifications, in order to be able to measure the same temperature points with higher air mass flow. In addition, the location of all the control elements of the installation could be optimized in order to be able to operate them remotely.

- Carry out studies of the evaporation phase of the urea jet in the same air flow conditions. This can be done using the "Schlieren" optical technique directly in the existing visualization chamber, since it has the necessary optical accesses.

- In this work, it was seen that the high cooling temperatures of the injector would enhance the atomization process caused by the change

of the fluid properties. This result is particularly important due to the need of better atomization inside the exhaust gas line, therefore, a deeper study of the evaporation and flash boiling of the urea water solution is suggested.

- Equip the experimental installation with other elements of the after-treatment system, such as the mixer, in order to understand their influence on the spray evolution and mixing process.

- To implement CFD calculations that can reproduce the spray penetration and distribution of the urea-water solution. They can be initialized and validated with part of the data presented in this thesis. The suggested analysis would provide fundamental understanding of the flow behaviour and would complement the characterization in other regions of the spray that were not covered in this study.

Global Bibliography

Alano, Eduardo et al. "Compact SCR for Passenger Cars". In: *SAE Technical Paper*. SAE International, 2011. DOI: 10.4271/2011-01-1318 (cited on page 32).

Bardi, Michele. "Partial Needle Lift and Injection Rate Shape Effect on the Formation and Combustion of the Diesel Spray". PhD thesis. Universitat Politècnica de València, 2014. DOI: 10.4995/Thesis/10251/37374 (cited on page 5).

Bardi, Michele et al. "Engine Combustion Network: Comparison of Spray Development, Vaporization, and Combustion in Different Combustion Vessels". In: *Atomization and Sprays* 22.10 (2012), pp. 807–842. DOI: 10.1615/AtomizSpr.2013005837 (cited on pages 79, 110).

BASF. "AdBlue® Technical Leaflet". In: November (2006), pp. 1–6 (cited on pages 29, 103).

Baumgarten, C. *Mixture Formation in Internal Combustion Engines*. Springer: Berlin/Heidelberg, Germany, 2006 (cited on page 46).

Birkhold, Felix, Meingast, Ulrich, Wassermann, Peter, and Deutschmann, Olaf. "Modeling and simulation of the injection of urea-water-solution for automotive SCR DeNOx-systems". In: *Applied Catalysis B: Environmental* 70.1-4 (2007), pp. 119–127 (cited on page 147).

Blaisot, J. B. and Yon, J. "Droplet size and morphology characterization for dense sprays by image processing: Application to the Diesel spray". In: *Experiments in Fluids* 39.6 (2005), pp. 977–994. DOI: 10.1007/s00348-005-0026-4 (cited on pages 85, 135).

Blakeman, Phil, Arnby, Karl, Marsh, Per, Newman, Colin, and Smedler, Gudmund. "Optimization of an SCR Catalyst System to Meet EUIV Heavy Duty Diesel Legislation". In: *2008 SAE International Powertrains, Fuels and Lubricants Congress*. SAE International, 2008. DOI: https://doi.org/10.4271/2008-01-1542 (cited on page 28).

Bracho, G., Postrioti, L., Moreno, A., and Brizi, G. "Experimental study of the droplet characteristics of a SCR injector spray through optical techniques". In: *International Journal of Multiphase Flow* 135 (2021), p. 103531 (cited on pages 133, 134, 141).

Bracho, Gabriela. "Experimental and theoretical study of the direct diesel injection process at low temperatures". PhD thesis. E.T.S. Ingenieros Industriales, Universidad Politécnica de Valencia, 2011 (cited on pages 5, 69).

Brizi, Gabriele. "Experimental analysis of Urea-Water Solution injectors for automotive Selective Catalytic Reduction systems". PhD thesis. Universita degli Studi di Perugia, 2018 (cited on pages 16, 43, 44).

Brizi, Gabriele, Postrioti, Lucio, and Vuuren, Nic van. "Experimental analysis of SCR spray evolution and sizing in high-temperature and flash boiling conditions". In: *SAE International Journal of Fuels and Lubricants* 12.2 (2019), pp. 87–107. DOI: 10.4271/04-12-02-0006 (cited on pages 43, 95, 100, 133, 135).

Carreres, Marcos. "Thermal effects influence on the Diesel injector performance through a combined 1D modelling and experimental approach". PhD thesis. Universitat Politècnica de València, 2016. DOI: 10.4995/Thesis/10251/73066 (cited on page 95).

Chen, SK, Lefebvre, AH, and Rollbuhler, J. "Influence of geometric features on the performance of pressure-swirl atomizers". In: (1990) (cited on pages 144, 146).

De Rudder, Korneel and Chauvin, Corine. "Close coupled DOC - mixer - SCR for Tier 4 final". In: *7th AVL International Commercial Powertrain Conference* (2013), pp. 1–10 (cited on pages 38, 111, 132).

Degraeuwe, Bart and Weiss, Martin. "Does the New European Driving Cycle (NEDC) really fail to capture the NOX emissions of diesel cars in Europe?" In: *Environmental Pollution* 222.X (2017), pp. 234–241. DOI: 10.1016/j.envpol.2016.12.050 (cited on page 1).

Ferrari, A. and Paolicelli, F. "An indirect method for the real-time evaluation of the fuel mass injected in small injections in Common Rail diesel engines". In: *Fuel* 191 (2017), pp. 322–329. DOI: https://doi.org/10.1016/j.fuel.2016.11.053 (cited on page 39).

García-Contreras, Reyes et al. "Impact of regulated pollutant emissions of Euro 6d-Temp light-duty diesel vehicles under real driving conditions". In: *Journal of Cleaner Production* 286 (2021), p. 124927. DOI: https://doi.org/10.1016/j.jclepro.2020.124927 (cited on page 19).

Ghandhi, J B and Heim, D M. "An optimized optical system for backlit imaging". In: *Review of Scientific Instruments* 80.5 (2009). DOI: 10.1063/1.3128728 (cited on page 79).

Giechaskiel, Barouch et al. "Evaluation of NOx emissions of a retrofitted Euro 5 passenger car for the Horizon prize "Engine retrofit"". In: *Environmental Research* 166 (2018), pp. 298–309. DOI: https://doi.org/10.1016/j.envres.2018.06.006 (cited on pages 17, 18).

Gimeno, Jaime. "Desarrollo y aplicación de la medida de flujo de cantidad de movimiento de un chorro Diesel". PhD thesis. E.T.S. Ingenieros Industriales, Universidad Politécnica de Valencia, 2008. DOI: 10.4995/Thesis/10251/8306 (cited on pages 5, 64, 66, 67, 69).

Giraldo Valderrama, Jhoan Sebastián. "Macroscopic and microscopic characterization of non-reacting diesel sprays at low and very high injection pressures". In: November (2018) (cited on pages 5, 45).

Guildenbecher, D. R., López-Rivera, C., and Sojka, P. E. "Secondary atomization". In: *Experiments in Fluids* 46.3 (2009), pp. 371–402. DOI: 10.1007/s00348-008-0593-2 (cited on page 50).

Halonen, Sauli, Kangas, Teija, Haataja, Mauri, and Lassi, Ulla. "Urea-Water-Solution Properties: Density, Viscosity, and Surface Tension in an Under-Saturated Solution". In: *Emission Control Science and Technology* 3.2 (2017), pp. 161–170. DOI: 10.1007/s40825-016-0051-1 (cited on page 103).

Hulkkonen, Tuomo, Sarjovaara, Teemu, Kaario, Ossi, Hamalainen, Ismo, and Larmi, Martti. "Experimental Study of Conical Diesel Nozzle Orifice Geometry". In: *Atomization and Sprays* 25.6 (2015), pp. 519–538. DOI: 10.1615/AtomizSpr.2015010383 (cited on page 79).

Iwamoto, Masakazu et al. “Removal of nitrogen monoxide through a novel catalytic process. 2. Infrared study on surface reaction of nitrogen monoxide adsorbed on copper ion-exchanged ZSM-5 zeolites”. In: *The Journal of Physical Chemistry* 96.23 (1992), pp. 9360–9366. DOI: 10.1021/j100202a055 (cited on page 27).

Johnson, Timothy and Joshi, Ameya. “Review of Vehicle Engine Efficiency and Emissions”. In: *SAE Technical Paper Series* 1 (2018), pp. 1–23. DOI: 10.4271/2018-01-0329 (cited on page 1).

Jung, Yongjin, Manin, Julien, Skeen, Scott A, and Pickett, Lyle M. “Measurement of Liquid and Vapor Penetration of Diesel Sprays with a Variation in Spreading Angle”. In: *SAE Technical Paper 2015-01-0946* (2015). DOI: 10.4271/2015-01-0946 (cited on page 79).

Kalghatgi, Gautam. “Is it really the end of internal combustion engines and petroleum in transport?” In: *Applied Energy* 225 (2018), pp. 965–974. DOI: https://doi.org/10.1016/j.apenergy.2018.05.076 (cited on page 1).

Kapusta, Łukasz Jan. “LIF/Mie Droplet Sizing of Water Sprays from SCR System Injector using Structured Illumination”. In: *Proceedings of ILASS2017 - 28th European Conference on Liquid Atomization and Spray Systems* September (2017), pp. 580–587. DOI: 10.4995/ilass2017.2017.5031 (cited on pages 121, 136).

Kapusta, Łukasz Jan, Sutkowski, Marek, Rogóż, Rafał, Zommara, Mohamed, and Teodorczyk, Andrzej. “Characteristics of Water and Urea–Water Solution Sprays”. In: *Catalysts* 9.9 (2019), p. 750. DOI: 10.3390/catal9090750 (cited on pages 2, 3, 44, 46, 97, 149).

Kapusta, Łukasz Jan and Teodorczyk, Andrzej. “Laser diagnostics for urea-water solution spray characterization”. In: *MATEC Web of Conferences* 118.00029 (2017), p. 00029. DOI: 10.1051/matecconf/201711800029 (cited on page 136).

Kapusta, Łukasz Jan et al. “Low-Pressure Injection of Water and Urea-Water Solution in Flash-Boiling Conditions”. In: *SAE Powertrains, Fuels & Lubricants Meeting*. SAE International, 2020 (cited on pages 95, 110, 111).

Kim, Chang Su and Park, Sung Young. “A design-variable-based computational study on the unsteady internal-flow characteristics of the urea-SCR injector for commercial vehicles”. In: *Defect and Diffusion Forum* 379 (2017), pp. 64–72. DOI: 10.4028/www.scientific.net/DDF.379.64 (cited on pages 2, 111, 121, 132).

Koebel, M., Elsener, M., and Kleemann, M. "Urea-SCR: a promising technique to reduce NOx emissions from automotive diesel engines". In: *Catalysis Today* 59.3 (2000), pp. 335–345. DOI: 10.1016/S0920-5861(00)00299-6 (cited on page 2).

Kohl, Arthur L. and Nielsen, Richard B. "Control of Nitrogen Oxides". In: *Gas Purification* II (1997), pp. 866–945. DOI: 10.1016/b978-088415220-0/50010-0 (cited on page 20).

Leach, Felix et al. "Fast Coriolis mass flow metering for monitoring diesel fuel injection". In: *Flow Measurement and Instrumentation* 58 (2017), pp. 1–5. DOI: https://doi.org/10.1016/j.flowmeasinst.2017.09.009 (cited on page 39).

Lecompte, Matthieu, Raux, Stephane, and Frobert, Arnaud. "Experimental Characterization of SCR DeNOx-Systems: Visualization of Urea-Water-Solution and Exhaust Gas Mixture". In: *SAE Technical Paper Series* 1 (2014). DOI: 10.4271/2014-01-1524 (cited on pages 3, 40).

Lee, Sang In and Park, Sung Young. "Numerical analysis of internal flow characteristics of urea injectors for SCR dosing system". In: *Fuel* 129 (2014), pp. 54–60. DOI: 10.1016/j.fuel.2014.03.031 (cited on page 2).

Lefebvre, Arthur H. and McDonell, Vincent G. *Atomization and Sprays.* Vol. 45. 5. CRC Press, 1990, p. 1435. DOI: 10.1016/0009-2509(90)87140-N (cited on pages 45, 47, 48).

Liao, Yujun, Furrer, Roman, Dimopoulos Eggenschwiler, Panayotis, and Boulouchos, Konstantinos. "Experimental investigation of the heat transfer characteristics of spray/wall interaction in diesel selective catalytic reduction systems". In: *Fuel* 190 (2017), pp. 163–173. DOI: 10.1016/j.fuel.2016.11.035 (cited on page 3).

Lieber, Christian, Koch, Rainer, and Bauer, Hans-jörg. "Microscopic Imaging Spray Diagnostics under High Temperature Conditions : Application to Urea – Water Sprays". In: *Applied sciences* (2019). DOI: 10.3390/app9204403 (cited on page 43).

Liu, Gang and Gao, Pu-Xian. "A review of NOx storage/reduction catalysts: mechanism, materials and degradation studies". In: *Catal. Sci. Technol.* 1 (4 2011), pp. 552–568. DOI: 10.1039/C1CY00007A (cited on page 27).

Manin, Julien, Bardi, Michele, and Pickett, Lyle M. "Evaluation of the liquid length via diffused back-illumination imaging in vaporizing diesel sprays". In: *The Proceedings of the International symposium on diagnostics and modeling of combustion in internal combustion engines.* Vol. 8. Fukuoka, 2012, pp. 665–673. DOI: 10.1299/jmsesdm.2012.8.665 (cited on page 79).

Manin, Julien, Bardi, Michele, Pickett, Lyle M., Dahms, Rainer N., and Oefelein, Joseph C. "Microscopic investigation of the atomization and mixing processes of diesel sprays injected into high pressure and temperature environments". In: *Fuel* 134 (2014), pp. 531–543. DOI: 10.1016/j.fuel.2014.05.060 (cited on pages 79, 85).

Mariani, Alessandro, Cavicchi, Andrea, Postrioti, Lucio, and Ungaro, Carmine. "A Methodology for the Estimation of Hole-to-Hole Injected Mass Based on Spray Momentum Flux Measurement". In: *SAE Technical Paper Series* 1 (2017). DOI: 10.4271/2017-01-0823 (cited on page 39).

Miles, Richard B. "Optical diagnostics for high-speed flows". In: *Progress in Aerospace Sciences* 72 (2015), pp. 30–36. DOI: 10.1016/j.paerosci.2014.09.007 (cited on page 79).

Montenegro, G. et al. "CFD analysis applied to the design of aqueous urea SCR dosing system with reduced risk of solid deposit formation". In: *THIESEL 2018 Conference on Thermo- and Fluid Dynamic Processes in Direct Injection Engines High-pressure*. 2018 (cited on pages 38, 111).

Munnannur, Achuth, Chiruta, Mihai, and Liu, Z Gerald. "Thermal and Fluid Dynamic Considerations in Aftertreatment System Design for SCR Solid Deposit Mitigation". In: *SAE Technical Paper Series* 1.1 (2012). DOI: 10.4271/2012-01-1287 (cited on page 111).

Oh, Jungmo and Lee, Kihyung. "Spray characteristics of a urea solution injector and optimal mixer location to improve droplet uniformity and NOx conversion efficiency for selective catalytic reduction". In: *Fuel* 119 (2014), pp. 90–97. DOI: 10.1016/j.fuel.2013.11.032 (cited on pages 2, 3, 110, 111).

Payri, Francisco and Desantes, Jose Maria. *Motores de combustion interna alternativos*. Editorial Universitat Politecnica de Valencia, 2011 (cited on pages 1, 24).

Payri, R., Bracho, G., Soriano, J. A., Fernández-Yáñez, P., and Armas, O. "Nozzle rate of injection estimation from hole to hole momentum flux data with different fossil and renewable fuels". In: *Fuel* 279.March (2020), p. 118404. DOI: 10.1016/j.fuel.2020.118404 (cited on pages 39, 104).

Payri, R., García, J. M., Salvador, F. J., and Gimeno, J. "Using spray momentum flux measurements to understand the influence of diesel nozzle geometry on spray characteristics". In: *Fuel* 84.5 (2005), pp. 551–561. DOI: 10.1016/j.fuel.2004.10.009 (cited on pages 64, 65, 69).

Payri, R., Salvador, F. J., Gimeno, J., and Bracho, G. "A new methodology for correcting the signal cumulative phenomenon on injection rate measurements". In: *Experimental Techniques* 32.1 (2008), pp. 46–49. DOI: 10.1111/j.1747-1567.2007.00188.x (cited on pages 38, 67).

Payri, Raul, Bracho, Gabriela, Gimeno, Jaime, and Moreno, Armando. "A Methodology for the hydraulic characterization of a Urea-Water Solution injector by means of Spray Momentum Measurement". In: *ILASS - Europe 2019, 29th Conference on Liquid Atomization and Spray Systems* September (2019), pp. 2–4 (cited on pages 38, 93).

Payri, Raul, Bracho, Gabriela, Gimeno, Jaime, and Moreno, Armando. "Investigation of the urea-water solution atomization process in engine exhaust-like conditions". In: *Experimental Thermal and Fluid Science* 108.June (2019), pp. 75–84. DOI: 10.1016/j.expthermflusci.2019.05.019 (cited on pages 2, 3, 79, 83, 85, 110, 121, 140).

Payri, Raul, Bracho, Gabriela, Marti-Aldaravi, Pedro, and Viera, Alberto. "Near field visualization of diesel spray for different nozzle inclination angles in non-vaporizing conditions". In: *Atomization and Sprays* 27.3 (2017), pp. 251–267. DOI: 10.1615/AtomizSpr.2017017949 (cited on page 79).

Payri, Raul, Garcia-Oliver, Jose Maria, Bardi, Michele, and Manin, Julien. "Fuel temperature influence on diesel sprays in inert and reacting conditions". In: *Applied Thermal Engineering* 35.1 (2012), pp. 185–195. DOI: 10.1016/j.applthermaleng.2011.10.027 (cited on page 79).

Payri, Raul, Garcia-Oliver, Jose Maria, Xuan, Tiemin, and Bardi, Michele. "A study on diesel spray tip penetration and radial expansion under reacting conditions". In: *Applied Thermal Engineering* 90 (2015), pp. 619–629. DOI: 10.1016/j.applthermaleng.2015.07.042 (cited on page 110).

Payri, Raul, Gimeno, Jaime, Bracho, Gabriela, and Moreno, Armando. "Spray characterization of the Urea-Water Solution (UWS) injected in a hot air stream analogous to SCR system operating conditions ." In: *WCX SAE World Congress Experience* 2019-01-0738 (2019), pp. 1–9. DOI: 10.4271/2019-01-0738.Abstract (cited on pages 79, 85, 110, 143, 146).

Payri, Raul, Salvador, Francisco Javier, Gimeno, Jaime, and Viera, Alberto. "10 Tagung Diesel- und Benzindirekteinspritzung 2016-2017". In: *10. Tagung Diesel- und Benzindirekteinspritzung 2016*. Ed. by Helmut Tschöke and Ralf Marohn. 1. Springer, 2017, pp. 133–152. DOI: 10.1007/978-3-658-15327-4 (cited on page 79).

Payri, Raul, Salvador, Francisco Javier, Marti-Aldaravi, Pedro, and Vaquerizo, Daniel. "ECN Spray G external spray visualization and spray collapse description through penetration and morphology analysis". In: *Applied Thermal Engineering* 112 (2017), pp. 304–316. DOI: 10.1016/j.applthermaleng.2016.10.023 (cited on page 110).

Payri, Raul, Viera, Juan Pablo, Wang, Hua, and Malbec, Louis-Marie. "Velocity field analysis of the high density, high pressure diesel spray". In: *International Journal of Multiphase Flow* 80 (2016), pp. 69–78. DOI: 10.1016/j.ijmultiphaseflow.2015.10.012 (cited on page 79).

Payri, Raul et al. "Momentum Flux Measurements on an ECN GDi Injector". In: *SAE Technical Paper 2015-01-1893*. Vol. 1. 2015. DOI: 10.4271/2015-01-1893 (cited on page 39).

Payri, Raul et al. "Computational study of urea-water solution sprays for the analysis of the injection process in SCR-like conditions". In: *Industrial & Engineering Chemistry Research* (2020). DOI: 10.1021/acs.iecr.0c02494 (cited on page 102).

Payri, Raúl, Bracho, Gabriela, Martí-Aldaraví, Pedro, and Moreno, Armando. "Using momentum flux measurements to determine the injection rate of a commercial Urea Water Solution injector". In: *Flow Measurement and Instrumentation* 80 (2021), p. 101999. DOI: https://doi.org/10.1016/j.flowmeasinst.2021.101999 (cited on pages 2, 38, 66, 100, 133).

Pickett, Lyle M, Manin, Julien, Payri, Raul, Bardi, Michele, and Gimeno, Jaime. "Transient Rate of Injection Effects on Spray Development". In: *SAE Technical Paper 2013-24-0001* (2013). DOI: 10.4271/2013-24-0001 (cited on page 39).

Pilch, M. and Erdman, C. A. "Use of breakup time data and velocity history data to predict the maximum size of stable fragments for acceleration-induced breakup of a liquid drop". In: *International Journal of Multiphase Flow* 13.6 (1987), pp. 741–757. DOI: 10.1016/0301-9322(87)90063-2 (cited on page 49).

Postrioti, Lucio, Brizi, Gabriele, Ungaro, Carmine, Mosser, Mark, and Bianconi, Francesco. "A methodology to investigate the behaviour of urea-water sprays in high temperature air flow for SCR de-NOx applications". In: *Fuel* 150.x (2015), pp. 548–557. DOI: 10.1016/j.fuel.2015.02.067 (cited on pages 42, 43, 136).

Postrioti, Lucio, Caponeri, Giulio, Buitoni, Giacomo, and Van Vuuren, Nic. "Experimental Assessment of a Novel Instrument for the Injection Rate Measurement of Port Fuel Injectors in Realistic Operating Conditions". In: *SAE International Journal of Fuels and Lubricants* 10.2 (2017), pp. 1–8. DOI: 10.4271/2017-01-0830 (cited on pages 38, 39).

Raff, Michael, Weingarten, Erik, and Muslija, Manuel. "Denoxtronic 5.3 – A modular system for applications worldwide". In: *19. Internationales Stuttgarter Symposium*. Ed. by Michael Bargende, Hans-Christian Reuss, Andreas Wagner, and Jochen Wiedemann. Wiesbaden: Springer Fachmedien Wiesbaden, 2019, pp. 113–127 (cited on pages 33, 34).

Reitz, R D et al. "IJER editorial: The future of the internal combustion engine". In: *International Journal of Engine Research* (2019), p. 146808741987799. DOI: 10.1177/1468087419877990 (cited on page 14).

Reitz, Rolf D. "Atomisation and other breakup regimes of a liquid jet". PhD thesis. Ph.D. Thesis, Princeton University, 1978 (cited on pages 45, 47).

Reitz, Rolf Deneys and Bracco, Frediano V. "Mechanism of breakup of round liquid jets". In: *Encyclopedia of Fluids Mechanics* 3 (1984). Ed. by N Cheremisnoff, pp. 233–249 (cited on page 46).

Salvador, Francisco Javier. "Estudio teórico experimental de la influencia de la geometría de toberas de inyección Diésel sobre las características del flujo interno y del chorro". PhD thesis. Valencia: E.T.S. Ingenieros Industriales. Universidad Politécnica de Valencia, 2003 (cited on page 5).

Shahariar, G. M.Hasan and Lim, Ock Taeck. "A study on urea-water solution spray-wall impingement process and solid deposit formation in urea-scr denox system". In: *Energies* 12.1 (2019). DOI: 10.3390/en12010125 (cited on page 111).

Shi, Xian, Deng, Jun, Wu, Zhijun, and Li, Liguang. "Effect of Injection Parameters on Spray Characteristics of Urea-SCR System". In: *SAE International Journal of Engines* 6.2 (2013), pp. 873–881. DOI: https://doi.org/10.4271/2013-01-1067 (cited on pages 41, 42).

Siebers, Dennis L. "Liquid-Phase Fuel Penetration in Diesel Sprays". In: *SAE Technical Paper 980809* (1998), pp. 1–23. DOI: 10.4271/980809 (cited on page 79).

Soare, Vlad. "Phase Doppler Measurements in Diesel Dense Sprays: Optimisation of Measurements and Study of the Orifice Geometry Influence over the Spray at Microscopic Level". PhD thesis. E.T.S. Ingenieros Industriales, Universidad Politécnica de Valencia, 2007 (cited on page 5).

Spiteri, A., Srna, A., and Dimopoulos Eggenschwiler, P. "Characterization of sprays of water and urea-water solution from a commercial injector for SCR DeNOx applications". In: *The Proceedings of the 13th Stuttgart International Symposium "Automotive and Engine Technology"*. 2013 (cited on page 41).

Spiteri, Alexander and Dimopoulos Eggenschwiler, Panayotis. "Experimental fluid dynamic investigation of urea-water sprays for diesel selective catalytic reduction-denox applications". In: *Industrial and Engineering Chemistry Research* 53.8 (2014), pp. 3047–3055. DOI: 10.1021/ie404037h (cited on pages 3, 40, 41, 121).

Strots, Vadim O., Santhanam, Shyam, Adelman, Brad J., Griffin, Gregory A., and Derybowski, Edward M. "Deposit formation in urea-scr systems". In: *SAE International Journal of Fuels and Lubricants* 2.2 (2010), pp. 283–289. DOI: 10.4271/2009-01-2780 (cited on page 111).

Tang, Chenglong, Feng, Zehao, Zhan, Cheng, Ma, Wen'an, and Huang, Zuohua. "Experimental study on the effect of injector nozzle K factor on the spray characteristics in a constant volume chamber: Near nozzle spray initiation, the macroscopic and the droplet statistics". In: *Fuel* 202 (2017), pp. 583–594. DOI: https://doi.org/10.1016/j.fuel.2017.04.078 (cited on page 136).

Triantafyllopoulos, Georgios, Katsaounis, Dimitrios, Karamitros, Dimitrios, Ntziachristos, Leonidas, and Samaras, Zissis. "Experimental assessment of the potential to decrease diesel NOxemissions beyond minimum requirements for Euro 6 Real Drive Emissions (RDE) compliance". In: *Science of the Total Environment* 618.x (2018), pp. 1400–1407. DOI: 10.1016/j.scitotenv.2017.09.274 (cited on page 2).

Varna, Achinta, Spiteri, Alexander C., Wright, Yuri M., Dimopoulos Eggenschwiler, Panayotis, and Boulouchos, Konstantinos. "Experimental and numerical assessment of impingement and mixing of urea-water sprays for nitric oxide reduction in diesel exhaust". In: *Applied Energy* 157 (2015), pp. 824–837. DOI: 10.1016/j.apenergy.2015.03.015 (cited on pages 2, 3, 121, 136).

Venegas, Oscar. "Estudio del fenómeno de la cavitación en la inyección Diesel mediante la visualización del flujo interno en orificios transparentes." PhD thesis. Universitat Politècnica de València, 2014. DOI: 10.4995/Thesis/10251/37375 (cited on pages 5, 46).

Viera, Juan Pablo. "Experimental study of the effect of nozzle geometry on the performance of direct-injection diesel sprays for three different fuels". PhD thesis. Universitat Politècnica de València, 2017. DOI: 10.4995/Thesis/10251/81857 (cited on page 5).

Vuuren, Nic van, Postrioti, Lucio, Brizi, Gabriele, Ungaro, Carmine, and Buitoni, Giacomo. "Experimental Analysis of the Urea-Water Solution Temperature Effect on the Spray Characteristics in SCR Systems". In: *SAE Technical Paper Series* 1 (2015). DOI: 10.4271/2015-24-2500 (cited on pages 3, 110, 121).

Vuuren, Nic van, Ungaro, Carmine, Brizi, Gabriele, Buitoni, Giacomo, and Postrioti, Lucio. "AUS-32 Injector Spray Imaging on Hot Air Flow Bench". In: *SAE 2015 World Congress and Exhibition*. SAE International, 2015. DOI: https://doi.org/10.4271/2015-01-1031 (cited on pages 2, 3).

Yang, Liuhanzi et al. "Experimental Assessment of NOx Emissions from 73 Euro 6 Diesel Passenger Cars". In: *Environmental Science and Technology* 49.24 (2015), pp. 14409–14415. DOI: 10.1021/acs.est.5b04242 (cited on page 1).

Yang, Zhiwen et al. "Real-world gaseous emission characteristics of Euro 6b light-duty gasoline- and diesel-fueled vehicles". In: *Transportation Research Part D: Transport and Environment* 78 (2020), p. 102215. DOI: https://doi.org/10.1016/j.trd.2019.102215 (cited on page 19).

Zeldovich, Yakov Borisovich. "Oxidation of nitrogen in combustion and explosions". In: *Selected Works of Yakov Borisovich Zeldovich, Volume I*. Princeton University Press, 2014, pp. 404–410 (cited on page 21).

Zhan, Reggie, Li, Wei, Eakle, Scott, and Weber, Phillip. "Development of a Novel Device to Improve Urea Evaporation, Mixing and Distribution to Enhance SCR Performance". In: 2010. DOI: 10.4271/2010-01-1185 (cited on page 32).

Zhao, Hua. *Advanced direct injection combustion engine technologies and development: diesel engines*. Vol. 2. Elsevier, 2009 (cited on pages 24, 25).

Zhao, Le et al. "Evaluation of Diesel Spray-Wall Interaction and Morphology around Impingement Location". In: *SAE Technical Paper 2018-01-0276* (2018). DOI: 10.4271/2018-01-0276 (cited on page 143).

Zheng, Guanyu. "Development of Air-Assisted Urea Injection Systems for Medium Duty Trucks". In: *SAE Technical Papers* 2017-Septe.September (2017). DOI: 10.4271/2017-24-0112 (cited on pages 2, 111).